NOVEL PLASMONIC DEVICES
FOR
NANO-PHOTONICS APPLICATIONS

A DISSERTATION
SUBMITTED TO THE DEPARTMENT OF ELECTRICAL AND
ELECTRONICS ENGINEERING AND GRADUATE SCHOOL OF
ENGINEERING AND SCIENCE OF
BILKENT UNIVERSITY
IN PARTIAL FULFILLMENT OF THE REQUIREMENTS
FOR THE DEGREE OF
DOCTOR OF PHILOSOPHY

By
Levent Şahin
July, 2013

I certify that I have read this thesis and that in my opinion it is fully adequate, in scope and in quality, as a dissertation for the degree of Doctor of Philosophy.

_____

Prof. Dr. Ekmel Özbay (Supervisor)

I certify that I have read this thesis and that in my opinion it is fully adequate, in scope and in quality, as a dissertation for the degree of Doctor of Philosophy.

_____

Prof. Dr. Gönül Turhan Sayan

I certify that I have read this thesis and that in my opinion it is fully adequate, in scope and in quality, as a dissertation for the degree of Doctor of Philosophy.

_____

Prof. Dr. Orhan Aytür

I certify that I have read this thesis and that in my opinion it is fully adequate, in scope and in quality, as a dissertation for the degree of Doctor of Philosophy.

_____

Prof. Dr. Oğuz Gülseren

I certify that I have read this thesis and that in my opinion it is fully adequate, in scope and in quality, as a dissertation for the degree of Doctor of Philosophy.

_____

Assoc. Prof. Dr. Vakur B. Ertürk

Approved for the Graduate School of Engineering and Science:

_____

Prof. Dr. Levent Onural
Director of the Graduate School

ABSTRACT

NOVEL PLASMONIC DEVICES FOR NANO-PHOTONICS APPLICATIONS

Levent Şahin
Ph.D. in Electrical and Electronics Engineering
Supervisor: Prof. Dr. Ekmel Özbay
July, 2013

Plasmonics have attracted a great deal of interest because of their potential to design novel photonics devices which have unique optical properties. This dissertation focuses on novel plasmonic device designs for photonics applications.

Electromagnetic properties of metamaterials are characterized and the resonance mechanism of Split Ring Resonator (SRR) structure is investigated. Furthermore, novel SRR-based metamaterial structures are studied. We demonstrated the significant plasmonic enhancement in the transmission characteristics through a sub-wavelength aperture by utilizing SRR resonances.

Electrical tuning of plasmonic resonance with varying gate bias by using graphene is observed. Also, electrical properties of graphene is investigated. Fabrication of electrically gated graphene based plasmonic structures are realized. In addition, we utilized metamaterials to design novel photonic devices and we experimentally studied and numerically

verified the novel propagation characteristics of graphene-based photonic devices and 3D nanostructures. The proposed structures are designed, simulated, fabricated and measured. The simulations and experimental results are in good agreement and shows significant enhancement of transmission characteristics of plasmonic devices. The dimensions of the structures that are designed in our work is less than 10 times smaller than the incident wavelength ($r/\lambda \sim 0.1$) which is a desired property for enhanced light confinement of sensors. Also, the gate tuning of SRR's plasmonic resonance is the first demonstration in the contemporary literature according to our knowledge.

Keywords: Plasmonics, Photonics, Metamaterial, Split Ring Resonator (SRR) Structure, Graphene, Tunable Resonances, 3D Direct Writing, Enhanced Transmission, Sub-wavelength Aperture

ÖZET

NANO-FOTONİK UYGULAMALAR İÇİN YENİ PLAZMONİK CİHAZLAR

Levent Şahin
Elektrik ve Elektronik Mühendisliği, Doktora
Tez Yöneticisi: Prof. Dr. Ekmel Özbay
Temmuz, 2013

Plazmonik kendine has optik özellikleri olan yeni fotonik cihazların geliştirilmesindeki potansiyeli nedeniyle büyük ilgi çekmektedir. Bu Tez, fotonik uygulamalar için yeni plazmonik cihaz tasarımlarına odaklanmaktadır.

Metamalzemelerin elektromanyetik özellikleri tanımlanmakta ve Yarıklı Halka Rezonatörü (YHR) yapısının rezonans mekanizması incelenmektedir. Bunun yanında, YHR temelli yen metamalzeme yapıları çalışılmıştır. YHR rezonanslarından faydalanarak dalga boyu altı aralıktan plazmonik geçirgenlikte önemli oranda artış gözlemlendi.

Grafen kullanarak plazmonik rezonansın değişken geçit meyili ile elektriksel ayarlanması gözlemlendi. Aynı zamanda, grafenin elektriksel özellikleri incelendi. Elektriksel geçitli grafen temelli plazmonik yapılar gerçekleştirildi. Ayrıca, yeni fotonik cihazların tasarımı için metamalzemeler kullanıldı ve grafen temelli fotonik cihazlar ile 3B nanoyapıların yeni yayılma özellikleri deneysel olarak çalışıldı ve benzetim ile doğrulandı. Önerilen yapılar tasarlandı, benzetim yapıldı,

üretildi ve ölçüldü. Benzetim çalışmaları ve ölçümler benzer sonuçlar verdi ve önerilen yeni yapıların kullanılması ile plazmonik cihazların geçirgenlik özelliklerinde önemli oranda artış gözlemlendi. Çalışmamızda tasarlanan yapıların boyutları gelen dalganın dalga boyundan 10 kat (r/λ~0.1) daha küçüktür ve bu sensorler için gereken artırılmış ışık toplanması amacıyla istenmektedir. Ayrıca, çalışmamızdaki YHR'nin plazmonik rezonansının geçit ayarlanması bildiğimiz kadarıyla güncel literatürdeki ilk gösterimdir.

Anahtar Sözcükler: Plazmonik, Fotonik, Metamalzeme, Yarıklı Halka Rezonatörü Yapısı, Grafen, Ayarlanabilen Resonanslar, 3B Doğrudan Yazım, Artırılmış Geçirgenlik, Dalga Boyu Altı Aralık

To my son, for greeting me with a bright smile

ACKNOWLEDGEMENT

I would like to express my sincere gratitude to my thesis supervisor Prof. Ekmel Özbay for his invaluable guidance and motivation. His support, encouragements and suggestions taught me much about systematically approaching to research study. I am grateful to Nanotechnology Research Center (NANOTAM) for the facilities and working environment provided for me to perform the research study.

I would like to thank to the members of my thesis committee, Prof. Dr. Gönül Turhan-Sayan, Prof. Dr. Orhan Aytür, Prof. Dr. Oğuz Gülseren and Assoc. Prof. Dr. Vakur B. Ertürk for reading the manuscript and commenting on the dissertation.

Special thanks and gratitude to Prof. Dr. Eric Mazur who supervised my research work at Harvard University while I was a visiting scientist. His research group provided support, encouragement and valuable ideas towards the realization some of the research work presented in this dissertation. Special thanks to my friend Dr. Kevin Vora for his support during my research work at Harvard.

During my dissertation work, I had the opportunity to work with a number of collaborators. I would like to thank to Kevin Vora, Phillip Munoz, Erdem Demircioğlu, A. Burak Turhan, Yasemin Kanlı and Semih Çakmakyapan for discussions on various aspects of research study.

I would like to thank Republic of Turkey, Prime Ministry (PM) for the permission to the study on the dissertation. Also, my special thanks to Dr. Orhan Şengül for his continuous support and encouragement. I would like to thank TÜBITAK - BİDEB (The Scientific and Technological Research Council of Turkey - The Department of Science Fellowships and Grant Programmes) for their support during my dissertation.

Last but not the least; I would present my endless thanks to my parents, Şaziye and Sayit Şahin; and to my beloved wife Dr. Fatma Başıbüyük-Şahin for their endless support, encouragement and love. This dissertation could not be completed without their support. I dedicate this labor to my son, the newest member of my family. He came into our life during the final stage of my Ph.D. study and helped me to overcome any worries and trouble.

CONTENTS

List of Figures

List of Tables

Chapter 1

Introduction

1.1 Motivation

Plasmonics is a growing new research field of science as a result of unique optical properties of metallic nanostructures that can be utilized to manipulate transmission and propagation characteristics of light. Nanometallic structures' optical properties stem from the ability to support collective electron excitations which is called plasmons.

Plasmons are defined as the coupled electromagnetic waves which propagates through its path between a metal and a dielectric interface. The increasing interest on plasmons stem from ability to confine light to nanoscale regions which can be much smaller than the wavelength of light. Therefore, plasmonics can provide nanoscale confinement and localization which is related to coupling of surface plasmons and waveguiding, and active functionality on the nanoscale.

Light can couple the free-electron excitations near the metallic surfaces as a result of its interaction with metal nanostructures. Surface plasmon-related electromagnetic resonances are related to surface details of the nanostructure which creates significant novel research areas for control of light. The control of light opens up significant opportunities for scientist to design plasmonic devices which are candidates to solve contemporary engineering challenges. In addition to providing novel devices, plasmonic devices lead to scaling down the sizes of optical devices and components. On the other hand, there are several challenges to overcome. The most prominent one is the Ohmic losses which impose fundamental constraint at optical frequencies. Also fabrication at nanoscale accuracy is a problem. We cannot control the geometry well without nanoscale precision at fabrication.

Metamaterial based plasmonic devices are prominent candidates for designing novel optical devices. Therefore, we will investigate the metamaterial based photonic devices in our dissertation.

Metamaterials have shown significant potential in recent years due to their scientific-breakthrough properties and applications to create novel devices that exhibit specific electromagnetic properties. The main idea behind the metamaterials is to manipulate constitutive parameters of artificially designed materials to obtain peculiar electromagnetic properties.

Since, response of materials to an incident electromagnetic wave is determined by their constitutive macroscopic electromagnetic parameters, the dielectric permittivity (ε) and magnetic permeability (μ), we can design artificial materials that respond to incident electromagnetic

waves in a desired characteristics. Ordinary materials generally have positive ε and μ, which restrict the design of novel devices. However, new structures called metamaterials are proposed for realizing novel response characteristics that do not occur in nature. The phrase "meta" means "beyond" in Greek, which refers the novel electromagnetic characteristics of metamaterials that are not available in nature. The engineered response of metamaterials has the potential to make a dramatic impact on the design of novel electromagnetic devices; as they provide the possibility to achieve novel physical phenomena that cannot be achieved with conventional, naturally occurring materials.

V. Veselago was the first scientist who theoretically suggested metamaterials with simultaneously negative dielectric permittivity and magnetic permeability at 1968 [1]. After a long time later, increasing interest in this topic started by the seminal works of J.B. Pendry *et al.* [2] and D.R. Smith *et al.* [3]. Since metamaterials offer new physical phenomena, there is an increasing amount of interest and a large amount of literature has been accumulated on metamaterials [4-16]. Also novel applications such as superlenses [17, 18], enhanced magnetic resonance imaging [18], hyperlenses [20, 21], cloaking [22], and semiconductor metamaterials [23] are achieved.

At the beginning, the research activities of metamaterial based photonics were mainly focused on obtaining artificial materials with negative permeability and negative index properties. However, new research fields for the applications of metamaterials have emerged lately. These research fields are mostly related to the transmission and propagation properties of novel structures.

In addition, there are wide varieties of study on metamaterials to change the transmission characteristics of several structures, which are restricted to several physical restrictions that cannot be overcome by ordinary materials. Transmission through a sub-wavelength hole is another contemporary research topic because of its applications of critical importance ranging from biomaterials to microscopy. The last century concluded with a very important discovery by Ebbesen [24]; sub-wavelength holes in a thin metal film can transmit electromagnetic waves much more strongly at certain frequencies than the Bethe's prediction [25] by utilizing hole arrays. Ebbesen's discovery (extraordinary transmission phenomenon) and new fabrication techniques opened up significant opportunities to design novel devices.

Also we studied graphene-based photonic devices. Graphene is an extraordinary material which is believed to have outstanding applications in photonics. Therefore, design of graphene-based novel photonic systems is an active research field. However, exciting opportunity to design novel photonic devices using graphene structures has not been fully exploited. Electrical tuning of plasmonic resonance with varying gate bias by using graphene is observed.

In the present dissertation, we investigated the transmission and propagation properties of metamaterials. We utilized metamaterials to design novel photonic devices and we experimentally studied and numerically verified the novel propagation characteristics of graphene-based photonic devices and 3D nanostructures.

1.2 Outline of the thesis

This dissertation is organized into 5 chapters. We investigated novel plasmonic devices for nano-photonics applications. We experimentally studied and numerically verified the propagation characteristics of novel plasmonic devices. Besides this introductory chapter which is aimed to provided a brief introduction of the dissertation, the content of the chapters are organized as follows:

In Chapter 2, the metamaterial based plasmonics is introduced and design of novel devices are investigated. Several novel structures to increase the transmission through a sub-wavelength aperture is investigated. The negative dielectric permittivity and negative magnetic permeability phenomenon are discussed. In addition, the negative index of refraction of left-handed metamaterials is demonstrated.

Chapter 3 is about the Nobel-winning graphene material's possible applications on photonics. Several novel structures to utilize promising properties of graphene is investigated. Finally, electrical tuning of plasmonic resonance by using graphene is observed with varying gate bias. This effect is studied with theoretical modeling and confirmed experimentally.

Chapter 4 is devoted to 3D nanostructures fabricated with femto-second laser writing which can be a base for new optical devices. Measurements and simulations are performed in order to observe 3D fabrication.

Furthermore, refractive index increase with increasing filling factor of FCC lattice is verified by using the retrieval procedure.

Finally, Chapter 5 provides a concise summary of the work presented in this dissertation Moreover, the future research directions and future work are provided in this chapter.

Chapter 2

Metamaterial based Plasmonics

2.1. Introduction

Metamaterials are artificially made structures with tailored sub-wavelength unit cells. They emerged with new and unusual properties which were previously unattainable in natural materials.

Over the past eight years, metamaterials have shown tremendous potential in many disciplines of science and technology. First designs were microwave devices that proved the concept. After that, operating frequency of metamaterials increased over the years [26]. This tremendous increase in operation frequency is a result of miniaturizing SRR devices. Challenging the limitations arising from scaling of microwave metamaterial designs to optical frequencies is one of the major research area of plasmonics nowadays. Because, optical metamaterials opens up significant opportunities to design an entire new generation of miniaturized passive and active optical elements.

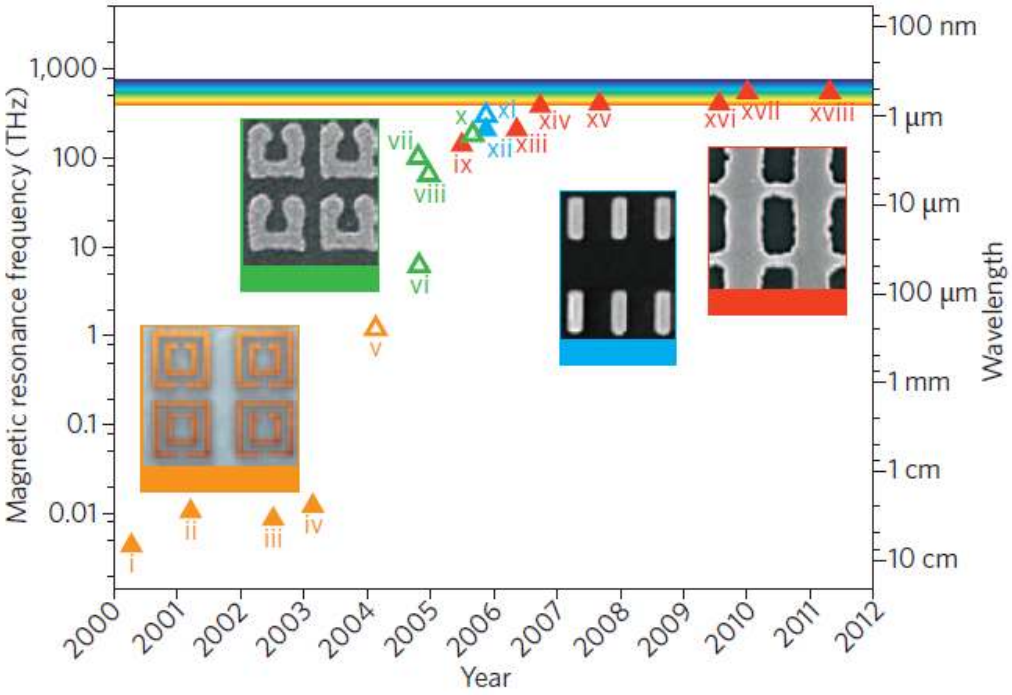

Figure 2.1: Development of metal-based metamaterial as a function of operation frequency and time. Orange: double SRRs; purple: transmission-Line structures [29], copyright (2004) by the American Physical Society; green: U-shaped SRRs; blue: metallic cut-wire pairs; red: double fishnet structures. The five insets show optical or electron micrographs of the five kinds of structure. Reprinted by permission from Macmillan Publishers Ltd: [Nature Photonics] [12].

Metamaterials design started with the design of first negative permittivity devices, thin metal wires. After that SRRs are suggested by Pendry et. al. to demonstrate negative permeability [2]. Obtaining both negative permittivity and permeability paved the wave of negative refractive index. Negative refractive index phenomenon created new opportunities to design novel devices especially at optical regime. Therefore, microwave devices are scaled down to obtain optical devices. However, fabrication of optical metamaterials and loss issues is still a challenge for researchers.

Main drawbacks of metal-based metamaterials, which are need to be overcome, are conduction loss and anisotropy [26].

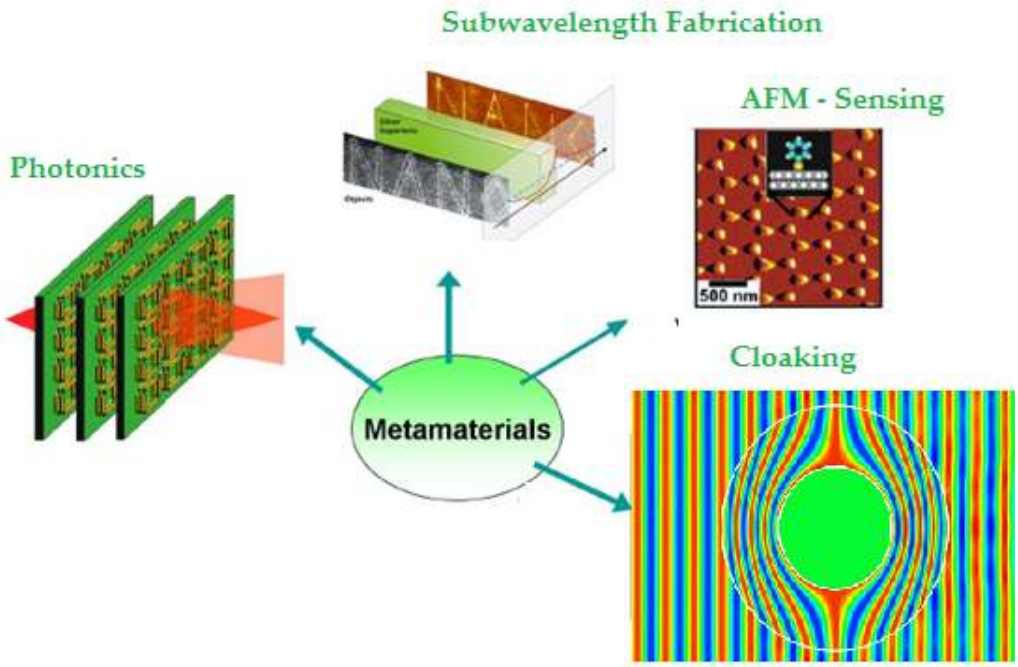

Figure 2.2: Potential applications such as subdiffraction imaging, sensing, cloaking [36].

Metamaterials are the pioneer devices of compact and novel photonic devices [27]. Artificially designed metamaterials are proposed to mimic bulk materials [3]. Since, we can design each elements in a bulk metamaterial, we can design frequency response of the metamaterial which is not available property of natural materials. Moreover, we can modulate the spectral response by including active elements. [12].

Unit cell of metamaterial is at the scale of sub-wavelength. Therefore, ultra compact photonic devices which are only several wavelengths in footprint is a possibility. Plasmonic resonance which emanates from metallic ring of SRR at optical regime is the driving force for optical metamaterial. Plasmons created by the SRR's metallic ring accumulated at

resonance frequency and creates high spatial field density which makes novel metamaterial-based devices possible.

Plasmons are defined as the coupled electromagnetic waves which exists between a metal and a dielectric interface. The increasing interest on plasmons stem from ability to confine light to nanoscale regions which can be much smaller than the wavelength of light. Therefore, plasmonics can provide nanoscale confinement and localization which is related to coupling of surface plasmons and waveguiding, and active functionality on the nanoscale. Plasmonic spatial localization and high density of states is superior to other methods on the same scale [30].

Light can couple the free-electron excitations near the metallic surfaces as a result of its interaction with metal nanostructures. Surface plasmon-related electromagnetic resonances are related to surface details of the nanostructure which creates novel research paths for control of light. The control of light opens up significant opportunities for scientist to design plasmonic devices which are candidates to solve contemporary engineering challenges. In addition to providing novel devices, plasmonic devices lead to scaling down the sizes of optical devices and components. On the other hand, there are several challenges to overcome. The most prominent one is the Ohmic losses which impose fundamental constraint at optical frequencies. Also fabrication at nanoscale accuracy is a problem. We cannot control the geometry well without nanoscale precision at fabrication.

In this section, we demonstrate metamaterial based plasmonic devices operating at microwave and optical frequencies. Resonance characteristic

of SRR is investigated for both microwave and light. Also the effect of geometrical parameters on the resonance of SRR is discussed. We made several transmission measurements and simulations; and observed enhanced transmission over a common frequency range.

2.2. Metamaterials

Metamaterials are the artificial structured materials which have unique properties to interact with waves that are not usually found in nature. Development of artificial dielectric media which are used for designing metamaterials has become a remarkable research area due to its potential for creating new devices that exhibit unusual electromagnetic properties [36]. The applications of novel dielectric media in various areas such as imaging, lensing, optical fibers, and lasers require the effective control of the transmission and propagation of electromagnetic waves. As we control permittivity and permeability values of a structure, we can design metamaterials. The metamaterial's constitutive parameters (ε,μ) can be determined to a desired value which are great candidates to be used in several applications ranging from focusing without a diffraction limit to extraordinary transmission through sub-wavelength apertures.

Electromagnetic response of materials is determined by the fundamental constitutive parameters, the dielectric permittivity (ε), the magnetic permeability (μ) and the conductivity (σ). The combined effect of permittivity and permeability determine the response of a lossless material to an incident electromagnetic field. Most of the natural structures have positive permittivity and permeability. Due to the absence of magnetic charges, it is rather difficult to have negative

permeability structures, while negative permittivity is obtained below the plasma frequency of periodic sub-wavelength metallic wires at microwave frequencies as shown theoretically [39, 40] and experimentally [41]. The phenomenon of negative refraction of electromagnetic wave in media with negative permittivity and permeability was first suggested by Vesalago in 1968 [1]. A material that has both negative permittivity and permeability was predicted to have negative refractive index, the reversal of Doppler Effect [1, 51] and Cerenkov radiation [52]. Materials with negative index of refraction ($n<0$) demonstrate the unusual behavior that the propagation direction of electromagnetic wave is opposite to the direction of the energy flow. In other words, the phase velocity and group velocity are antiparallel, which is an extraordinary behavior of left-handed materials that may open up significant opportunities to develop novel electromagnetic devices.

Negative permittivity is demonstrated by utilizing periodic metallic wire arrangements at the microwave regime [39-41]. Dielectric permittivity is negative below the plasma frequency of a metallic wire array and no electromagnetic wave can propagate at the negative permittivity spectrum as long as the permeability remains positive. No material with negative permeability was suggested until the seminal work of Pendry *et al.* [2], where a periodic arrangement of novel resonator structures called Split Ring Resonators (SRRs) was employed to obtain negative permeability around the resonance frequency. Afterwards, Smith *et al.* experimentally demonstrated a novel type of materials, composite metamaterials, by stacking thin wires and SRRs [3, 45] so that left-handed propagation band was observed at frequencies where both the dielectric

permittivity and magnetic permeability of this composite metamaterial were both negative.

Negative index of refraction is theoretically [1, 46] and experimentally [47] verified where both permittivity and permeability are both negative. Negative index of refraction for left-handed materials has been confirmed in agreement with various other studies [46-50, 53].

The fundamental postulate for the large-scale (macroscopic) electromagnetic phenomena is described by Maxwell's Equations. Therefore, the theoretical analysis of metamaterials starts with Maxwell's Equations.

Electromagnetic field solutions at every point in space must satisfy the Maxwell's Equations which are expressed in time domain as follows:

$$\nabla \times \overline{E} = -\frac{\partial \overline{B}}{\partial t} \quad \text{(Faraday's Induction Law)} \tag{2.1}$$

$$\nabla \times \overline{H} = \frac{\partial \overline{D}}{\partial t} + \overline{J} \quad \text{(Generalized Ampere's Circuital Law)} \tag{2.2}$$

$$\nabla \bullet \overline{D} = \rho \quad \text{(Gauss' Law)} \tag{2.3}$$

$$\nabla \bullet \overline{B} = 0 \quad \text{(Conservation of Magnetic Flux)} \tag{2.4}$$

Also, the mathematical statement of "conservation of electric charge" is given by the Continuity Equation:

$$\nabla \bullet \overline{J} = -\frac{\partial \rho}{\partial t} \tag{2.5}$$

which is linearly dependent on Maxwell's Equations.

The vector and scalar quantities in Eqn. 2.1 through Eqn. 2.5 are functions of both space variables and time.

We considered the uniform plane wave excitation at a given angular frequency w for the simplicity of our analysis. Using the e^{+jwt} convention, the mathematical expressions for the $\overline{E}$ and $\overline{H}$ fields of a uniform plane wave in phasor domain can be given as

$$\overline{E} = \overline{E_0} e^{+j\bar{k}\bullet\bar{r}} \tag{2.6.a}$$

$$\overline{H} = \overline{H_0} e^{+j\bar{k}\bullet\bar{r}} \tag{2.6.b}$$

where $\bar{k}$ is the propagation vector, $\bar{r}$ is the position vector and the wave is assumed to propagate in a simple (linear, homogeneous and isotropic), lossless and source-free media with constitutive relations

$$\overline{B} = \mu\overline{H} \tag{2.7.a}$$

$$\overline{D} = \varepsilon\overline{E} \tag{2.7.a}$$

The reduced Maxwell's equations for monochromatic, isotropic plane wave can be derived in phasor domain as;

$$\bar{k} \times \overline{E} = -w\mu\overline{H} \tag{2.8}$$

$$\bar{k} \times \overline{H} = w\varepsilon\overline{E} \tag{2.9}$$

Moreover, the simplest dispersion relation for the isotropic, homogeneous and lossless materials can be derived as:

$$k^2 - w^2 \mu\varepsilon = 0 \tag{2.10.a}$$

$$k^2 = w^2 n^2 \tag{2.10.b}$$

where n, the refractive index of the medium, is given by

$$n = \sqrt{\mu\,\varepsilon} \tag{2.11.a}$$

or, for a composite medium with effective medium parameters μ_{eff} and ε_{eff}, given by

$$n = \sqrt{\mu_{eff}\,\varepsilon_{eff}} \tag{2.11.b}$$

The dispersion relation (Eqn. 2.10.a) is the equation defines the propagation of wave. As we can see, ε and μ are the only material properties in Eq. 2.10.a. Therefore, we can state that the dielectric permittivity (ε) and magnetic permeability (μ) of a material are the characteristic parameters of the material for a lossless media. On the other hand, Eqn. 2.10.b states that as both ε and μ become negative, the refractive index (n) does not change its sign; however, the Maxwell's relations show the effect of simultaneous negative dielectric permittivity and magnetic permeability. The materials with simultaneous negative ε and μ exhibit unique properties that are different from ordinary positive ε and μ materials [1].

As can be seen in Eqns. (2.8) and (2.9), $\{\overline{E}, \overline{H}, \overline{k}\}$ form a right-handed orthogonal coordinate system for materials with positive ε and μ. In case both ε and μ are negative, an interesting result arises; $\{\overline{E}, \overline{H}, -\overline{k}\}$ forms a left-handed orthogonal coordinate system.

In addition, since the sign of Poynting Vector ($\overline{P}$) is independent of the sign of ε and μ (Eqn. 2.12), the direction of the energy flow does not change:

$$\overline{\mathrm{P}} = \overline{E} \times \overline{H} \tag{2.12}$$

Therefore, the direction of the power flow never changes. However, the wave propagation direction is opposite to the direction of power flow in left-handed metamaterials. In other words, this result causes the famous effect of an antiparellel phase and group velocity, the reversal of the Doppler Shift [51], and Cerenkov radiation [52].

For materials with negative ε and positive μ or vice versa. Electromagnetic waves become evanescent as a result of imaginary propagation constant (k). When, both ε and μ are negative, the wave can propagate as a result of $\varepsilon\mu > 0$ (real propagation constant, k). So far, we analyzed the situation when ε and μ are both positive and negative. If the signs of ε and μ are opposite ($\varepsilon\mu < 0$), then the electromagnetic waves are reflected totally and evanescent waves occur. Also the reflection is reversed and the exciting new phenomena occurs with these kind of materials.

Transmission properties of a lossless (or very low loss) material are determined by its dielectric permittivity and magnetic permeability.

Therefore, we firstly investigate the phenomenon of negative permittivity. Then, the negative permeability phenomenon and negative index metamaterials which possess both negative permittivity and negative permeability will be investigated.

2.2.1. Negative Permittivity

Negative dielectric permittivity is dominant for metals at optical frequencies as a result of the plasma frequency of metals. Under a specific frequency called plasma frequency, the real part of permittivity parameter of a plasma medium is negative. However, it is hard to have negative dielectric permittivity at lower frequencies, such as near infrared and the microwave regime; because, the dissipation dominates in metallic media as a result of significant increase in the dissipation of the plasmon's energy in the system [40-41]. Therefore, the dielectric permittivity becomes purely imaginary. In 1996, Pendry *et al.* proposed the arrangement of periodic metal wires for the depression of the plasma frequency into the near infrared and GHz band [39]. The physical mechanism behind Pendry *et al.*'s suggestion is the confinement of electrons into thin wires for enhancing the effective electron mass through self-inductance. Therefore, the proposed structure has negative permittivity at microwave frequencies by using suitable parameters. The plasma frequency of the periodic thin wire array is given by making detailed analytical derivations as follows [39]:

$$w_p^2 = \frac{n_{eff} \cdot e^2}{\varepsilon_0 \cdot m_{eff}} = \frac{2\pi \cdot c_0^2}{a^2 \cdot \ln \frac{a}{r}} \tag{2.13}$$

where, c_0 is the speed of light, a is the lattice parameter and r is the radius of each wire (see Figure 2.3).

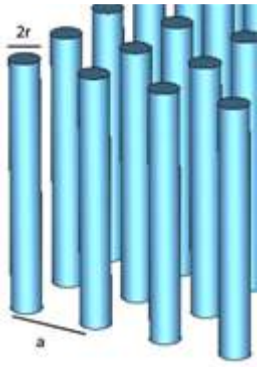

Figure 2.3: The schematic representation of a periodic metallic wire array. a is the lattice constant and r is radius of a single wire.

Eqn. 2.13 states the fact that the plasma frequency can be expressed in terms of the macroscopic parameters of the array structure (a, r) instead of the microscopic quantities (effective electron mass-m_{eff}, effective electron density-n_{eff}). Moreover, the parameters of the metallic wire array lattice (a, r) are much smaller than the wavelength. When all the lattice parameters (a, r) of the thin metallic wires are much smaller than the wavelength ($a \ll \lambda$, $r \ll \lambda$), the response of the wire array can be interpreted by the effective medium theory. Therefore, an effective dielectric permittivity (ε_{eff}) can be used to define the dielectric permittivity parameter of the material/medium. In other words, the periodic array of metallic wires appears to be an effective homogeneous material having an effective dielectric permittivity with negative real part.

We calculated the plasma frequency of various fictitious thin wire arrays and made simulations in before [38] in order to confirm the theoretical expectations.

The model of Pendry *et al.* was further improved in various other studies [3]. Different approaches such as the one which models a periodic metallic wire array by using circuit models have been proposed [55]. We used the abovementioned model for microwave devices. On the other hand, we used the plasma frequency parameter of metals for optical simulations.

2.2.2. Negative Permeability

Designing a material with negative permeability is much more difficult than designing one with negative dielectric permittivity. The lack of a magnetic charge in nature is the main reason behind the difficulty of obtaining negative permeability materials. Since the magnetic response of natural materials is not strong at microwave frequencies, the magnetic moment of atom or molecules cannot be utilized effectively. Therefore, we need to have a strong magnetic dipole moment effect obtained artificially. In 1999, Pendry *et al.* suggested several types of periodically arranged resonator structures that give strong enough magnetic response to an incident electromagnetic field [2].

The periodic thin wire array that was mentioned in the previous chapter responds to an incident electromagnetic field such that the effective dielectric permittivity of the structure becomes negative below the plasma frequency, but its permeability remains positive. Since, a magnetic dipole moment can be created by a current carrying conductor loop; a metallic ring structure provides a suitable structure to obtain a strong magnetic response. However, the rings should also have capacitive elements such as splits in order to be resonant at wavelengths much

larger than the diameter of the rings. Also, the structures are periodic arrangements of arrays in order to couple each other and increase the magnetic resonance. The strong magnetic resonance gives rise to negative permeability over a narrow resonance band.

The widely used structure for having negative permeability at microwaves is a Split Ring Resonator (SRR) structure [2] which is composed of two conducting rings with splits where the split locations are 180 degrees apart from each other. The splits are used to make the SRR resonant at wavelength much larger than the diameter of the SRR. The gap between the rings, splits, and inner split ring are all used to increase the capacitance that enables a decrease in the resonance frequency of the structure. If the largest dimension of the SRR is much smaller than the wavelength of the resonance frequency, the response of a periodic arrangement of the SRR array can be analyzed by the effective medium theory such as we have mentioned in the case of the thin wire array. Therefore, an effective magnetic permeability (μ_{eff}) can be used to define the permeability parameter of the resulting material/medium.

The critical frequencies and effective permeability (μ_{eff}) for the SRR structure are analytically derived as [2]:

$$w_{mp} = \sqrt{\frac{3 \cdot d \cdot c^2}{\left(1 - \frac{\pi \cdot r^2}{a^2}\right)\pi^2 \cdot r^3}} \tag{2.17}$$

$$w_0 = \sqrt{\frac{3 \cdot d \cdot c^2}{\pi^2 \cdot r^3}} \tag{2.18}$$

$$\mu_{eff} = 1 - \frac{\frac{\pi \cdot r^2}{a^2}}{1 + \frac{2\sigma \cdot j}{wr\mu_0} - \frac{3dc^2}{\pi^2 r^3 w^2}} \tag{2.19}$$

where, c is the speed of light in vacuum, a is the lattice constant for a unit cell, μ_0 is the magnetic permeability constant of vacuum, r is the radius of the inner ring and σ is the conductivity of the cylinder surface per unit area.

The capacitance introduced into the system by the splits and the gap between the rings collaborates with the inductance introduced into the system by the metallic rings in order to resonate. Figure 2.6 shows the typical μ_{eff} form of a SRR as a function of angular frequency w under the assumption that the metallic rings are made of a perfect electric conductor (PEC) [2]:

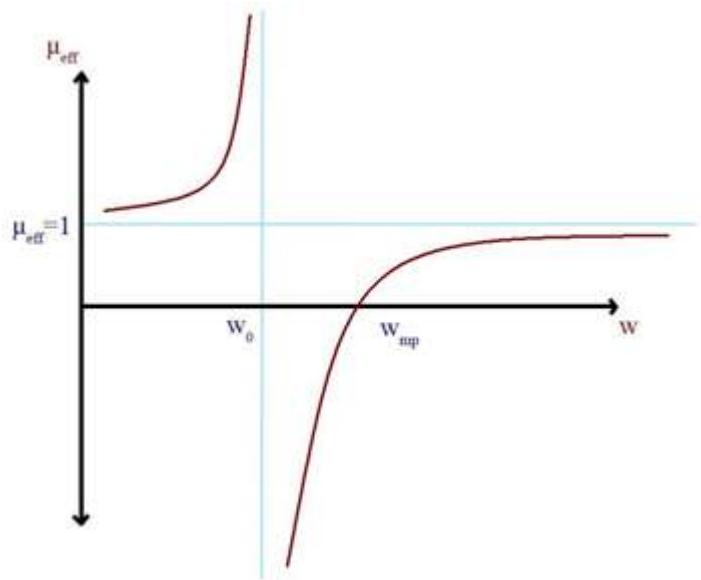

Figure 2.4: μ_{eff} -w diagram for ideal single SRR structure [15].

SRR's negative permeability is not very effective and useful for light. However, SRR's strong magnetic resonance is the most prominent structure to design plasmonic devices.

SRR is the most common structure that is used for the design of novel materials, such as metamaterials [56-64]. Resonator characteristics of SRRs will be used in our thesis to propose novel methods for providing enhanced (extraordinary) transmission through sub-wavelength apertures. Therefore, we need a detailed analysis of SRR, which is provided in the following sections.

Negative Index Metamaterials

The refraction phenomenon, occurring when an incident wave is transmitted from one medium to another, is governed by the well known subject to Snell's Law of refraction which is stated as:

Snell's Law:

$$n_1 \sin\Theta_1 = n_2 \sin\Theta_2 \tag{2.20}$$

If both media (n_1, n_2) are filled by right-handed materials, the wave propagation vectors of the incident and transmitted wave fall into the different half spaces with respect to the surface normal [65]. However, when the incident wave is transmitted to a left-handed medium from a right-handed medium, refraction occurs in an unusual manner. Namely, when the incident waves are transmitted from a right-handed medium to a left-handed medium (negative dielectric permittivity and negative magnetic permeability), the refraction problem dictates that the wave

vector of the incident wave and the transmitted wave are both on the same side with respect to surface normal [1].

Smith *et al.* have shown through an analysis of the points of a constant phase of a modulated plane wave, in which the group and phase velocities undergo negative refraction at the interface between a positive and negative index material [66].

In our previous work [38], we simulated the negative refraction through a fictitious left-handed slab material in which the Drude Dispersion model for effective dielectric permittivity and the Lorentz Dispersion Model for the effective magnetic permeability are used.

The resonance behavior of a material is described by the so-called Lorentz Model, containing the resonance frequency w_0 and the damping factor δ:

$$\mu_{eff}(w) = \mu_{\infty} \times (1 - \frac{\frac{\mu_s}{\mu_{\infty}} \times w_m'^{\,2} - w_m'^{\,2}}{w^2 - j\delta w - w_m'^{\,2}}) \tag{2.21}$$

where, w_m' is the magnetic plasma frequency in which μ_{eff}=0.

Considering the specific plasma frequency w_p, the correspondent relative permittivity is given by the *Drude Model*:

$$\varepsilon_{eff} = \varepsilon_{\infty} - \frac{w_p^{\,2}}{w \times (w - iv_c)} \tag{2.22}$$

where, v_c is the collision frequency.

The ε_{eff} (Drude Model) [38, 177] and μ_{eff} (Lorentz Model) [39, 177] of the medium and the simulation results can be obtained by utilizing CST Microwave Studio by utilizing retrieval algorithms.

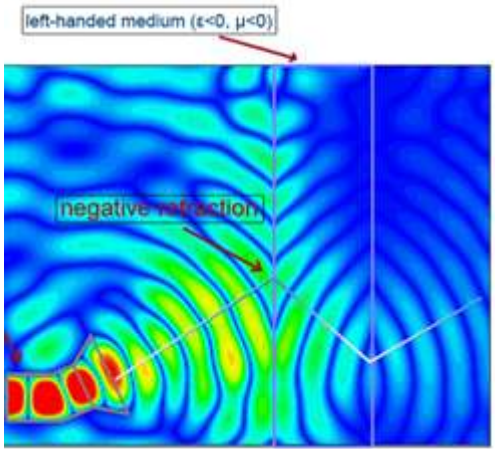

Figure 2.5: Negative refraction of electromagnetic wave through a left-handed medium[38].

The phase fronts in the left-handed medium show that the wave propagates towards the source side (first incidence plane) which is closer to the source side, instead of propagating towards the second incidence plane. This shows us the opposite direction of group velocity and wave velocity. This new phenomenon, negative refractive index material, inspires new geometrical optics devices called flat lenses. A possible perfect focus without the usual constraints imposed by wavelength can be achieved by negative refractive index materials, which are capable of restoring not only the phase of propagating waves but also the amplitude of evanescent states [67]. These new focusing devices are called "perfect lenses". Consequently, this extraordinary refraction mechanism opened

up new research areas such as superlenses [18, 37], cloaking [22], and semiconductor metamaterials [23].

Metamaterials are firstly illustrated at microwave regime; because the wavelength at microwave is much more larger compared to light and therefore subwavelength structures at microwave are fabricated at first. As the fabrication techniques advanced, metamaterial fabrication progress to optical frequencies (Figure 2.6)

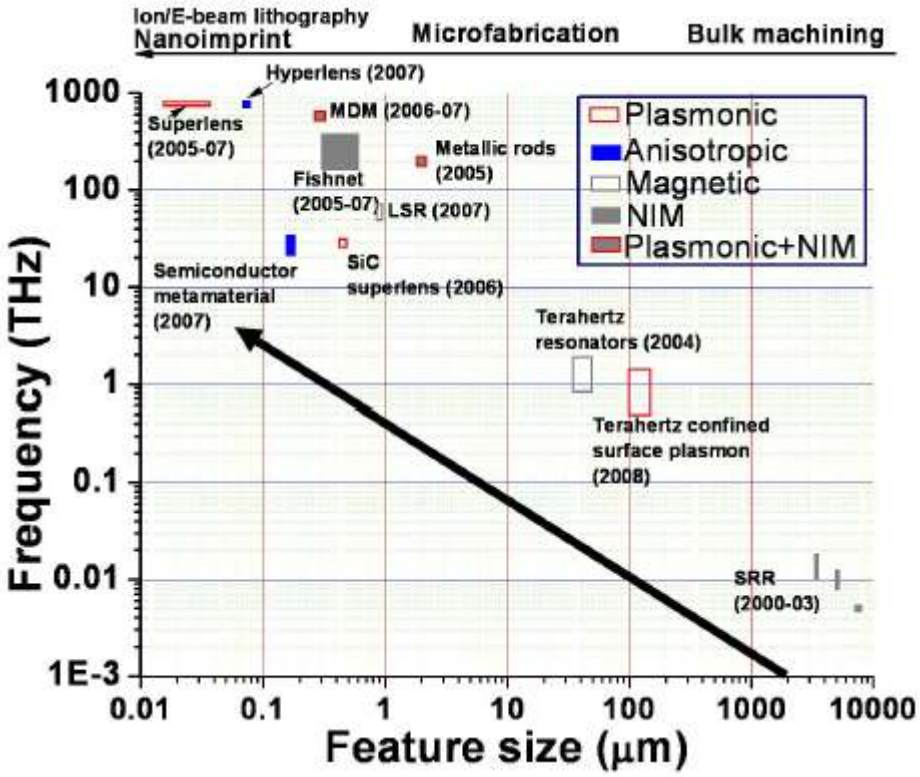

Figure 2.6: Progress made in scaling metamaterials from microwave to optical frequencies. Feature size denotes lattice or unit cell size as appropriate. Suitable fabrication tools corresponding to feature size are listed at the top [36].

Resonator structures which used for designing metamaterials are firstly designed at microwave frequencies and after that they are scaled down to mid-infrared frequencies [31] (e.g. L-shaped resonators operating at

60THz). Scaling down from mid infrared maker magnetic response deviates largely as a result of deviation of metal from lossless perfect conductor characteristics. However, further scaling requires a different approach because of deviation of metal from perfect conductor behavior at higher frequencies [71]. First near infrared magnetic resonance device was fabricated using a wire sandwich structure. Sandwich structure is fabricated by sandwiching a dielectric layer between two metal films. The magnetic resonance response stem from antiparallel current supported by the wire pair. These structures are the ancestors of "fishnet" structures [38, 72] which were designed by combining with long metal wires to have negative refraction for at telecommunication wavelength (1550nm). Development of metamaterials operating at telecommunication wavelengths opens up significant practical opportunities because it can pioneer to novel optical devices communication industry.

Metamaterials deduce their extraordinary properties mostly from the surface plasmon waves. Surface plasmons are collective oscillations of free electrons on the surface of metallic nanostructures. Surface plasmons are characterized by their subwavelength property and ability to couple light nanoscale devices more effectively which is a significant opportunity for novel plasmonic devices. By utilizing surface plasmons we amplify evanescent waves, which enables scientist to design subdiffraction resolution optical imaging, detection of chemical and biological agents with a single molecule sensitivity. Since the application possibilities are endless, more research on metamaterials will be conducted in the future and abovementioned applications are only the pioneers of novel metamaterial devices. The most prominent candidate for novel plasmonic

metamaterials is Split Ring Resonator structures that is used for designing artificial materials, metamaterials.

2.3. Split-Ring Resonator (SRR) Structures

2.3.1 Introduction

As we discussed above, electromagnetic response of materials is determined by constitutive parameters: The magnetic response of materials is determined by the magnetic permeability (μ), while the electric response of the materials is determined by the dielectric permittivity (ε). The combined effect of permittivity and permeability determine the response of material to incident electromagnetic field. Electric charges designate the electric response of materials. Since there is no magnetic charge in nature, it is rather difficult to have negative permeability structures, while negative permittivity is obtained below the plasma frequency of periodic sub-wavelength metallic wires at microwave frequencies. Therefore, the magnetic property of available structures should be modified to obtain artificial magnetic-like charges and create magnetic dipole moment. The search for magnetic-like charges show results at late 1990s. Sir John Pendry came up with an idea of utilizing periodic array of swiss-roll and split-ring resonator (SRR) structures for obtaining magnetic response to an incident electromagnetic field [2]. Since SRRs can be manufactured easily than swiss-role structures and exhibit stronger magnetic response, the most dominant and commonly used structure is the Split Ring Resonator (SRR) structure. SRRs have been studied extensively in literature so far. There are experimental [74-76] and numerical simulation studies [85-88] on the

transmission characteristics of SRRs. Analytical models are suggested to better model the resonance characteristics of SRRs [90-92]. The majority of the studies on SRR are performed in the microwave regime; but, there is an increasing amount of interest on the studies of magnetic resonance of SRRs at near infrared spectrum [93].

The fascinating property of SRR is the strong magnetic resonance which is due to the additional capacitive elements such as splits and gap between the rings. A typical Split Ring Resonator (SRR) structure is given in Figure 2.7.

.

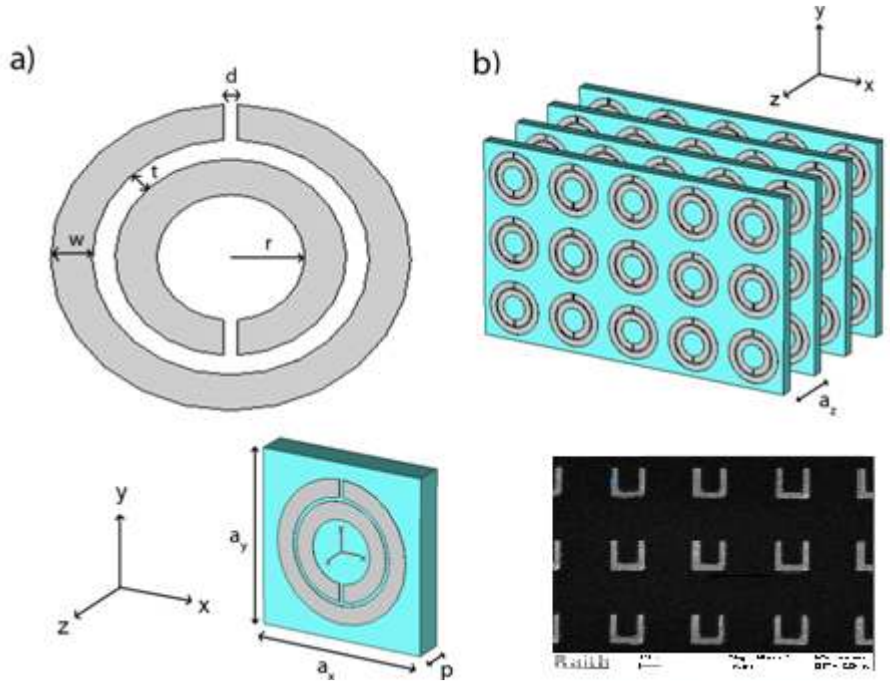

Figure 2.7: Schematics of a) single SRR b) periodic arrangement of SRR array (microwave and optical replica).

The capacitive elements (splits and gap) are utilized to achieve magnetic resonance at wavelengths much larger than the diameter of the rings.

There can be one or two rings depending on the application. The second ring is actually used for increasing the capacitance of the structure. For instance, second ring is hard to fabricate for optical applications. But it is very practical for microwave. Two rings with splits oriented oppositely. Also, there are several split ring resonator structures such as single-split ring structures and split rings with several splits [38].

Since, the periodic arrangement of the SRR (Figure 2.7.b) increases the magnetic response of SRR by strong coupling between the resonators, the unique properties such as negative permeability emerges. Also, since all parameters of SRR (a, r, d, t, w, p) are much smaller than wavelength, the response of SRR array is fit to effective medium theory. Therefore, an effective magnetic permeability (μ_{eff}) and effective dielectric permittivity (ε_{eff}) can be used to define the two fundamental material parameters of the structure/medium.

2.3.2. Electromagnetic Resonance Mechanism of SRR

Since, split ring resonator structures are strong magnetic resonators and they respond incident electromagnetic wave by both electrical and magnetic resonance in particular bandwidths, magnetic resonance characteristics of SRRs are available for very narrow bandwidth. Also, the SRRs respond to the magnetic component of the incident wave if the incident electromagnetic wave is excited with the appropriate polarization [73, 81]. Moreover, periodically arranged SRR array is shown to exhibit negative permeability ($\mu_{eff} < 0$) for frequencies close to magnetic resonance frequency (w_m) of the SRR structure [2]. Since the periodic arrangement of the SRR slightly changes the magnetic response

of SRR by coupling between the SRRs, the resonance behavior of a single SRR can also be observed by the frequency response of periodic arrangement of SRRs [73, 77]. Periodic arrangement of SRR arrays are utilized to investigate the magnetic response of SRRs; because the combined effect of periodic SRR array reveals the magnetic properties of SRR more clearly than a single SRR and negative permeability values can be obtained by strong magnetic response of SRR array.

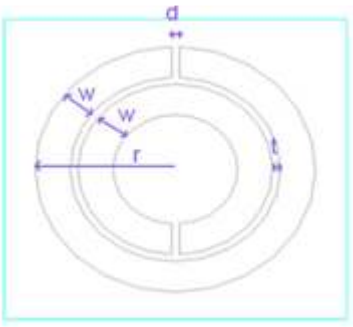

Figure 2.8: Schematic Representation of an SRR a) SRR structures modeled at Lumerical. w: width of metal, d: gap distance, t: gap between two concentric rings, h: thickness of metal.

We used two different simulation software: 1) CST Microwave Studio for microwave which is a three dimensional full-wave solver employing the finite integration technique [177], 2) Lumerical FDTD Solutions for infrared which uses finite difference time domain method [178].

We used a previous works' [38] design parameters for estimating the parameters of SRR that will work in infrared frequency regime. For our previous work, the largest length of the SRR is 7.2 mm. Since as we scale down the size of a structure, the frequency/wavelength response for this structure scales up proportionally. This method would work for certain wavelength. Further scaling requires a different approach because of deviation of metal from perfect conductor behavior at higher frequencies

than mid-infrared. Here, we need only a rough guess. Afterwards, we will optimize our structure. In addition, since fabrication of circular nano-scale features is very hard, we used square type SRR for optical coupling which is circular-type SRRs for microwave regime and we used a single ring SRR version because alignment of concentric ring cannot be achieved very sensitive at optical regime.

As we know the resonance of 7.2 mm single ring SRR structure is at 4.1 GHz ($\lambda \cong 75$ mm) [38], we can roughly scale to desired wavelength. In order to obtain a response at $\lambda \cong 1.55$um, we have to start with a design of SRR length of $7.2mm * \left(\frac{1.55 * 10^{-6}}{75 * 10^{-3}} \right) = 148nm$. Also, the same scaling is done for both the split width and width of the metallic ring:

$$l = 7.2mm * \left(\frac{1.55 * 10^{-6}}{75 * 10^{-3}} \right) = 148nm$$

$$d = 0.2mm * \left(\frac{1.55 * 10^{-6}}{75 * 10^{-3}} \right) = 4.1nm$$

$$w = 0.9m * \left(\frac{1.55 * 10^{-6}}{75 * 10^{-3}} \right) = 18.6nm$$

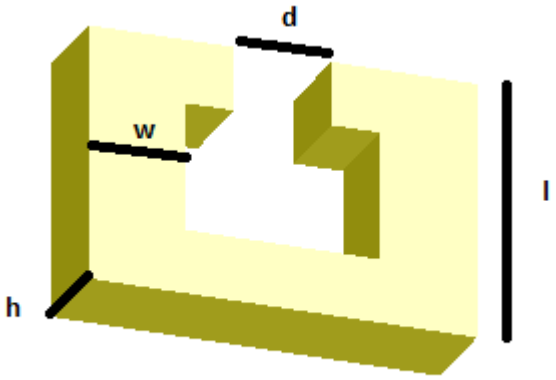

Figure 2.9: Single ring SRR structure modeled at Lumerical. w: width of metal, d: gap distance, h: thickness of metal.

As a rule of thumb, we take periodicity of SRR as two time the maximum length for all perpendicular directions to propagation. Since 4.1 nm and 18.6 nm is very small features for contemporary fabrication devices, we increased d, t, h and w to 50 nm which is safe for fabrication. Also we used an optically thick sapphire (Al_2O_3). Thus, we used the following parameters for simulation (Figure 2.9):

l=148nm (After Optimizaition: 200nm)

w=50nm

d=h=50nm

Thickness of the sapphire substrate: 5um

Since the scaling down is not ideal process, we did not get a resonance at 1.55um. Then we made optimization and find the correct parameters to get resonance at approximately telecommunication frequency (1.55um-see Figure 2.10).

Phase Match Layer's (open boundary conditions) are employed along the propagation direction . Periodic boundary conditions are used for the rest of the directions. Therefore the SRR structure with its sapphire substrate is assumed to be periodic and infinite along the directions perpendicular to the propagation direction. The dip of the transmission data gives the electromagnetic resonance frequency of the structure.

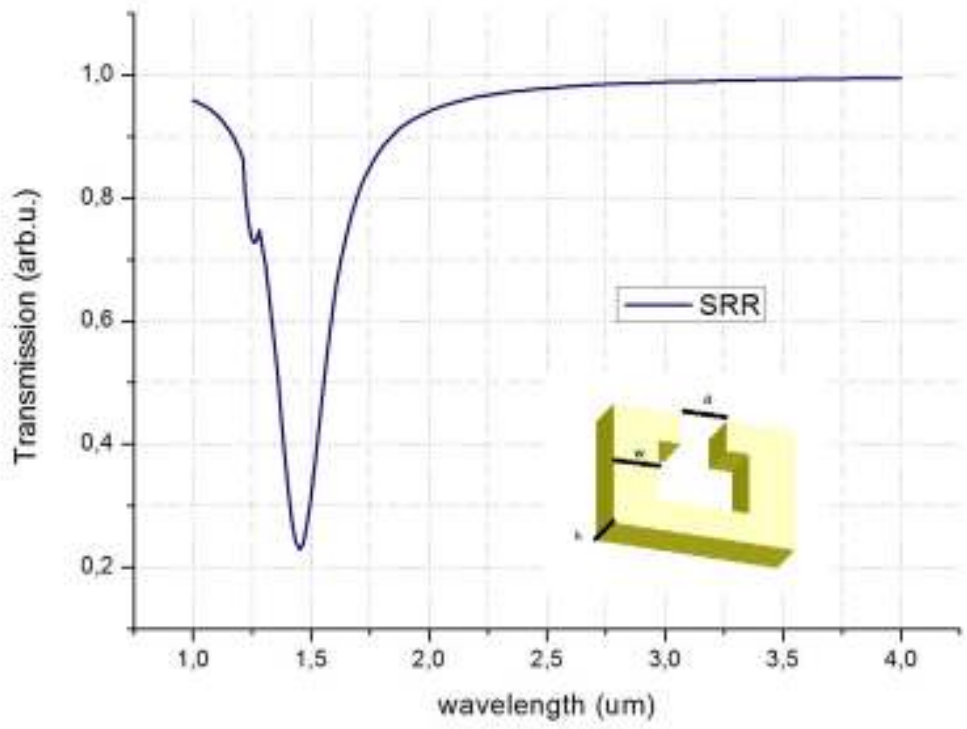

Figure 2.10: Simulation Results of SRR (l=200 nm, w=d=h 50 nm).

The resonances of SRRs not only the electromagnetic resonances but also, the periodicity of SRR may cause a band gap too. Therefore, a bandgap in the transmission spectrum of periodic SRR array medium may be due to the electromagnetic resonance or periodicity (Bragg gaps) [59]. Identification can be done by using a closed SRR (CSRR) structure in

which the splits of the SRR is closed. Since the splits of SRR play a key role in the electromagnetic resonance, closing the splits will annihilate this resonance but Bragg gaps will remain. We made numerical simulations by closing the splits of the structures in Figure 2.9. The simulation results for CSRR structure are demonstrated with results of SRR in Figure 2.11:

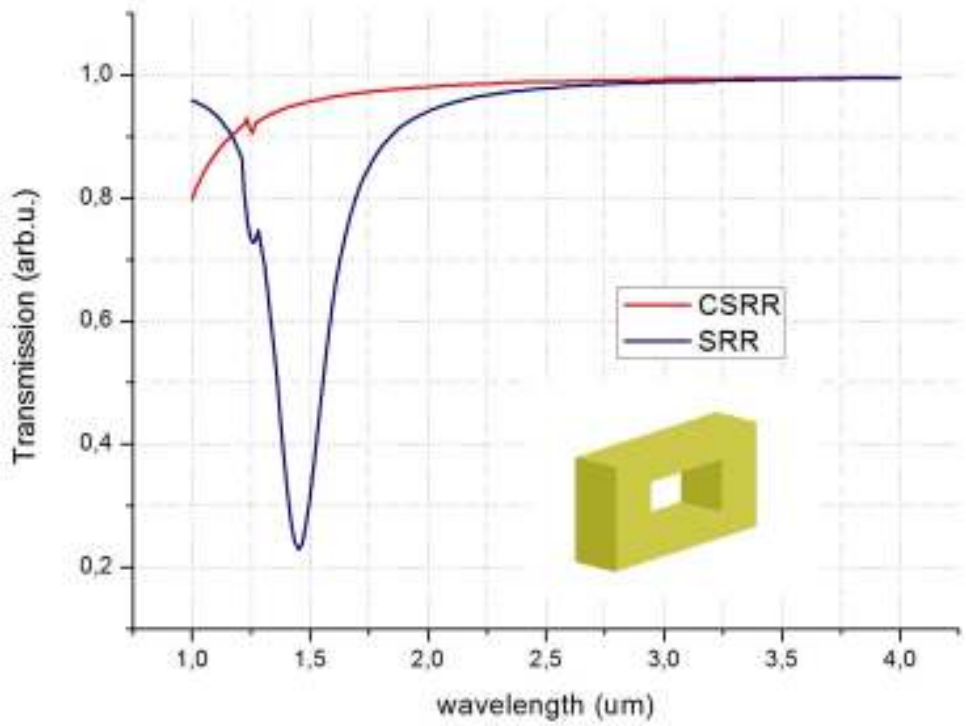

Figure 2.11: Simulation results of a SRR and CSRR structures. CSRR structure is depicted in the inset CSRR (l=200 nm, w=h= 50 nm).

We observed a dip at 1.47 um in the transmission spectrum of SRR (Figure 2.11). However, no dip is observed for CSRR structure. The splits are very crucial for magnetic resonance and removing the splits of SRR prevents current to flow between the arms of splits. Therefore, the

resonance is destroyed. So, the dip is due to resonance; because, closing the splits destroys the dips at that wavelength.

Note that, the maximum length of the SRR (l = 200n m) is less than 0.1λ for the resonance at $\lambda \cong 1.5$um. Therefore, electromagnetic resonance can be achieved by SRR structures with sub-wavelength dimensions which open up significant opportunities to design novel sub-wavelength devices. So, the major reason of the increasing amount of interest on SRR is not only the ability of achieving negative permeability but also achieving resonance with sub-wavelength dimensions. The structures that we proposed in this chapter for increasing the transmission of electromagnetic waves through sub-wavelength apertures are based on novel resonator structures and utilize the sub-wavelength resonance mechanism. We will discuss these novel structures in the following section.

2.4. Plasmonic Enhancement of Light/Wave

Plasmonics is a dominant research area for designing novel devices that utilizes the unique optical properties of metallic nanostructures to guide and deviate light/wave at subwavelength scales (nanometer scale for light). Concentrating light or create localized fields are traditionally the domain of dielectric devices. As the fundamental laws of diffraction suggests, these dielectric devices can not focus light to region less than half-wavelength, and dielectric resonators have electromagnetic volumes (v_m) limited to $v_m \approx \left(\frac{\lambda}{2}\right)^3$ [32]. Metallic nanostructures are not limited with these limitations. Therefore, plasmonics is the leading tool for enhancement of light/wave.

The simplest structure of scientific study is probably a simple hole in a screen. However, the study and debates on the characterization of a hole in a screen have been ongoing for centuries. In the middle of the 17th century, Grimaldi described diffraction form circular aperture, which contributed the foundation of classical optics [94, 95]. As classical optics suggests, the description of Grimaldi was valid only for a circular apertures having diameters much larger than the excitation wavelength.

Since interest in the microwave regime (longer wavelengths compared to the optical the wavelengths) increased in the 1940s as a result of World War II, the interest in the electromagnetic characterization of small (sub-wavelength) holes also increased. In 1944, Bethe gave a theoretical analysis of electromagnetic wave transmission through a sub-wavelength circular hole (aperture) in a perfectly conducting metal screen of zero thickness and suggested that the amplitude of the transmitted wave is proportional to the square of the area of sub-wavelength aperture with $k \cdot (r/\lambda)^4$ where the radius (r) of the aperture is much smaller than the wavelength (λ) of incident electromagnetic wave ($r<<\lambda$) [25]. In other words, the transmitted wave is proportional to the square of the aperture area and is inversely proportional to the fourth power of the excitation signal's wavelength.

According to Bethe's ideal theoretical structure, the transmission spectra for an aperture of radius $r<<\lambda$ has a rapidly decreasing transmission with the increased wavelength of incident field by the power of four. We have simulated and confirmed the Bethe's expectation by simulating the transmission spectra of a circular hole as shown in Figure 2.12 where k is an arbitrary constant to overlap the simulation results and $k \cdot (r/\lambda)^4$ curve

for comparison. Power of four is valid for microwave simulations in which PEC approximation is valid (Figure 2.12.a). However, the transmission spectra for an aperture of radius r<<λ has a rapidly decreasing transmission with the increased wavelength of incident field by the power of three for optical simulations as a result of non ideal metallic characteristics of metallic screen (Figure 2.12.b).

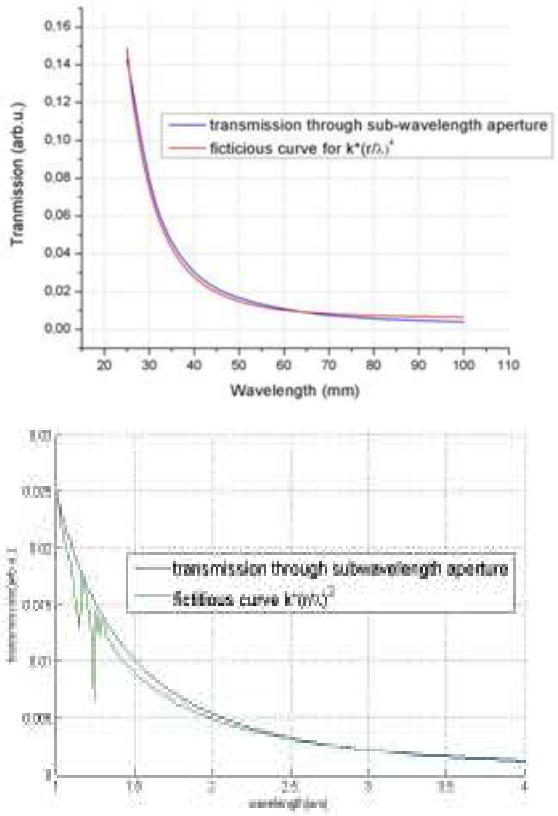

Figure 2.12: Theoretical suggestion of Bethe (λ^{-4} decrease) and the simulation results of transmission through a sub-wavelength aperture where r< $\lambda/10$.

Also, an aperture in real life has a lateral dimension, which makes an aperture a waveguide-like structure and deviates the transmission result from Bethe's ideal theory. This situation is more dominant at optical regime. Because later dimension of the hole will be much more comparable to wavelength. This waveguide structure modifies the

dispersion relation of the incident field and the monotonic increase of transmission becomes distorted between a frequency band: There exists a specific frequency (wavelength) at which an incident wave in a given mode cannot be maintained (cut-off frequency/wavelength) as shown in Figure 2.13 [95].

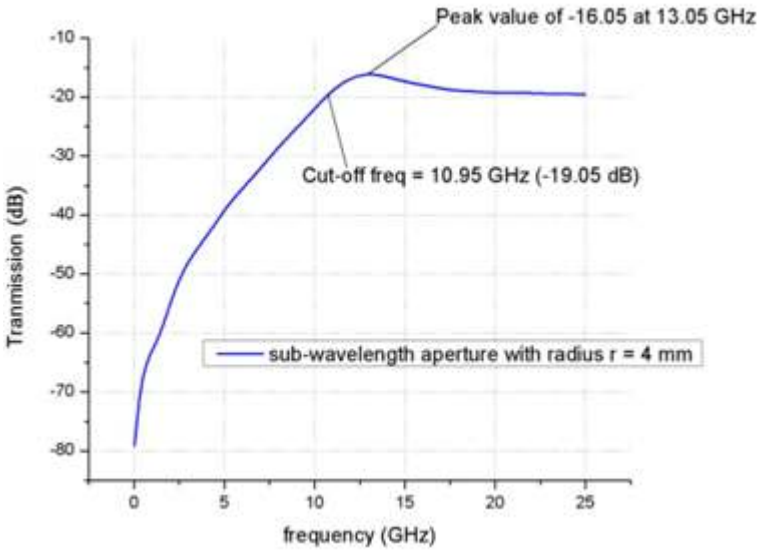

Figure 2.13: Transmission through a sub-wavelength aperture[23].

Annular apertures that resemble coaxial waveguides are supposed to have a TEM_0 mode without a cut-off [97, 121, 122]. However, there exists a cut-off frequency and also an extraordinary transmission peak: Several studies have shown that single sub-wavelength apertures have peaks (Figure 2.13) in their transmission spectrum as a result of the constructive excitation of propagating, surface and evanescent modes [95, 114]. In addition, the cut-off frequency cannot be sharply defined while considering metals at optical regime (with finite conductivity); because the transmission regime goes continuously from the propagative to evanescent regime as the wavelength increases [95].

When the finite conductivity of the metal is taken into account, the cut-off wavelength of the aperture is larger compared to an aperture in a perfectly conducting plane [102]. Also, transmission through a sub-wavelength aperture further decreases due to the non-zero depth of the aperture [103, 104]. All of these studies reveal that Bethe's theory holds for idealized situations, in which the enhancement of electromagnetic wave propagation beyond the limit of Bethe's suggestion could be obtained by utilizing novel methods to improve the coupling of incident wave and aperture [98-101].

Advances in the characterization and fabrication techniques enable researchers to reduce severe effects of extremely high transmission losses and diffraction of electromagnetic waves through sub-wavelength aperture transmission. In 1998, "extraordinary optical transmission (EOT) through a sub-wavelength hole array in a metal screen" phenomena was reported by the seminal work of Ebbesen *et al.* [24]. It has been shown that the coupling of light with the Surface Plasmons (SP) of a two dimensional array of sub-wavelength holes in turn causes a strong enhancement of transmitted light, which is above the limit of Bethe's prediction. This new era has attracted the interest of researchers on the enhancement of "light/electromagnetic wave" transmission through sub-wavelength apertures. Various studies on the characterization of EOT phenomenon approved the involvement of Surface Plasmons; and also showed that the interplay between light and the resonant excitation of SPs, which are induced by a periodic array of holes, causes the EOT [106-109].

The EOT phenomenon and new fabrication techniques opened up significant opportunities to new research areas and applications such as new probes for the scanning near-field optical microscope (SNOM) [110, 111], near-field optical recording [112, 113], nano-scale lithography [114-116] tracking single molecule (fluorescence spectroscopy) [111, 117], ultrafast miniature photodetector [118].

2.4.1 Device Coupling

In this section, plasmonic transmission enhancement through a single sub-wavelength aperture by device (SRR) coupling is discussed. The effective coupling is achieved by placing a Split Ring Resonator (SRR) structure in the near field of an aperture. Figure 2.14 shows the proposed SRR structure in front of the aperture.

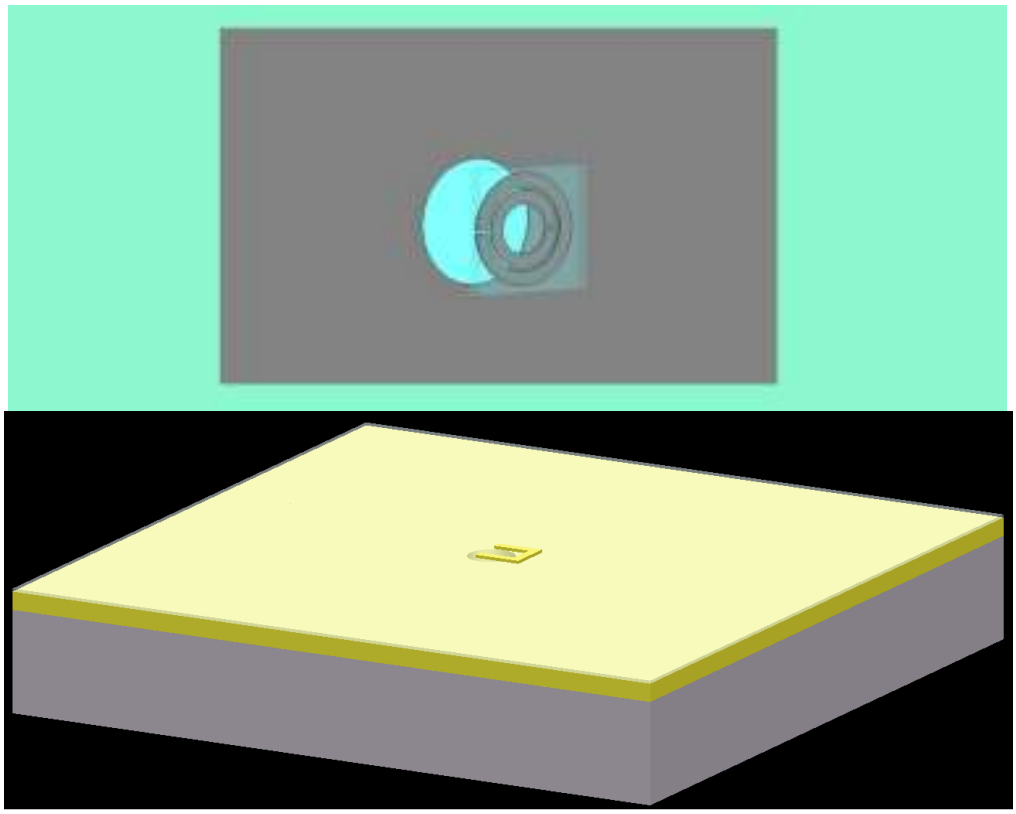

Figure 2.14: Schematic representations of SRR devices for a) Microwave Regime b) Optical Regime.

The SRR structure that we used is a type of electromagnetic resonator that gives rise to strong resonance and a high intensity of electromagnetic waves in between splits of the SRR [73]. A detailed analysis of SRRs is provided above. In this work, we use a well-known SRR structure that has been used in a variety of research studies [59, 73, 81].

We start with a device designed for microwave [162]. Because, working microwave is easier in terms of fabrication and metals resemble PECs which makes life easier for designing processes. After that, we start working on optical replica of enhancement by device coupling which is harder to design and fabricate as a result of deviating from PEC characteristics and approaching the atomic scale effects.

Firstly we start with our microwave regime design:

Surface Plasmons are propagating resonant modes confined to metallic surfaces that is caused by the coupling between the free surface charges of metal and the incident electromagnetic field at the interface separating a dielectric media and a metal. Since metals have very high conductivities at microwave frequencies (i.e. they behave similar to PECs in the microwave spectrum); surface plasmons are not supposed to exist at the microwave frequency regime. Therefore, there has been a debate on the existence of EOT phenomena at microwave frequencies [119, 120]. As a matter of fact, SPs are not considered to exist in the microwave region; but the "Spoof Surface Plasmons", that are very similar to SPs, are formed between a dielectric substrate and a metal layer at microwave frequencies [119]. SPs and Spoof SPs serve similarly to guide the electromagnetic wave to the aperture in order to obtain an enhanced transmission. In our

work, we obtained enhanced transmission at microwave frequencies in which the metals behave like perfect conductors. Therefore, localized surface plasmons do not contribute to the enhancement process. In addition, since grating structures are not used in our approach, there is no significant contribution of surface waves to the enhanced transmission. As we will show in the following sections, the strong localized fields around SRR-based novel structures couple to the incident electromagnetic field through a resonant process, causing a strong extraordinary transmission.

Split-ring resonator structures that we used for microwave are composed of two concentric copper rings with splits oriented at opposite sides. Figure 2.15 shows a schematic representation of the SRR that we used. The gap between the inner and outer rings (t); and the width of the splits (d) are 0.2 mm, the metal width (w) is 0.9 mm, and the outer radius of the SRR structure is 3.6 mm. SRR is deposited on a commercial FR4 dielectric board with a thickness of 1.6 mm [79].

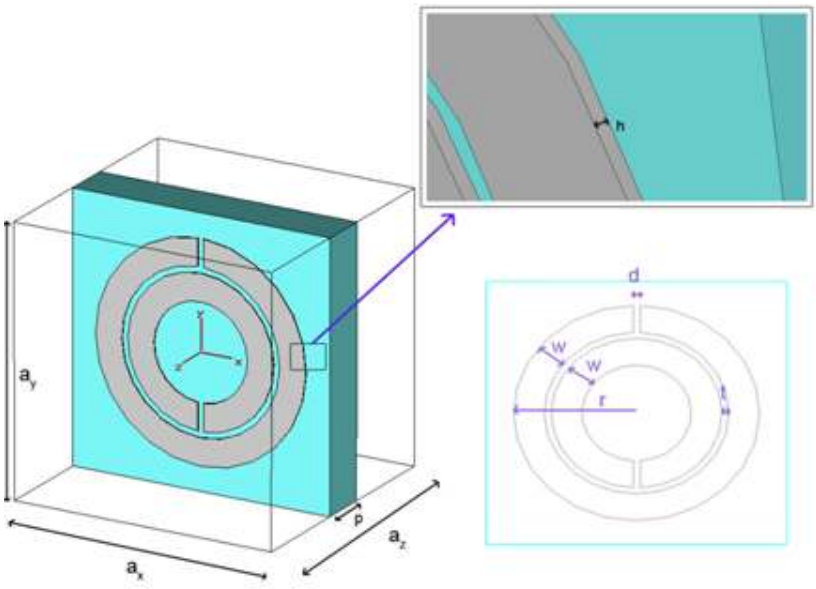

Figure 2.15: Schematic drawing of Split Ring Resonator structure used for microwave.

We also employed a square plate with a size of L x L (L = 200 mm), which is composed of a copper metal with a thickness of 30 μm and 1.6 mm thick commercial FR-4 PCB substrate. The deposited metal on the FR-4 substrate has an aperture that has a radius of 4 mm at the center of the substrate. The radius of the aperture is 4 mm, which is comparable with the largest size of the SRR (outer diameter = 3.6 mm).

Electromagnetic behavior of SRRs is bianisotropic [38]. Since there are four different combinations of SRR alignment, response of an SRR to electromagnetic waves for four different configurations of SRR is dissimilar. Therefore, we tried all combinations to find the best alignment for enhanced transmission.

As we know from previous studies [38, 81, 88], there are two types of resonance mechanisms (electrical and magnetic resonance) for SRRs and the magnetic resonance can only be excited for the parallel-oriented-SRR

structures where the magnetic component of the incident field ($\overline{H}$) is perpendicular to the SRR plane. Thus, there is magnetic resonance two parallel alignment options. On the other hand, there exists electrical due to the asymmetry of these SRR structures with respect to the incident electromagnetic field's electric component ($\overline{E}$) [88]. Since different resonance mechanisms play a role for different orientations of an SRR, the response of the SRR strongly depends on its orientation. Therefore, we checked all possible combinations to find best enhancement.

In this work, we proposed; and both experimentally and numerically verified an approach that utilizes the resonance of split ring resonator structures, which are placed in the close vicinity of a sub-wavelength aperture. The work presented in this section was appeared as a journal article in Physical Review Letters [162].

Firstly, we performed numerical simulations to observe the theoretical results of our novel approach. The numerical simulations, which are performed by the commercially available software (CST Microwave Studio), confirmed enhanced transmission through a sub-wavelength aperture via placing an SRR in the front of the aperture. Open boundary conditions are applied along all directions, in which perfect electric conductor approximation for the metal structures is introduced as minor approximations for simulations. Since the metals are very good conductors at the microwave spectrum and the open boundary conditions can be obtained by using enough absorbers around the measurement setup; the approximations that are used in the simulations are reasonable and acceptable. The dielectric constant of the FR-4 dielectric substrate is taken as $\varepsilon = 3.6$ with a tangent loss of $\delta = 0.01$. We checked different

alignment combinations of SRR structure in front of the 4 mm radius circular aperture. The transmission enhancement of the SRR structure is found maximum when the outer split of the SRR is placed at the centerline of aperture (see Figure 2.16).

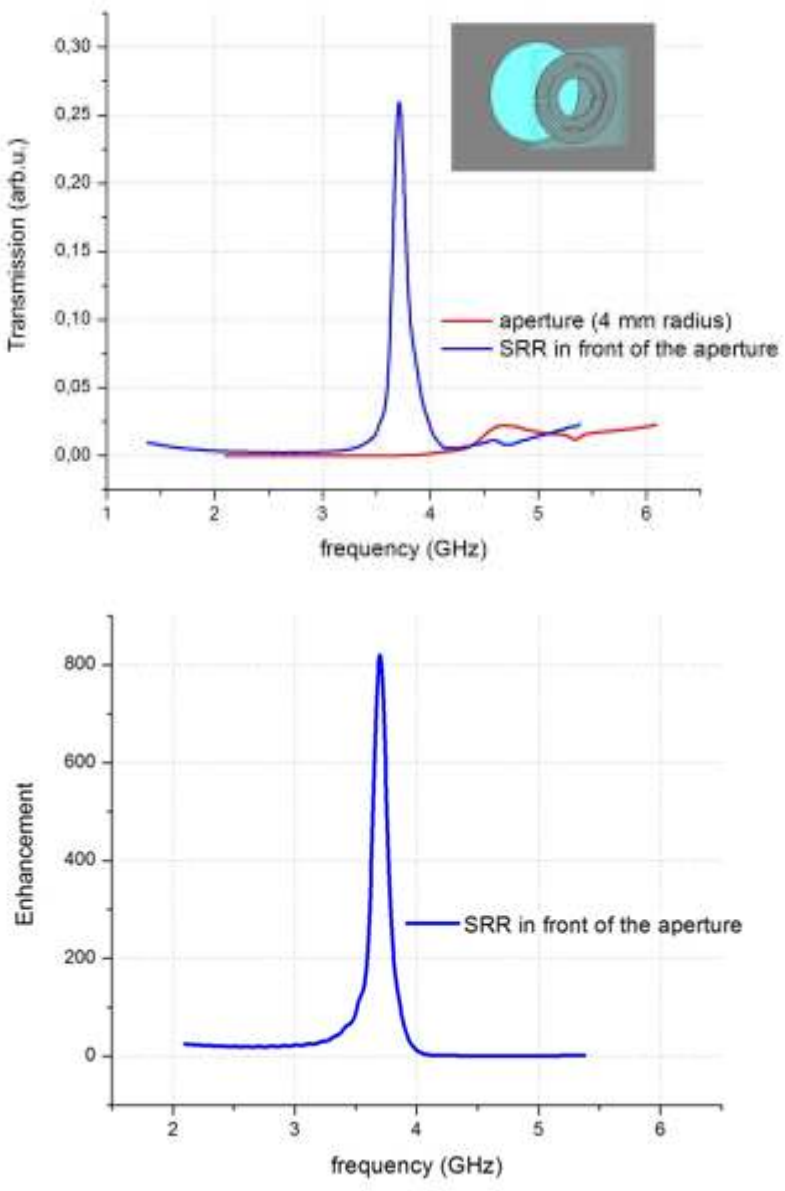

Figure 2.16: a) Transmission spectrum of optimized version of proposed structure (inset is a) the schematic of optimum alignment) b) enhancement spectrum.

The transmission is significantly increased by utilizing a single SRR in the optimum orientation and location. 820-fold transmission enhancement, which is defined as the ratio of transmitted electromagnetic wave intensity through SRR and aperture to transmitted electromagnetic wave intensity through only aperture, is realized at 3.71 GHz. Note that the resonance wavelength at 3.71 GHz is ($\lambda = \frac{c}{f}$) approximately 80 mm and the aperture radius (r = 4 mm) is approximately 0.05λ, which is considered as sub-wavelength. This is the smallest aperture size to wavelength ratio in the contemporary literature according to our knowledge.

The enhancement results revealed that enhancement over 800-fold is achieved when the SRR is placed 0.1 mm away from the aperture and the outer split of the SRR is placed at the centerline of the aperture. The propagation direction of the incident wave is perpendicular to the SRR plane. Therefore, the magnetic component of the incident field ($\overline{H}$) is parallel to the SRR plane. The enhancement stems from electric resonance of SRR.

The numerical simulation results showed the enhanced transmission through sub-wavelength aperture by utilizing SRR coupling. Therefore, we fabricated the abovementioned device to confirm our simulation results by experiments. The structures are fabricated with a process resolution of 100 um, which is the smallest length of our proposed structures. We used an experimental setup that is composed of an Agilent N5230A portable network analyzer, two waveguide ports and proper SMA cables. The waveguide ports are used as transmitter and receiver

and they are connected to the network analyzer with SMA cables. Figure 2.17 shows the setup used for transmission experiments.

Figure 2.17: Experimental setup used in measurements.

Metallic plate with a 4 mm radius circular aperture is placed 0.1 mm away from the transmitter antenna and the receiver antenna is located 5 cm away from the transmitter antenna, as we modeled in numerical simulations. Waveguide ports are employed as transmitter and receiver antennas. The propagation of wave is perpendicular to aperture plane, E-field vector extends from one of the tips of gap to the other tip.

As we expected, very high transmission enhancement is achieved, when SRR is placed 0.1 mm away from the aperture and the outer split of the SRR is placed at the centerline of the aperture.

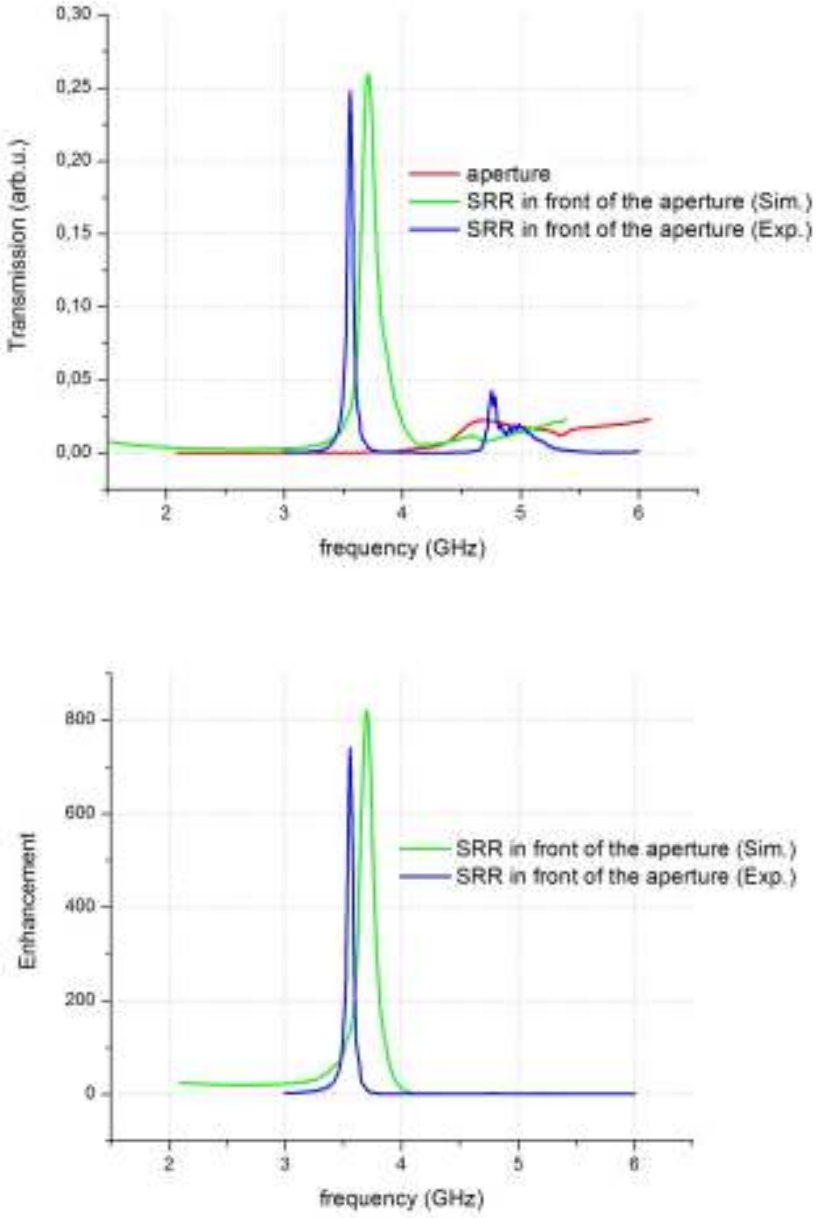

Figure 2.18: a) Transmission spectrum, b) Enhancement spectrum.

The experimental and numerical transmission results are in good agreement and transmission through sub-wavelength aperture is significantly increased as shown in Figure 2.18. 820-fold enhancement with numerical simulation and 740-fold enhancement with experimental results is observed by utilizing a single SRR only, in the near field of a sub-wavelength aperture. The strong localization of electromagnetic field,

caused by electrical resonance of SRR, enabled a significant enhancement of transmission (740-fold) through sub-wavelength aperture, which is the highest value reported in literature to our knowledge.

The experimental results are in good agreement with the numerical simulations. Minor differences between the simulations and experimental results can be attributed to the misalignment of the SRR in the experiments and the deviation of the electrical parameters of the materials from their ideal values used in the simulations.

As demonstrated so far, enhanced transmission by SRR coupling is polarization dependent which utilizes the resonance of a circular bianisotropic split ring resonator that is placed in the close vicinity of a sub-wavelength aperture. Other possible SRR geometries such as single ring with single cut resonators [81], rectangular SRR structures [83, 84] and elliptical SRRs [78] are also possible options to obtain enhanced transmission for specific polarizations of the incident wave. So far, we demonstrated a novel enhanced transmission device at microwave regime. We will further discuss the possible optical replica of SRR coupling and plasmonic enhancement applications.

Dipole resonances can be produced by shrinking the size of macroscopic metallic devices such that their resonance enter the optical regime. An optical SRR device can be designed by miniaturizing macroscopic version. SRRs are strong resonators in which incident electromagnetic wave creates a circulating and oscillating electric current that generates a magnetic dipole moment normal to the SRR plane. In a simple manner, SRR can be regarded as a half-wave antenna rolled into an almost closed

circle. Therefore, we will utilize the antenna property of SRR to focus surface plasmons on the aperture. As a result of focusing surface plasmons, we tried to obtain a transmission enhancement at optical regime.

Numerical simulations to observe the theory of our novel approach is performed by using a numerical simulation software, Lumerical. We confirmed enhanced transmission through a sub-wavelength aperture via placing an SRR in the front of the aperture.

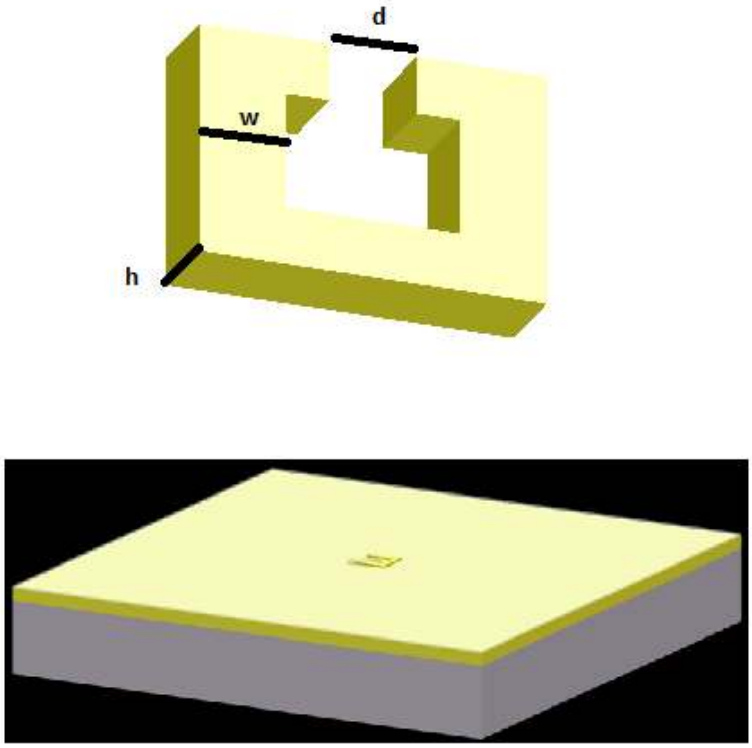

Figure 2.19: Schematic Representation of SRR coupling aperture.

Split-ring resonator structures that we used for infrared is a single ring structure Figure 2.19 shows a schematic representation of the SRR that we used. Since we aim to obtain an enhancement at telecommunication wavelength (1.55um), we used the design parameters that we found at

Section 2.3 which shows resonance at 1.55um. We used an optically thick sapphire (Al_2O_3). Thus, we used the following parameters for simulation (Figure 2.19):

l=200nm

w=d=t=h=50nm

Thickness of the sapphire substrate: 5um

Phase Match Layer's (open boundary conditions) are employed along the propagation direction . Periodic boundary conditions are used for the rest of the directions. Therefore the SRR structure with its sapphire substrate is assumed to be periodic and infinite along the directions perpendicular to the propagation direction. The dip of the transmission data gives the electromagnetic resonance frequency of the structure.

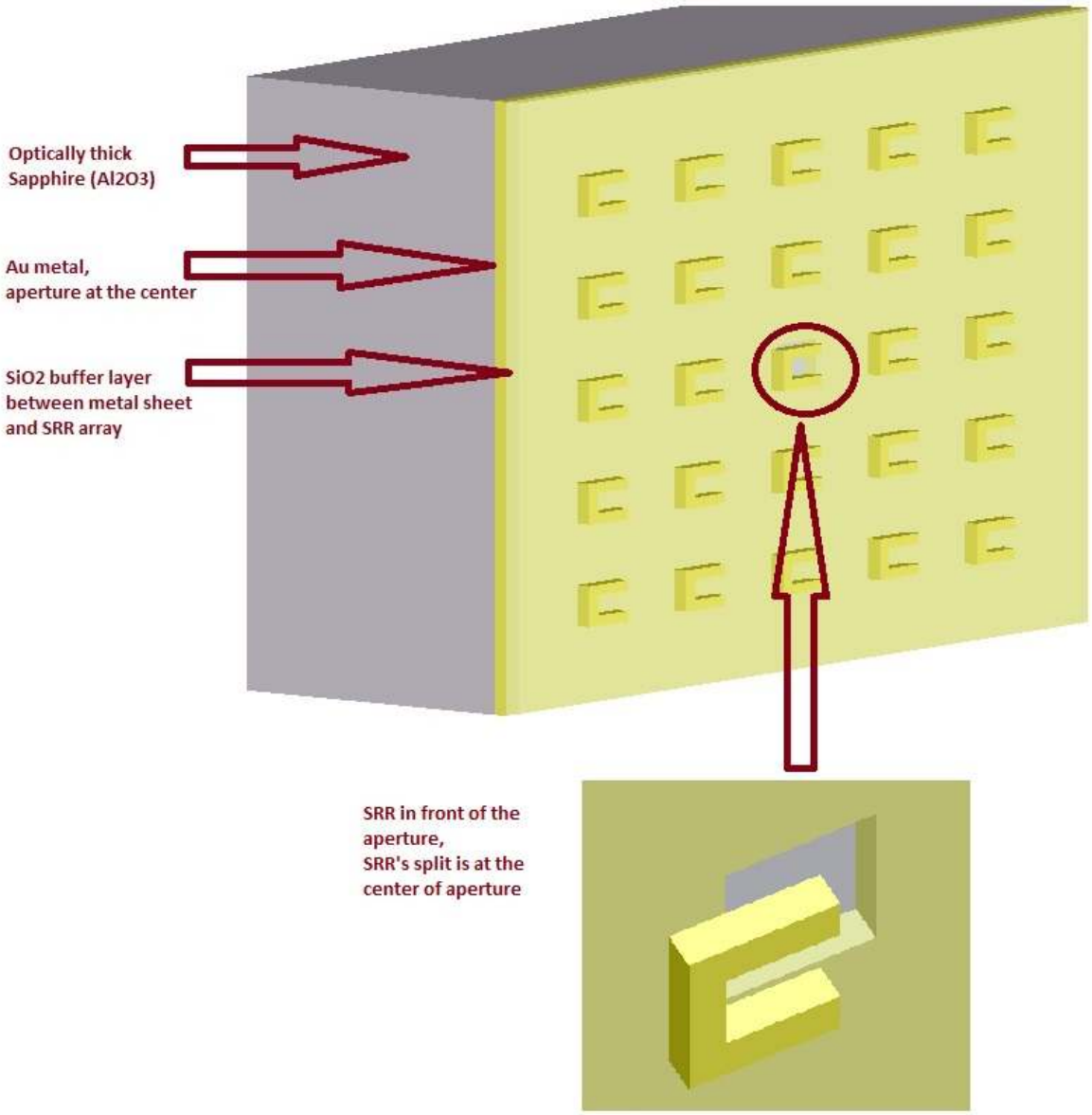

Figure 2.20: Suggested SRR coupling structure.

We checked different alignment combinations of SRR structure. The transmission enhancement of the SRR structure is found maximum when the split of the SRR is placed at the centerline of aperture.

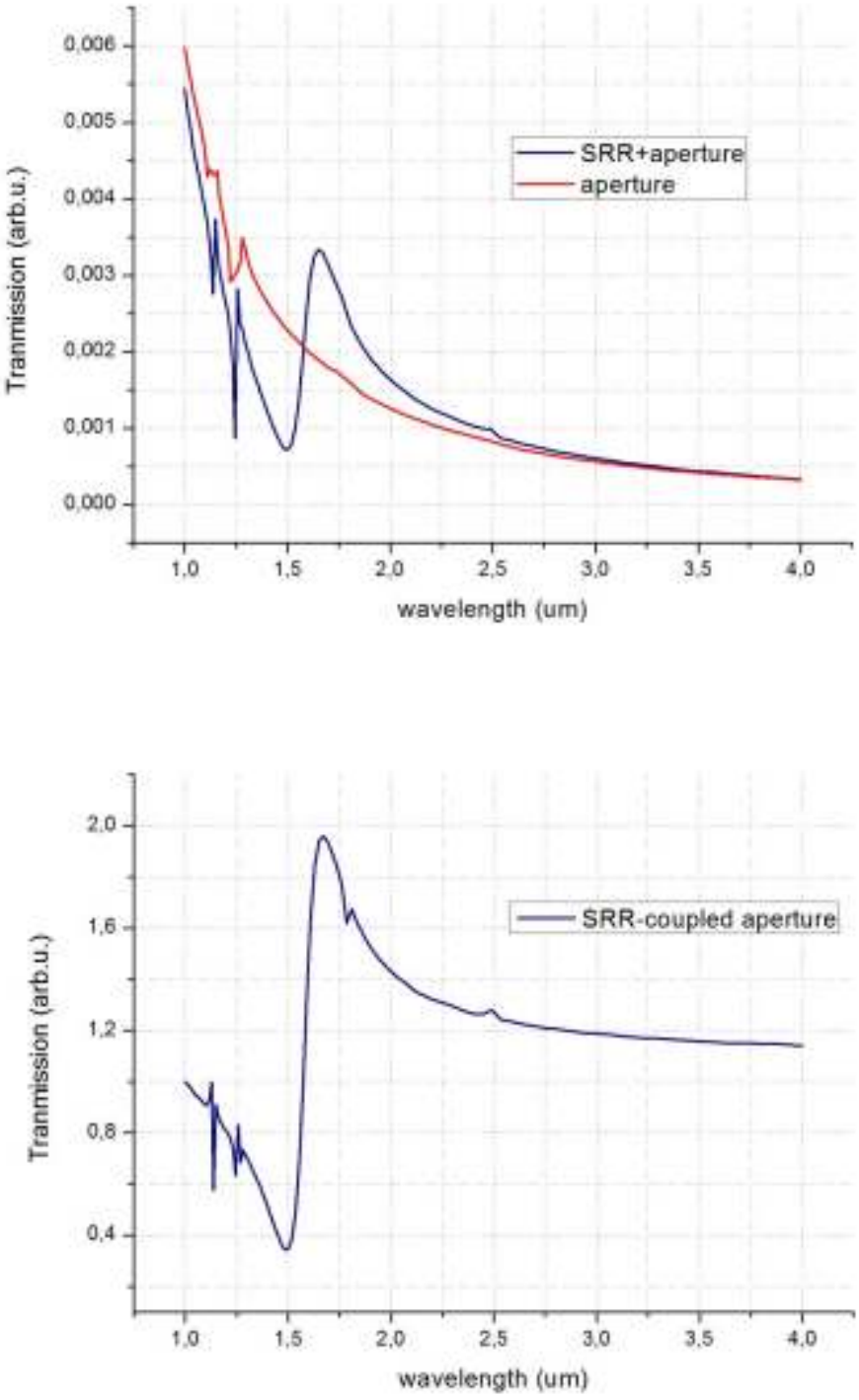

Figure 2.21: a) Transmission spectrum of the SRR-coupled aperture structure and a single aperture. b) Enhancement spectrum - Simulation Results.

The enhancement results revealed that enhancement over 200% is achieved (Figure 2.21) when the SRR is placed 50nm away from the aperture (50 nm thick SiO2 layer between SRR and aperture) and the split of the SRR is placed at the centerline of the aperture. The propagation direction of the incident wave is perpendicular to the SRR plane. The enhancement stems from electric resonance of SRR. The transmission is significantly increased by utilizing a single SRR in the optimum orientation and location. 200% transmission enhancement, which is defined as the ratio of transmitted electromagnetic wave intensity through SRR and aperture to transmitted electromagnetic wave intensity through only aperture, is realized at 1.55um. Note that the resonance wavelength at 1.55um and the aperture length (r = 200nm) is approximately 0.1λ, which is considered as sub-wavelength. This is a quite high enhancement for telecommunication wavelength.

2.4.2 Surface Manipulation

Plasmonic enhancement by utilizing SRR structures is also achieved by manipulating the surface. In this section, we will discuss novel structures that are utilized for enhancing the transmission of electromagnetic waves through a single sub-wavelength aperture. The manipulation of the aperture shapes is a promising approach for enhanced transmission through sub-wavelength apertures[82, 83]. There are wide varieties of study on metamaterials to change the transmission characteristics of several structures, which are restricted to several physical restrictions that cannot be overcome by ordinary materials. Transmission through a sub-wavelength hole is another contemporary research topic because of its

applications of critical importance ranging from biomaterials to microscopy.

The last century concluded with a very important discovery by Ebbesen [24]; sub-wavelength holes in a thin metal film can transmit electromagnetic waves much more strongly at certain frequencies than the Bethe's prediction [25] by utilizing hole arrays. Ebbesen's discovery (extraordinary transmission phenomenon) and new fabrication techniques opened up significant opportunities to design novel devices, such as new probes for the scanning near-field optical microscope (SNOM) [110, 111], near-field optical recording [112, 113], nano-scale lithography [114-116] tracking single molecule (fluorescence spectroscopy) [111, 117], and ultrafast miniature photodetector [118,126].

The study and debates on the characterization of wave propagation through a hole in a screen have been ongoing for centuries. In the middle of the 17th century, Grimaldi described diffraction from a circular aperture, which contributed to the foundation of classical optics [94, 95]. As classical optics suggests, Grimaldi's description was only for a circular aperture much larger than a wavelength. In 1944, Bethe gave a theoretical characterization of electromagnetic wave transmission through a sub-wavelength circular hole (aperture) in a perfect conductor metal screen of zero thickness, and suggested that the amplitude of the transmitted wave is proportional to the square of the area of a sub-wavelength aperture with $k \cdot (r/\lambda)^4$ where the radius (r) of the aperture is much smaller than the wavelength (λ) of the incident electromagnetic wave ($r << \lambda$) [25]. In other words, the transmitted wave is proportional to the square of the aperture area and is inversely proportional to the fourth

power of the excitation signal's wavelength. According to Bethe's ideal theoretical structure, the transmission spectra for an aperture of radius $r<<\lambda$ has a rapidly decreasing transmission with the increased wavelength of an incident field by a power of four. Bethe's theory holds true for idealized situations, in which the enhancement of electromagnetic wave propagation beyond the limit of Bethe's suggestion could be obtained by utilizing novel methods to improve the coupling of an incident wave and aperture [99-101, 136,137].

The advances in characterization and fabrication techniques enabled researchers to work more on decreasing the severe effects of extremely high transmission loss and the diffraction of light through a sub-wavelength aperture. In 1998, "extraordinary optical transmission (EOT)" phenomena were reported by the seminal work of Ebbesen et al. [24]. It was shown that the coupling of light with the surface plasmons (SP) of a two dimensional array of sub-wavelength holes in turn yields a strong enhancement of transmitted light, which is above the limit of Bethe's prediction. This new era has attracted the interest of researchers on the enhancement of "light/electromagnetic wave" transmission through sub-wavelength apertures. The following works [141-147] on the characterization of EOT phenomenon approved the involvement of surface plasmons; and also showed that the interplay between light and the resonant excitation of SPs, which are induced by a periodic array of holes, causes the EOT. The EOT phenomenon and new fabrication techniques opened up significant opportunities to new research areas and applications, such as new probes for the scanning near-field optical microscope (SNOM) [110, 111], near-field optical recording [112, 113],

nano-scale lithography [162-164], tracking a single molecule (fluorescence spectroscopy) [111, 117], and an ultrafast miniature photodetector [118].

Surface plasmons (SP) are the resonant excitations that are caused by the coupling between the free surface charges of metal and the incident electromagnetic field at the interface separating a dielectric medium with a metal. Since metals at microwave frequencies possess very high conductance (metals behave similar to PECs in the microwave spectrum); surface plasmons are not supposed to exist at the microwave frequency regime. Therefore, there has been a debate going on regarding a new way of explanation for EOT at microwave frequencies [119, 120]. In this approach, SPs are not considered to exist in the microwave regime, in which "spoof surface plasmons" that are very similar to SPs are formed between the dielectric substrate and metal at microwave frequencies [119]. SPs and spoof SPs serve in a similar way in order to guide the electromagnetic wave to the aperture in order to in turn obtain an enhanced transmission. In our present work, we obtained enhanced transmission at both microwave and optical frequencies wherein the metals act as perfect conductors for microwave and not ideal for optical regime. Therefore, localized surface plasmons contribute to the enhancement process for optical device structure but not for microwave structure. The driving force of enhancement process for light waves are the localized surface plasmons. As we will show in the following, the strong localized fields around split-ring resonator (SRR)-based novel structures couple to the incident electromagnetic field through a resonant process, causing a strong extraordinary transmission of electromagnetic waves.

Design and fabrication of sub-wavelength aperture structures:

We investigated novel structures that are utilized for the enhanced transmission of electromagnetic waves through a single sub-wavelength aperture. Previous studies have shown that an aperture with rectangular [104] and elliptical [102] shapes in turn yield enhanced transmission for the specific polarization of an incident electromagnetic wave. Furthermore, enhanced transmission through a sub-wavelength aperture, by utilizing SRR structures, was previously shown theoretically [161] and we showed experimentally in our previous work [162].

The manipulation of the aperture shapes is a promising approach for enhanced transmission through sub-wavelength apertures. In the present work, we utilized SRR-shaped apertures in order to increase the transmission though a sub-wavelength aperture by using the strong localization characteristics of SRR structures [81, 164-165].

The idea of an SRR-shaped aperture stems from the Babinet's principal [167]. By using the Babinet's principle, we can anticipate that the reflected fields of the SRR structure for a given incident polarization are supposed to be similar to the transmittance spectra of the complementary SRR-shaped aperture for orthogonal polarization. Since SRR is a strong resonator structure, there exists a dip in the transmittance spectra at the resonance frequency. The dip in the transmission spectrum of the SRR corresponds to a peak in the reflection spectrum. Therefore, we can utilize this peak in order to obtain enhanced transmission through sub-wavelength apertures according to Babinet's principle.

First, we performed simulations on an SRR structure at microwave frequencies. After that, we made optical replica of these devices. Split-ring resonator structures, which can be easily manufactured for microwave regime, comprise of two concentric copper rings with splits oriented at opposite sides. Figure 2.22 shows a schematic representation of the SRR that we used. The gap between the inner and outer rings (t); and the width of the splits (d) are 0.2 mm, the metal width (w) is 0.9 mm, and the outer radius of the SRR structure is 3.6 mm. SRR is deposited on a commercial FR4 dielectric board with a thickness of 1.6 mm which is used at previous works. [79, 165].

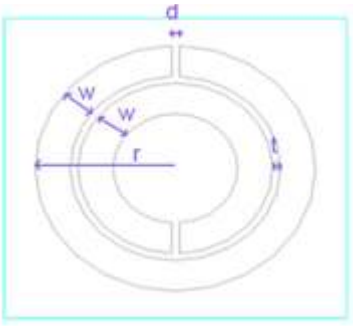

Figure 2.22: SRR structure.

The simulation that we performed at microwave for the single SRR structure was carried out by modeling a waveguide-like structure which is the same experimental setup that we will use for microwave measurements. Namely, two waveguide ports were used to obtain S-21 data. Open boundary conditions were employed along the propagation direction. Electric (E_t=0) and magnetic (H_t=0) boundary boundary conditions were used for direction parallel to propagation.

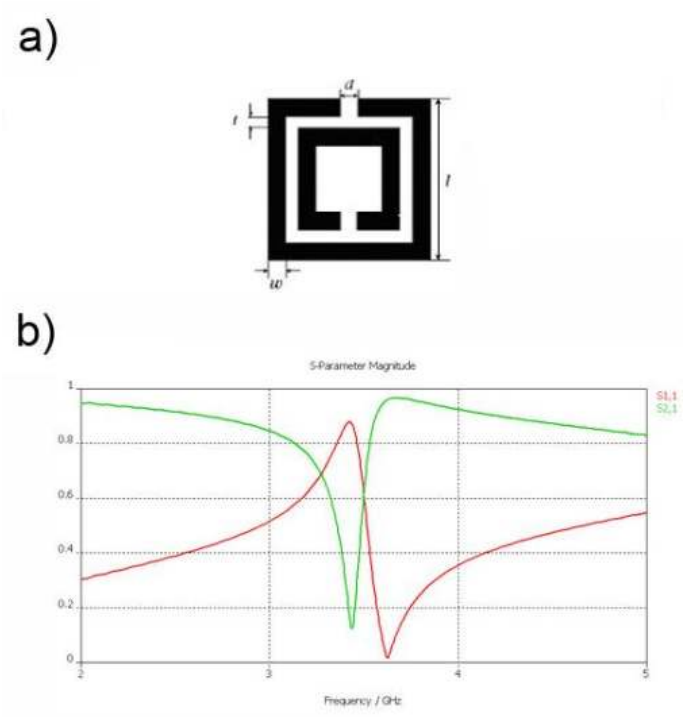

Figure 2.23: a) Schematic representation of SRR b) Transmission (S21) and reflection (S11) spectra of the SRR structure [8].

Figure 2.23.b shows the calculated transmission and reflection spectrum of the SRR structure. There is a peak in the reflection spectrum. Therefore, we expected to have a peak in the transmission spectrum of the SRR-shaped aperture for the orthogonal polarization of an incident wave (in accordance with Babinet's Principle).

The numerical simulations for microwave design were performed by the commercial available finite-difference time-domain (FDTD), Lumerical and CST Microwave Studios. Since the mesh sizes are reasonable for microwaves, we modeled the complete scene in a real electromagnetic measurement setup in order to decrease the deviations from the experimental results. Open boundary conditions were applied along all directions and perfect electric conductor (PEC) approximation was used for metal parts in the simulations of microwave device. Since

metals are very good conductors at the microwave spectrum and the open boundary conditions can be obtained by using absorbers around the measurement setup, the approximations that are used in the simulations are reasonable and acceptable.

The metallic plate with an aperture is placed 0.1 mm away from the transmitter antenna and the receiver antenna is located 5 cm away from the transmitter antenna. The SRR-shaped aperture is complementary to an exact replica of the SRR structure. The SRR-shaped aperture is modeled by subtracting the SRR structure from a square metal plate with a size of L x L (L = 200 mm). The metal plate is composed of a copper metal with a thickness of 30 μm and a 1.6 mm thick commercial FR-4 PCB substrate. Figure 2.24 shows a schematic representation of the SRR-shaped aperture that we used. The gap between the inner and outer rings (t); and the width of the splits (d) are 0.2 mm, the ring width (w) is 0.9 mm, and the outer radius of the SRR structure is 3.6 mm. The dielectric constant of the FR-4 dielectric substrate is taken as ε=3.6 with a tangent loss of δ=0.01.

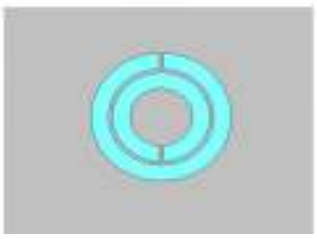

Figure 2.24: Schematic representation of the SRR-shaped aperture model (Gray parts are the metal plate and the blue parts are the gaps).

Figure 2.25 shows the calculated transmission result of the SRR-shaped aperture, which demonstrated an extraordinary transmission peak.

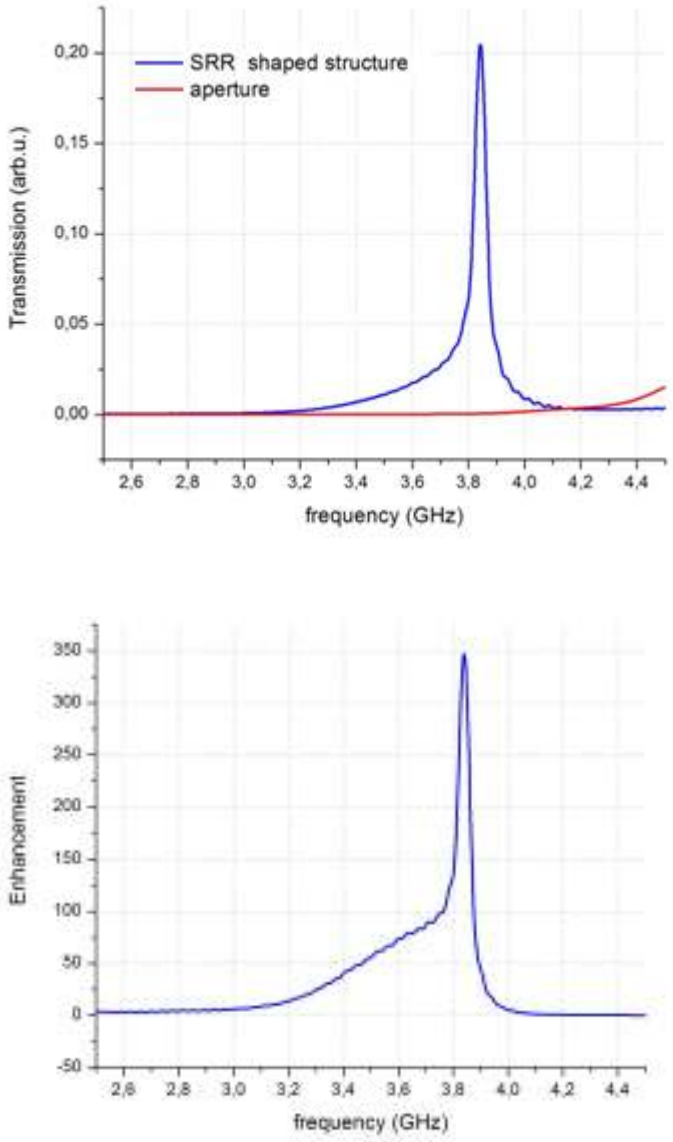

Figure 2.25: a) The calculated transmission spectrum of the SRR-shaped structure and a single aperture. b) Enhancement spectrum.

The enhancement in the transmission through an aperture is defined as; the ratio of the field intensity of the transmitted

electromagnetic wave through an SRR-shaped aperture to that through the aperture only.

Figure 2.25 shows the enhancement that was obtained by manipulating the shape of the aperture as the SRR-shaped aperture. We obtained a 346-fold transmission enhancement at 3.84 GHz. It is noteworthy that the enhancement peak is very close to the resonance frequency of the SRR structure that we used the parameters of it [162]. The resonance coupling of the incident electromagnetic wave to the SRR-shaped aperture causes the strong localization of the electric field at the splits and gaps of the SRR-shaped aperture. Therefore, the resonator characteristic of SRR is responsible for the confined electromagnetic waves in the SRR-shaped aperture. We checked the role of the SRR characteristics on the enhanced transmission through an SRR-shaped aperture by closing the split regions of the structure, in which the structure became a CRR (closed ring resonator)-shaped aperture (Figure 2.26.a). Since the resonant behavior of SRR diminishes by closing the splits, the role of the resonant structure of SRR on the enhancement mechanism of an SRR-shaped aperture is evident (Figure 2.25.b).

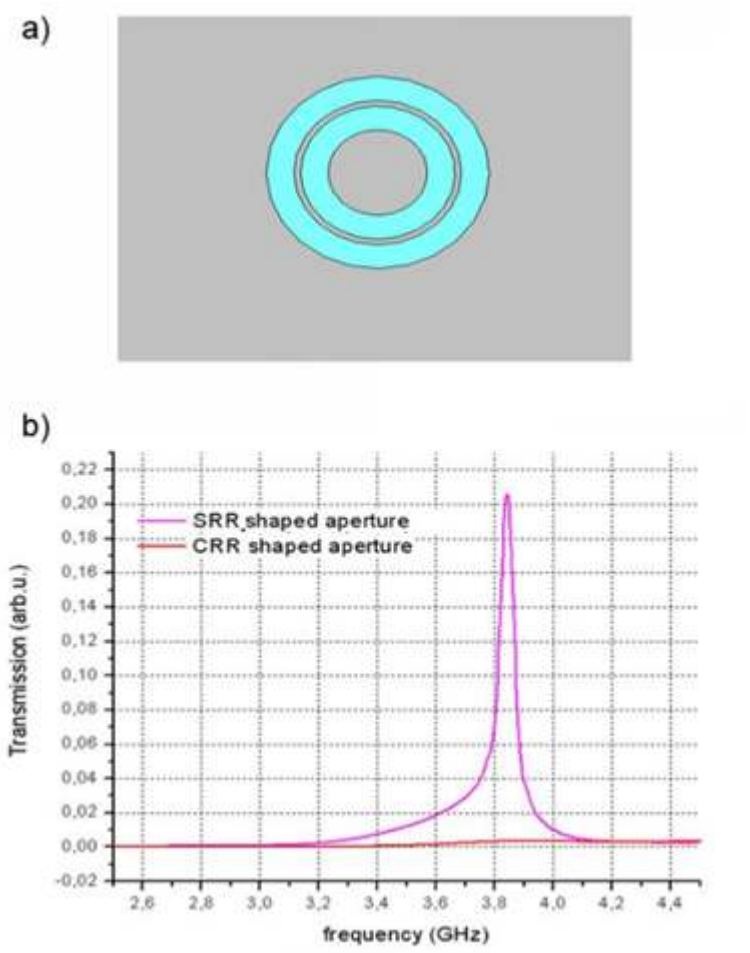

Figure 2.26: a) Schematic representation of the Closed Ring Resonator (CRR) shaped aperture. b) Transmission spectrum of the CRR-shaped aperture and the SRR-shaped aperture [8].

After the successful demonstration of enhanced transmission through SRR-shaped aperture, we simulated, manufactured, and measured several other types of split ring resonator structures in order to better characterize the novel approach/structure that we proposed. We performed a parametric study of an SRR-shaped aperture and we also investigated single-ring SRR-shaped apertures. We mostly used square shaped structures due to the ease of fabrication for the applications at optical frequencies. The schematic representations of the proposed structures are shown in Figure 2.27:

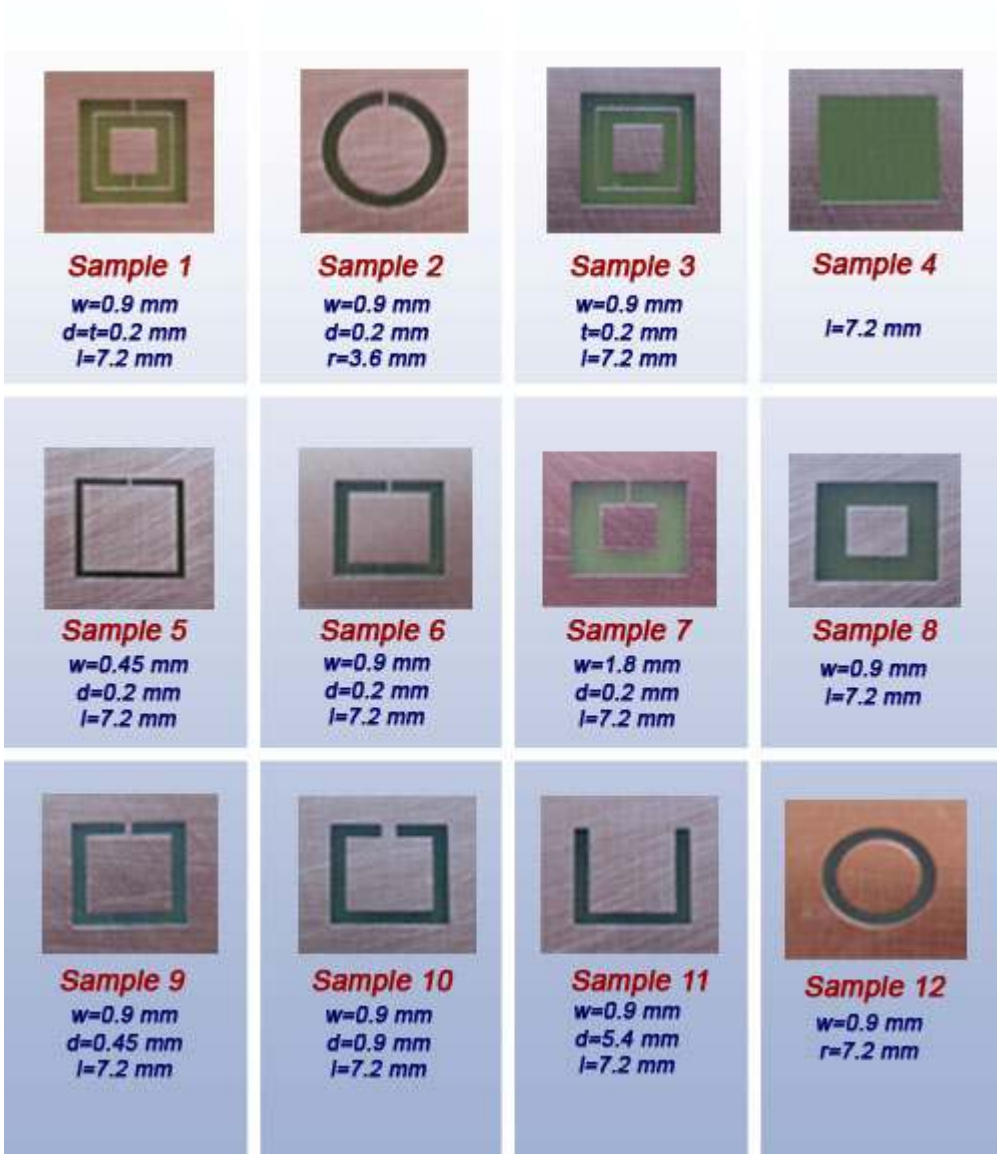

Figure 2.27: The schematics of the proposed SRR-shaped aperture structures.

We investigated the enhanced microwave transmission through sub-wavelength apertures for 12 different samples. The maximum length of all the samples was 7.2 mm, which corresponds to approximately 0.1λ at the resonance frequency of the SRR structures (~ 3-4 GHz).

We used an experimental setup comprising an Agilent N5230A portable network analyzer, two waveguide ports, and the proper SMA cables. The

waveguide ports were used as the transmitter and the receiver and were connected to the network analyzer with SMA cables. In the measurements, the metallic plate with an aperture was placed 0.1 mm away from the transmitter antenna and the receiver antenna was located 5 cm away from the transmitter antenna, just as we modeled in the numerical simulations. Waveguide ports were employed as transmitter and receiver antennas.

These samples were fabricated by using a CNC machine with a process resolution of 0.1 mm. Figure 2.28 displays the measured transmission spectra of the 12 samples. Also, the enhancement values of the experimentally measured samples simulations are shown in Figure 2.28:

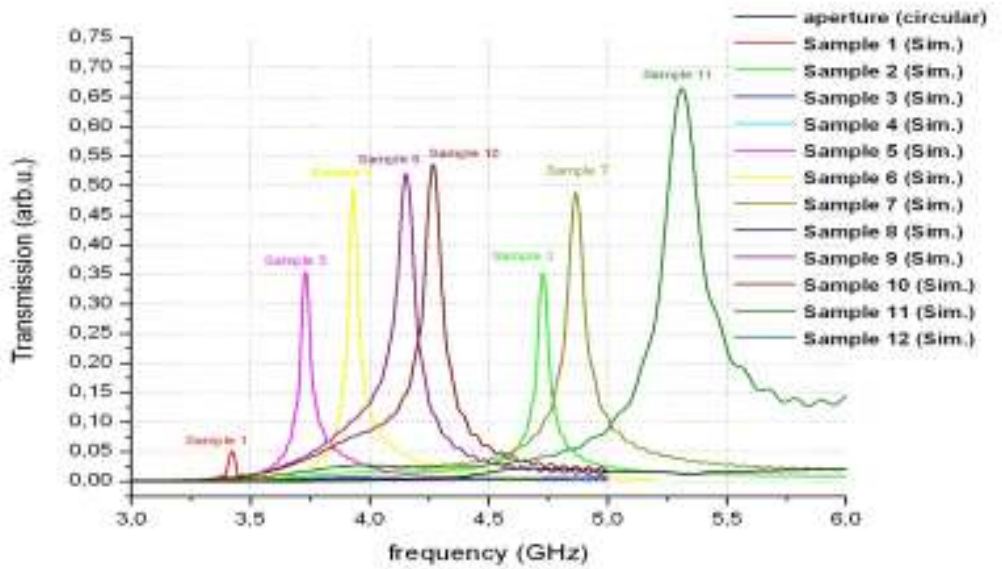

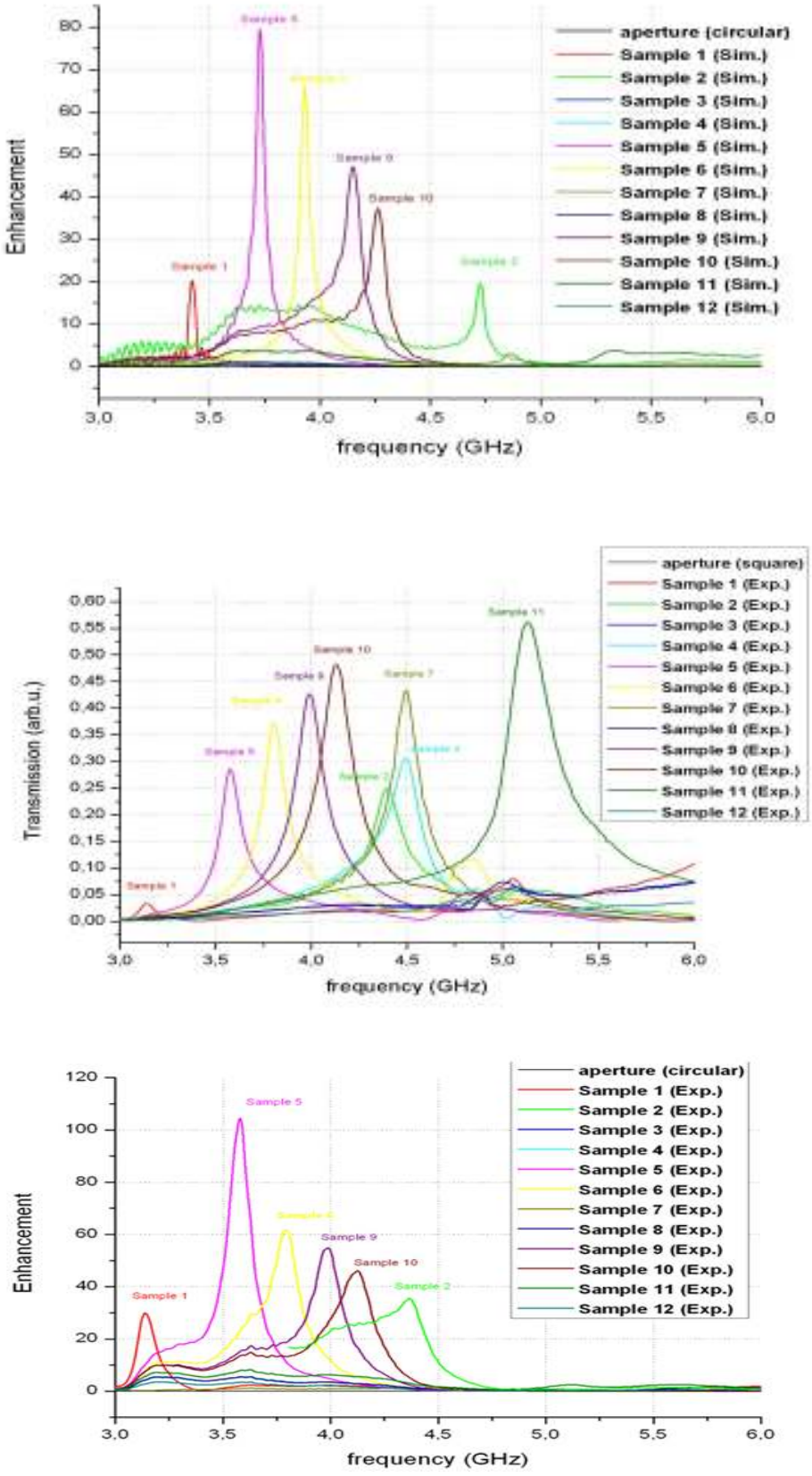

Figure 2.28: Transmission and enhancement spectrum of the proposed SRR-shaped apertures - Measured & calculated.

The experimental and numerical transmission results are in good agreement, which indicates that a significant enhancement was achieved by using our proposed structures. Transmission through the sub-wavelength aperture is significantly increased when SRR-shaped apertures are placed instead of only apertures. Moreover, we observed that the annular apertures (Samples 3, 8, and 12) transmit electromagnetic waves very close to the single aperture sample (Sample 4), which indicates that SRR-shaped apertures show superior performance versus annular apertures in terms of sub-wavelength aperture transmission. This also shows the effect of the resonant coupling mechanism via SRR-shaped apertures. The resonance of SRR enables the coupling of the incident wave to the transmitted wave. Figure 2.28 shows the enhancement values of the simulated structures.

Moreover, some of the peaks that are shown in transmission results are not available in enhancement results; because, transmission through a sub-wavelength aperture increases with the power of four as the frequency increases. Therefore, certain peaks at the end of the interested frequency spectrum disappear in the enhancement plot as a result of an increase in the transmission through the aperture at higher frequencies.

Sample-4 is the reference sample for our measurements. As we stated above, the sub-wavelength apertures transmit very poorly and diffract electromagnetic radiation in all directions. Therefore, all of the samples were designed on a 20 cm x 20 cm metal plate in order to better collect the transmitted wave and better isolate the incident wave and transmitted wave.

Sample-1 has the highest transmission wavelength (lowest radius to the wavelength ratio) as a result of the additional splits and rings compared to the other samples. Furthermore, we observed that as the ring width decreases the transmission enhancement and transmission peak frequency increases; this is because the decreased width of the SRR-shaped apertures increases the coupling between the plate at the center and the surrounding large plane, which increases the resonant coupling.

We also investigated the effect of a split width on the enhancement peak. The enhancement value of the samples decreases as we increase the split width. Furthermore, the resonance peak frequency increases with the increasing split width. The split width is very crucial for the resonance of SRR. The effect of increasing the split width is also very important for the application of our proposed structures at optical frequencies. Since the fabrication of the sample-11 is the easiest among all the others, it will be the best choice for higher frequencies. As we can see from the results, we obtained a significant transmission peak, which is very promising for higher frequency applications.

Finally, we investigated the effect of the shape of SRR on the enhancement. We fabricated sample-2 and sample-12 for observing the effect of the SRR-type. The transmission of sample-12 is as we expected, very low. However, we obtained a significant enhancement (35.58-fold) by only utilizing a small wire that makes the structure an SRR-shaped structure (Sample-2). We used a circular aperture (radius 3.6 mm) as the reference sample for circular SRR-shaped aperture structures for a fair comparison.

The metal that we used in our structures is very close to a perfect conductor at microwave frequencies. Therefore, localized surface plasmons do not contribute to the enhanced transmission. The enhancement stems from the strongly localized fields that are caused by the resonant process of SRR-shaped aperture to the sub-wavelength aperture.

After the successful demonstration of enhanced transmission through SRR-shaped aperture at microwave, we moved on the optical replica of these structures.

For optical regime, we used square shaped structures due to the ease of fabrication for the applications at optical frequencies. The schematic representations of the proposed structures are shown in Figure 2.29:

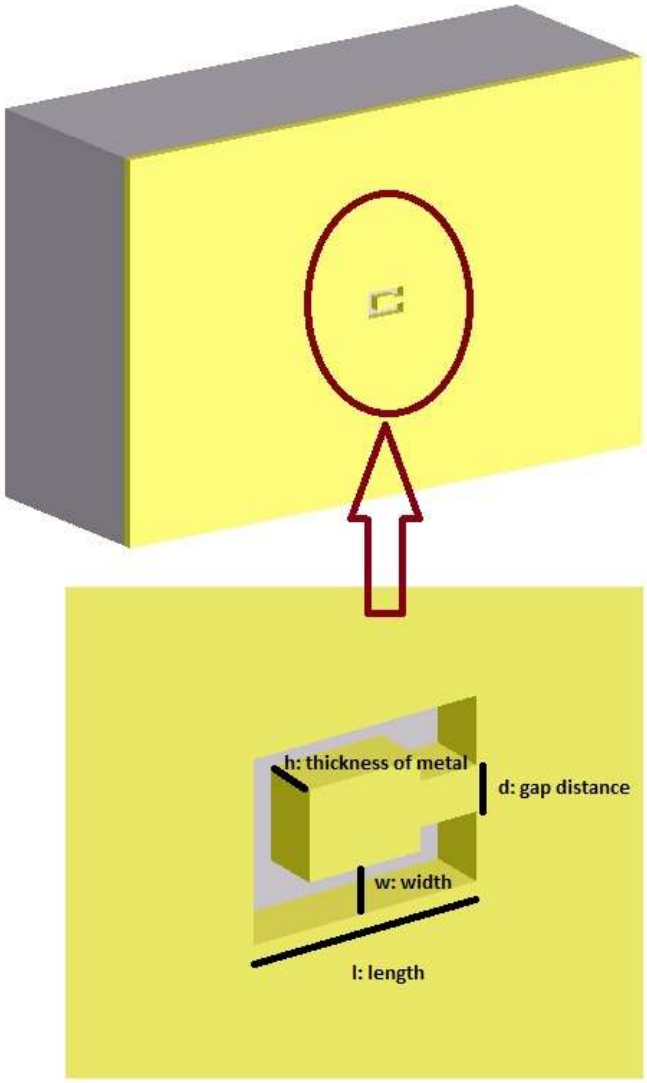

Figure 2.29: Schematic representation of optical SRR-shaped aperture.

The enhancement in the transmission through an aperture is defined as; the ratio of the field intensity of the transmitted electromagnetic wave through an SRR-shaped aperture to that through the aperture only.

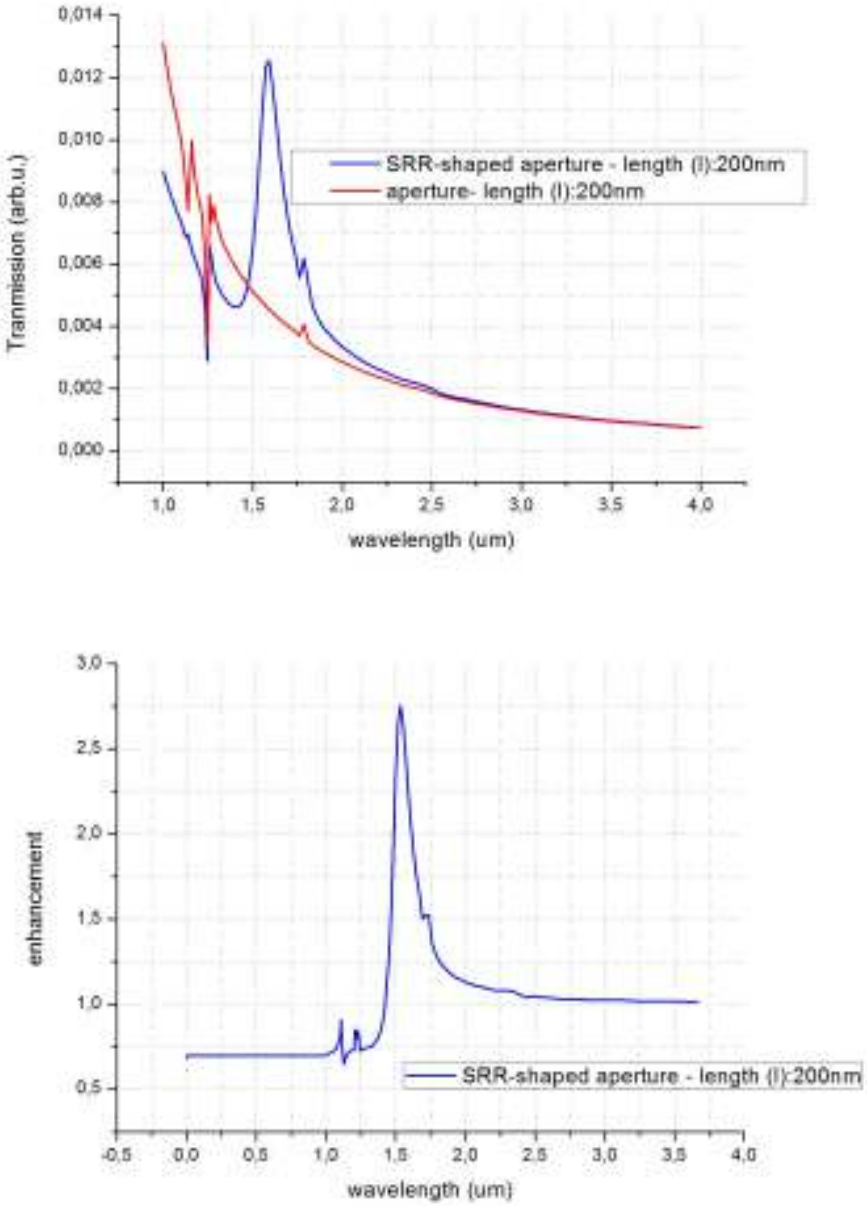

Figure 2.30: a) Transmission spectrum of the SRR-shaped structure and a single aperture. b) The enhancement spectrum (l=200 nm, w=h= 50 nm, d:100nm). - Simulation Results.

Figure 2.30 shows the enhancement that was obtained by manipulating the shape of the aperture as the SRR-shaped aperture. We obtained a 2.75-fold (%275) transmission enhancement at 1.55 um. It is noteworthy that the enhancement peak is very close to the resonance frequency of the SRR

structure. The resonance coupling of the incident electromagnetic wave to the SRR-shaped aperture causes the strong localization of the surface plasmons at the arm edges of the SRR-shaped aperture. Therefore, the resonator characteristic of SRR is responsible for the confined electromagnetic waves in the SRR-shaped aperture.

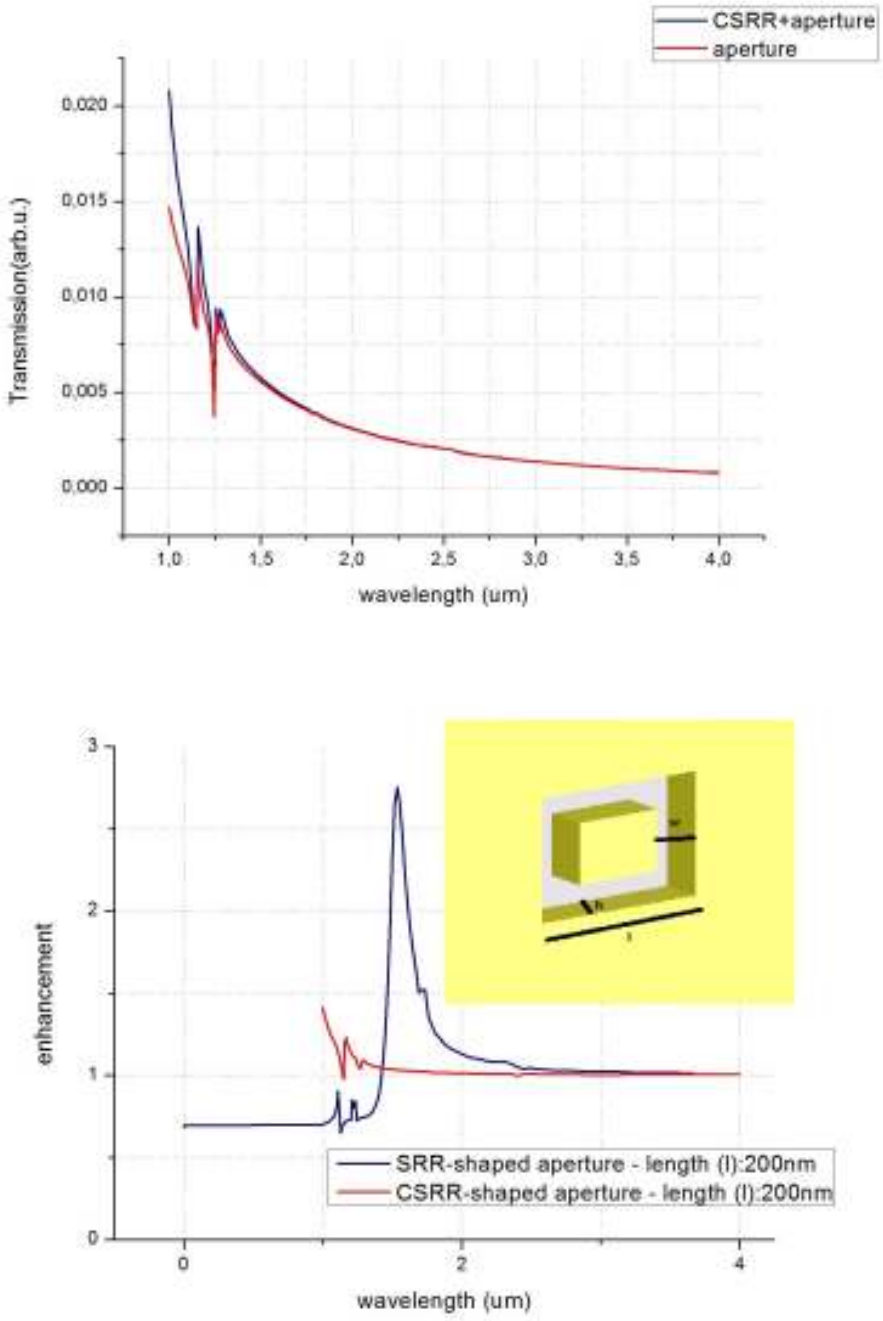

Figure 2.31: Simulation results of a SRR and CSRR structures. CSRR structure is depicted in the inset CSRR (l=200 nm, w=h= 50 nm), a) Transmission, b) Enhancement.

We checked the role of the SRR characteristics on the enhanced transmission through an SRR-shaped aperture by closing the split regions of the structure, in which the structure became a CRR (closed ring resonator)-shaped aperture (Figure 2.31-inset). Since the resonant behavior of SRR diminishes by closing the splits, the role of the resonant structure of SRR on the enhancement mechanism of an SRR-shaped aperture is evident.

Surface plasmons play a critical role in the transmission properties of an aperture and therefore important for enhanced transmission through subwavelength apertures. Enhanced transmission can be explained by diffraction assisted by the enhanced fields associated with surface plasmons [34, 119]. Surface plasmons can be created by texturing the metallic surface with a subwavelength pattern [35, 118, 119], which show that enhanced transmission from a subwavelength aperture is assisted by the guided mode of the coaxial waveguide and coupling to the surface plasmons. We used a similar approach to texture shape's itself. Transmission through the sub-wavelength aperture is significantly increased when SRR-shaped apertures are placed instead of the single aperture. The resonance of SRR-shaped aperture that we explained according to Babinet's Principle enables the coupling of incident wave to transmitted wave. In other words, we just inserted a small patch of metal in a subwavelength aperture and increased the transmission 275% which is a remarkable result. The extraordinary transmission result that was observed at the response of SRR-shaped aperture confirms that our expectation, which is based on Babinet’s Principle, holds. This novel approach opens up significant opportunities to utilize several resonator

structures for obtaining extraordinary transmission through sub-wavelength apertures. In the present work, we investigated SRR-shaped apertures for increasing the transmission through a sub-wavelength aperture both for microwave and optical regime.

2.4. Summary

In summary, we demonstrated several novel structures to increase the transmission through a sub-wavelength aperture. Enhanced transmission through a sub-wavelength aperture by placing a SRR structure in the near field of the aperture is achieved at both optical and microwave frequencies. 740-fold enhancement is obtained at microwave device and 200% enhancement is obtained at ~1.5um. Subsequently, we manipulated the shape of sub-wavelength aperture. We utilized SRR-shaped apertures in order to increase the transmission though a sub-wavelength aperture by using the strong localization property of SRR structures. We obtained a 104-fold enhancement by utilizing SRR-shaped apertures at microwave and 275% enhancement at 1.5um. The enhancement stems from the strongly localized fields caused by SRR-shaped apertures. The strongly localized fields are a result of the resonant process of SRR-shaped aperture to the sub-wavelength aperture which is spoof surface plasmons for microwave and surface plasmons for optical regime.

Enhanced transmission through a sub-wavelength aperture has been and will be subject of intense research due to a wide range of applications of this phenomenon. Our suggested structures are candidates to be used for future plasmonic applications.

Chapter 3

Graphene Based Metamaterials

3.1. Introduction

Graphene is an extraordinary material which is believed to have outstanding applications in photonics. Therefore, design of graphene-based novel photonic systems is an active research field. However, exciting opportunity to design novel photonic devices using graphene structures has not been fully exploited. Here, we report the design simulation and fabrication of novel SRR and graphene based metamaterial structures. We obtained promising results that can open up significant opportunities to design novel graphene-based photonic devices.

Graphene is a monolayer of carbon atoms which are arranged in a two-dimensional honeycomb lattice. It can be used for wrapping up into fullerenes (0D), for rolling into nanotubes (1D) or for stacking into 3D graphite [150,158,179]. Since graphene has interesting electrical and

mechanical properties, it is an attractive research material nowadays. Electron in a graphene monolayer behave as massless Dirac fermions where principles of quantum electrodynamics can be tested [181, 183, 185]. For instance, an electron in monolayer (atomically thick) graphene sheet has zero effective mass (Dirac Fermions) [186] and it can travel for micrometers without scattering, even at room temperature [183, 187]. Also, graphene exhibit many interesting and exotic properties ranging from ballistic electronic transport [188-190] to anomalous quantum Hall effect in electrical transport [186, 189] and tunable interband transitions [193, 194].

Graphene has exceptional optical properties. For instance, graphene exhibits saturable absorption constant as a consequence of Pauli blocking [182,195,196]. Moreover, non-equilibrium carrier result in hot luminescence [197, 198]. Graphene is a versatile optical material for nanophotonics applications [183] like metamaterials [199], photodetectors [200], light emitting devices and ultrafast lasers [201]. In particular, graphene with its planar nature, attracts an increasing research interest as a promising novel tool for nanoplasmonics and nanoscale electronics [202, 203].

Pioneering works of graphene were focused on single particle excitation of electrons. On the other hand, plasmonic properties of graphene layer, which is a result of collective excitations of 2D massless electrons, is an emerging research area nowadays. Plasmonic resonances in graphene give outstanding potential for designing novel optoelectronic devices by its remarkably high absorption [183, 204, 205] ($\pi a \approx 2.3\%$), where

$\alpha = \frac{e^2}{\hbar c} \approx \frac{1}{137}$ is the fine structure constant [183]. Since graphene plasmons are confined to volumes ($\approx \frac{1}{\alpha^3}$) of the order of 10^6 times smaller than the diffraction limit, graphene plasmons are superior to traditional metallic plasmonics; because, graphene-based structures exhibit stronger light-matter interactions as a result of better confinement of waves.

Electrical response at Terahertz frequencies are high enough to design plasmonic devices [206]. However, electrical control of plasmon resonance becomes a challenge at optical frequencies as a result of drastically reduced free electron responses with increasing frequency. Graphene which is a novel zero bandgap semiconductor [186, 189] is a great candidate to overcome this challenge. Since high frequency interband transition in graphene can be exploited through electrical gating [207], plasmon resonance of graphene-hybrid device like SRR can be modulated.

Surface plasmons have the characteristics of concentrating light into subwavelength volume which is one of the main tools of plasmonics [179-180, 207]. Plasmons in graphene is an active research field [28, 42-44, 212]. However, exciting opportunity to design novel metamaterials using graphene structures has not been fully exploited. It is desired to control the plasmon resonances. Controlling the plasmon resonance at optical regime is a challenge as a result of very weak response of gate-induced free electrons [207]. We achieved the control of infrared plasmon resonances by utilizing graphene-SRR system. We modulate the

resonance frequency of SRR by utilizing the gate-tunable optical transitions [193-194, 204-205].

Here, we report the design simulation and fabrication of a novel SRR and graphene based metamaterial structures. Namely, we report optical response of 2D metamaterial (SRR) structure layer on a monolayer graphene which confines plasmons. As we will show in the following, the strong localized fields around split-ring resonator (SRR)-based novel structures couple to the incident field through a resonant process, causing a strong localization of electromagnetic waves.

3.2. Electrical Gate Tuning

Plasmonics open up the way of focusing light into subwavelength volumes, which facilitates the manipulation of light at the nanoscale by guiding surface plasmons. Since dynamic control of the resonance of plasmonic devices is crucial for applications like sensors [82], nano-antennas [89] and compact optoelectronic devices[96,105,123]. Controlling plasmonic resonances dynamically is very desirable for plasmonic applications. Several plasmonic devices has been proposed to control plasmon resonances only at terahertz regime as a result of gate-induced free electrons in semiconductors have large response at low frequency range like terahertz [206,207]. Therefore, electrically controlling plasmonic resonances at optical regime by utilizing gate voltage dependent optical properties of metallic structures with graphene hybrid is an emerging research field and research challenge as a result of significantly decreased free electron responses with increasing frequency. Graphene is a great candidate to overcome this problem; because

graphene has the property of gate voltage controlled optical conductivity that makes graphene an electrically tunable plasmonic material [131-133,183,186]. Graphene's both the low frequency carrier response and the high frequency interband transition can be changed through electrical gating [194]. Changing the Fermi Level and carrier density by gate voltage which is also called electrostatic doping [138] is the reason behind the gate voltage dependent optical property of graphene.

In this work, dynamical control of mid-infrared plasmon resonance of hybrid Split Ring Resonator (SRR)-graphene structure by electrically tuning the graphene's optical property is demonstrated. We tuned the plasmonic resonance of a SRR structure by exploiting the gate-tunable optical transitions of graphene [138,139,193]. A plasmon resonance wavelength tuning range of 110 nm in MIR regime is demonstrated numerically. This work is the first demonstration of graphene based SRR tuning in the contemporary literature according to our knowledge.

Optical Parameters of Graphene:

Permittivity of a ordinary dielectric substrate is;

$$\varepsilon = \varepsilon_{real} + \varepsilon_{imag} = 1 + i\frac{\sigma}{w\varepsilon_0} \quad (1)$$

We need to find the conductivity of graphene to calculate permittivity.

For the sake of the clarity, we started with the general model found before[139]. For high frequencies, ω ≫ (kv, τ^−1), the dynamical conductivity is given by

$$\sigma(\omega) = \frac{e^2\omega}{i\pi\hbar}\left[\int_{-\infty}^{+\infty} d\varepsilon \frac{|\varepsilon|}{\omega^2}\frac{df_0(\varepsilon)}{d\varepsilon} - \int_{0}^{+\infty} d\varepsilon \frac{f_0(-\varepsilon) - f_0(\varepsilon)}{(\omega + i\delta)^2 - 4\varepsilon^2}\right] \quad (2)$$

where $f_0(\varepsilon)$ is the Fermi Function.

The Fermi function f(E) specifies how many of the existing states at the energy E will be filled with electrons. The function f(E) shows the probability that an available state at an energy E will be occupied by an electron (under equilibrium conditions). In other words, it is a probability distribution function.

$$f(E) = \frac{1}{1+e^{\frac{(E-E_F)}{k_B T}}} \quad (3)$$

where E_F is Fermi Energy or Fermi Level,

k_B is Boltzman Constant = $1.38x10^{-23}\frac{J}{K} = 8.6x10^{-5}ev/K$ and

T is absolute temperature at Kelvin.

E is the energy of the particle, and E_F is the Fermi Energy Level for the case of electrons in a semiconductor. At T = 0 K, the energy of the particle should be equal to the Fermi energy.

The first term in Eqn. (2) corresponds to the intraband electron–photon scattering processes. The second term in Eqn. (2), corresponds to interband electron transitions.

$$\sigma(w) = \sigma^{intra}(w) + \sigma^{inter}(w) \tag{4}$$

$$\sigma^{intra}(\omega) = \frac{e^2\omega}{i\pi\hbar} \int_{-\infty}^{+\infty} d\varepsilon \frac{|\varepsilon|}{\omega^2} \frac{df_0(\varepsilon)}{d\varepsilon} = \frac{ie^2|\mu|}{\pi\hbar(\omega + i\tau^{-1})} = \frac{2ie^2T}{\pi\hbar(\omega + i\tau^{-1})} \ln\left[2\cosh(\mu/2T)\right]$$

$\omega \Rightarrow \omega + i\tau^{-1}$

in order to take into account the electron – impurity scattering processes

$\mu \gg T$

(5)

where μ is E_F /$\hbar$ and for T=0 integral can be easily calculated[139],

$$\sigma(\omega) = -\frac{e^2\omega}{i\pi\hbar} \int_0^{+\infty} d\varepsilon \frac{f_0(-\varepsilon) - f_0(\varepsilon)}{(\omega + i\delta)^2 - 4\varepsilon^2} = \frac{e^2}{4\hbar}\left[\theta(\omega - 2\mu) - \frac{i}{2\pi} \ln \frac{(\omega + 2\mu)^2}{(\omega - 2\mu)^2}\right] \tag{6}$$

At the finite, but low temperatures, $\theta(w - 2\mu) \rightarrow \frac{1}{2} + \frac{1}{\pi}\arctan\left(\frac{w-2\mu}{2T}\right)$ substitution should be made in Eq. (6) [139].

The resulting surface conductivity formula of graphene is obtained as within the RPA limit [138]

$$\sigma_s(\omega) = \frac{i2e^2k_BT}{\pi\hbar^2(\omega + i\tau^{-1})} \ln\left[2\cosh\left(\frac{E_F}{2k_BT}\right)\right] + \frac{e^2}{4\hbar}\left[\frac{1}{2} + \frac{1}{\pi}\arctan\left(\frac{\hbar\omega - 2E_F}{2k_BT}\right) - \frac{i}{2\pi}\ln\frac{(\hbar\omega + 2E_F)^2}{(\hbar\omega - 2E_F)^2 + 4(k_BT)^2}\right] \tag{7}$$

where k is Boltzmann's constant, T is the absolute temperature, E_F is the Fermi Energy Level and t is the relaxation time.

Electron correlation is done by Random Phase Approximation. Graphene sheet conductivity which will be used to determine graphene permittivity

is derived within the RPA limit [138]. The random phase approximation (RPA) is an approximation method in condensed matter physics in which electrons are assumed to respond only to the total electric potential V(r) which is the sum of the external perturbing potential $V_{ext}(r)$ and a screening potential $V_{sc}(r)$ [142]. The external perturbing potential is assumed to oscillate at a single frequency. Therefore, the model yields via a self-consistent field (SCF) method [143] a dynamic dielectric function denoted by $\varepsilon RPA(k, \omega)$. What is meant by the random phase approximation is that the contribution to the dielectric function from the total electric potential is assumed to average out, so that only the potential at wave vector k contributes.

Since graphene is very thin (one atom layer) and we can state volume conductivity of graphene is surface conductivity over thickness of the graphene;

$$\sigma = \frac{\sigma_s}{t_{graphene}} \tag{8}$$

From Eqn(2), we deduced;

$$\varepsilon = 1 + \frac{i}{w\varepsilon_0 t_{graphene}} * \frac{i2e^2 k_B T}{\pi\hbar(w + i\tau^{-1})} * ln\left[2\cosh\left(\frac{E_F}{2k_B T}\right)\right] + \\ + \frac{e^2}{4\hbar}\left[\frac{1}{2} + \frac{1}{\pi}\arctan\left(\frac{\hbar w - 2E_F}{2k_B T}\right) - \frac{i}{2\pi} ln\left(\frac{(\hbar w + 2E_F)^2}{(\hbar w - 2E_F)^2 + 4(k_B T)^2}\right)\right] \tag{9}$$

$$\varepsilon = \varepsilon_{real} + \varepsilon_{imag} \tag{10}$$

where τ is the relaxation time.

We know every parameters of Eqn. (9) except relaxation time. We have to find an estimate of relaxation time in order to calculate.

In case of no electromagnetic field probed to graphene assumption, most of the transport properties of graphene sheets can be explained by scattering from charged impurities [144]. Therefore, charged impurities plays a role in finding relaxation time which is a function of conductivity [138,144]:

Graphene has a superior conductivity and mobility values are obtained as approximately 2.500 cm^2/Vs [155] for our samples at working wavelength range. There is a simple relation between mobility and conductivity. Let n be the number density of electrons, and let μe be their mobility. The electrical conductivity σ satisfies:[127,138]

$$\tau = ne\mu_e \frac{2h^2\mu_e}{g_s g_v e^2 E_F} \tag{11}$$

where $g_s = g_v = 2$ are the spin and valley degeneracy factors.

By using the measured conductivity values of graphene[157], conductivity is roughly calculated to find relaxation time which we will use in our structures.

In graphene, conductivity is shown to be dependent on charged impurity scattering [145,148,149]:

$$\sigma(n) = Ce\left|\frac{n}{n_{imp}}\right| + \sigma_{res} \quad (12)$$

where C is a constant, e is the electronic charge and σ_res is the residual conductivity at n = 0. $C = 5x10^{15}V^{-1}s^{-1}$ [149] and σ_{res} is measured from our graphene samples. While we know n_{imp} we can find n of our sample. As can be seen in Eqn.12, conductivity is charged impurity dependent. On the other hand, despite the zero carrier density near the Dirac points, graphene exhibits a minimum conductivity on the order of $\frac{4e^2}{h}$. This minimum value (σ_{min}) is called the quantum unit of conductance It is a result of local puddles of carriers that allow conduction which is a result of rippling of the graphene sheet or ionized impurities in the SiO2 substrate [149]. Although, theoretical studies suggest that the minimum conductivity should be $\frac{4e^2}{h}$; novel results show that minimum conductivity is of order $\frac{4e^2}{h}$ or greater and depend on impurity concentration [151]. Therefore we estimated the conductivity of graphene for a corresponding Fermi Level and derived the relaxation estimation by eqn (11).

After determining all the parameters, we calculated the permittivity of graphene for different Fermi Energy Levels. Fermi energy Levels are used to find the necessary gate voltage.

E_F of Dirac fermions scales with the 2D carrier denisty N [153,193] as;

$$Ef = \hbar v_F \sqrt{\pi N} \iff N = \frac{E_f^2}{h_{cap}^2 v_F^2 \pi} \quad (13)$$

where v_F is the Fermi velocity and $1.11x10^6 m/s$ is valid approximation for graphene [156].

Also; $N = \frac{C_g x V}{e}$ where Cg is the capacitance per unit area, $V=V_g - V_{CNP}$ where V_g is gate voltage and V_{CNP} is charge neutrality point (Dirac Point) [193]. The ultimate formula is:

$$E_F = \hbar v_F \sqrt{\frac{\pi C_g V}{e}} \tag{14}$$

We can deduce gate Voltage (V) for a specified Fermi Energy (E_F)

$$V = \frac{E_f^2 e}{\pi h\_cap^2 v_F^2 C_g} \tag{15}$$

Capacitance per unit area can be approximated by

$$C_g = \frac{\varepsilon A}{dx} \tag{16}$$

Since two our graphene structure is not exactly a parallel plate capacitor, a correction parameter (x) is added to calculate effective graphene thickness.

Permittivity is assumed to be 2.5 out of plane permittivity of graphene [138, 140] and d is take to be the graphene thickness (0.335 nm). Area is defined as the active area of our structure which is maximum unit cell size of SRR unit cell (~1um):

$$C_g = \frac{\left(2.5*\frac{8.852*10^{-12}F}{m}\right)*(1\mu m*1\mu m)}{0.335nm*x} * \frac{1}{(1\mu m*1\mu m)} = 66aF/x(\mu m)^2 \quad (17)$$

Therefore eqn.15 can be written as

$$V = \frac{E_f^2 e}{\pi h\_cap^2 v_F^2 \frac{(\varepsilon_r \varepsilon_0)}{d}} = \frac{E_f^2 (1.6*10^{-19}C)}{\pi(6.582*10^{-16}eVs)^2(1.11*10^6 m/s)^2(66aF/x(\mu m)^2)} \quad (18)$$

We come up with a very simple result for gate voltage and Fermi Energy;

$$V = 1.4457 * x * E_f^2 \quad (V) \quad (19)$$

where E_F is in eV. By using gate vs E_F values of a similar graphene gating structure work [138], we estimated x to be 125. So V is;

$$V = 180.71 * E_f^2 \quad (V) \quad (19)$$

V_g is;

$$V_g = V + V_{CNP}(V) \quad (20)$$

Also, we can easily switch to carrier density N by Eqn13.

In our numerical calculations, graphene is modelled as an effective medium which is valid as a result of extremely thin (sub-wavelength.) nature of it. We have calculated the real and imaginary part of graphene at 300K for different carrier concentrations and its corresponding gate voltages that we derived from Fermi Energy (Eqn.19&20). Also, we know the charge neutrality point of our structure as 80V by preliminary measurements (Figure 3.15). The numerical simulations were performed by using commercially available Lumerical Software package. Several calculations are done by Matlab.

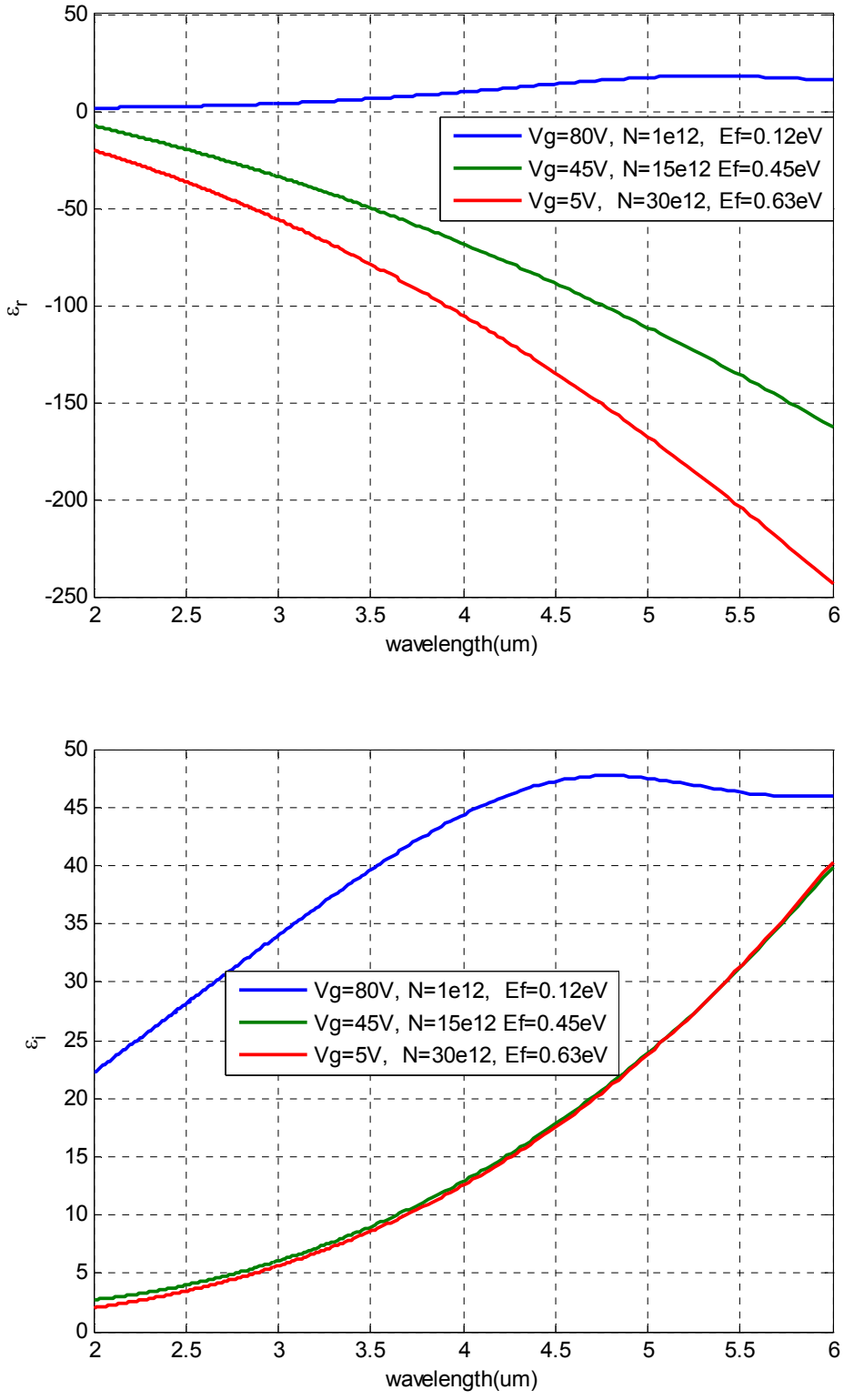

Figure 3.1: Permittivity of graphene obtained by RPA at 300K: a) real b) imaginary.

As we can see from Figure 3.1, electrical gating of graphene modulates both the real and imaginary parts of graphene's permittivity. Permittivity change is increased by increasing carrier concentration (gate modulation). Since the response of plasmonic resonance structures can be tailored by engineering the geometrical or optical parameters of the materials, we expect to obtain a shift in transmission spectrum of an graphene-hybrid SRR structure. Gated graphene has a shifted Fermi energy. The real part of permittivity has significant contribution from intraband transition which has maximum at $2E_F$ and the imaginary part of dielectric constant is dominated by interband transition [207]. Interband transition has a maximum at $2E_F$; because, all optical transitions below $2E_F$ contribute a negative susceptibility to graphene permittivity and transitions above $2E_F$ contribute a positive[138]. Therefore, when the photon energy is less than 2 times of fermi energy, the contribution from the interband transition diminishes (Pauli Blocking) and intraband transitions dominates the optical permittivity; as a result of Pauli Exclusion Principle: electron transitions are inhibited as the arrival states are occupied by more electron. In this region that covers our simulation spectrum (3-7um --> 0.2-0.6eV), real part of permittivity is dominant over the imaginary part of permittivity (Figure 3.1). Therefore, we can state that, carrier concentration dependent modulation of SRR resonance is possible as result of decrease in real part of permittivity when the carrier concentration increases.

Electromagnetic radiation cannot couple to plasmon excitation in graphene [180], but plasmon resonances can be excited by utilizing engineered plasmonic metamaterial devices called SRRs which have

dimensions much smaller than operating wavelengths. In our study, we utilized the results of previously studied SRR structures [33,81,162].

SRR is simply a ring with a gap. Figure 3.2 shows a schematic representation of SRR that we used in simulations and the fabricated structure. We directly scaled up the SRR structure, that we utilized at near infrared spectrum. (Section 2.3.2).

As we know the resonance of 148 nm single ring SRR structure is at 1.55um we can roughly scale to desired wavelength. In order to obtain a response at $\lambda \cong$ 4um, we have to start with a design of SRR length of $l = 148nm * \left(\frac{4 * 10^{-6}}{1.55 * 10^{-6}} \right) = 384nm$. Also, the same scaling is done for both the split width and width of the metallic ring:

$$l = 148nm * \left(\frac{4 * 10^{-6}}{1.55 * 10^{-6}} \right) = 384nm$$

$$d = 50nm * \left(\frac{4 * 10^{-6}}{1.55 * 10^{-6}} \right) = 130nm$$

$$w = 50nm * \left(\frac{4 * 10^{-6}}{1.55 * 10^{-6}} \right) = 130nm$$

However, we need optimization to obtain resonance exactly at 4.0 um (Figure 3.3).

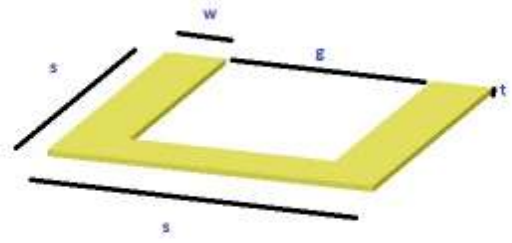

Figure 3.2: SRR model.

SRR-only optimized parameters are (for resonance at 4um):

s=530nm

g=150nm

w=190nm

a (lattice const.perpendic. to prop. dir.)=880nm

Since we changed the resonance interface of SRR by adding Silicon substrate and a buffer SiO2 layer, resonance frequency shifted and we made optimization to get resonance at 4.0um (Figure 3.3). The resonance spectrum of optimized Si+SiO2+SRR structure to resonate at 4um and its associated optimized parameters are obtained.

Si+SiO2+SRR+graphene optimized parameters are:

s=480nm

g=130nm

w=175nm

a (lattice const.perpendic. to prop. dir.)=840nm

thickness of Silicon substrate=2000nm

thickness of SiO2 buffer layer=285nm

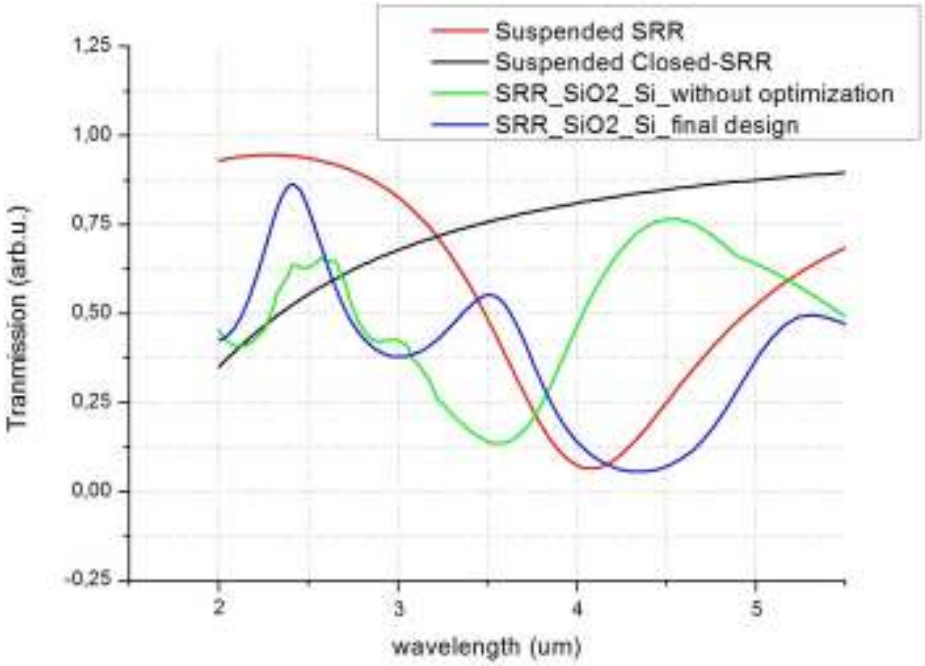

Figure 3.3: SRR and SRR-SiO2-Si spectrum.

After that, theoretical graphene permittivity results are utilized to add graphene model to our SRR+Si+SiO2 structure. Models at with different Fermi Energies (Gate Voltages) are used to simulate the gate voltage modulation of graphene-hybrid SRR structure. Graphene model is added to obtain SRR+graphene hybrid structure.

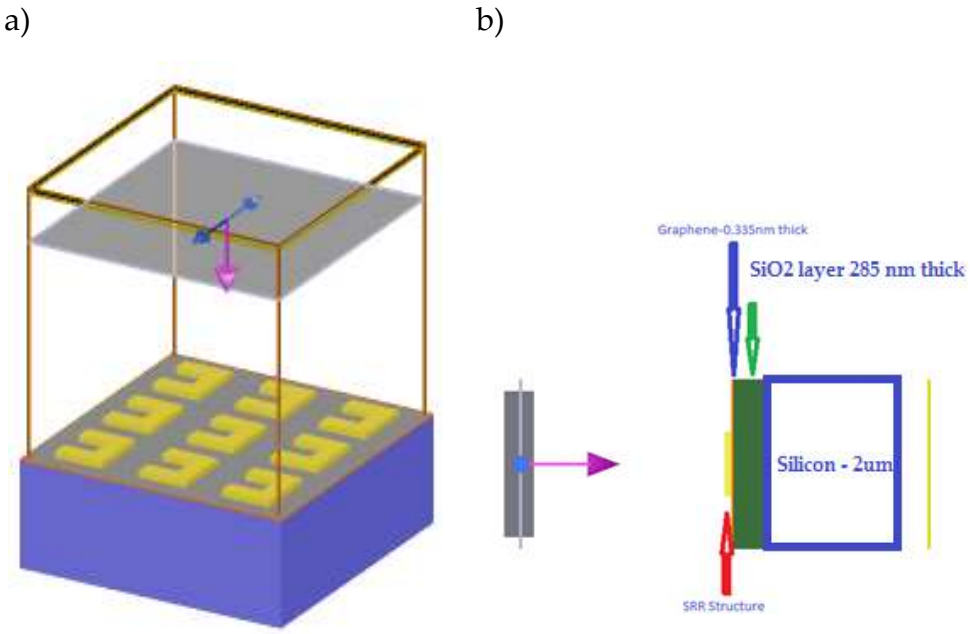

Figure 3.4: a) Schematic of graphene hybrid SRR structure, b) Device Configuration.

Permeability is 1; because of non-ferromagnetic nature of materials at IR and optical regime. Thickness of a typical graphene sample is 0.335 nm [186]. The unit cell of our metamaterial structure contains an SRR layer on top of graphene layer. The substrate under the graphene layer is Si+SiO2 Simulated transmission spectra for different gate voltages is found to be:

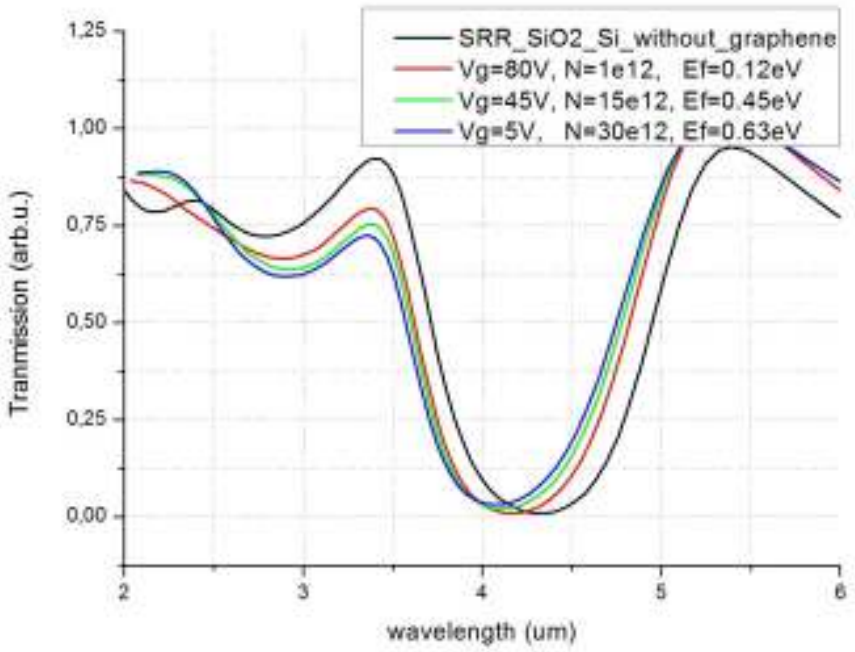

Figure 3.5: Simulated transmission spectra for different gate voltages and corresponding charge carrier concentrations.

As can be seen in Figure 3.5, graphene layer increases the resonance of SRR structure. We obtained a steeper dip when we use graphene layer in between SRR and silicon substrate. Better confinement of electromagnetic waves in atomically thick graphene layer further increases the resonance of SRR.

Sample	***Resonance (tuning range)***
SRR_SiO2_Si without graphene	4.30 um
Vg=80V, N=1e12, Ef=0.12eV	4.18 um (reference)
Vg=45V, N=15e12, Ef=0.45eV	4.12 um (2% of the resonance frequency)
Vg=5V, N=30e12, Ef=0.63eV	4.07 um (3% of the resonance frequency)

Table 3.1: Numerical results of resonances tuning for different gate voltages.

Dynamical gate control of SRR resonance using graphene is demonstrated numerically (Figure 3.5). Numerical results demonstrate electrical tuning of graphene-hybrid SRR over a broad wavelength range of 110 nm in the mid-infrared (4um) region (3% of the resonance frequency).

3.3. Design, Fabrication and Electrical Gating

The numerical simulation results presented so far confirmed the electrical tuning of plasmonic resonance by utilizing graphene. Therefore, we shall continue to make further progress by conducting experiments. The structures are fabricated and measured accordingly.

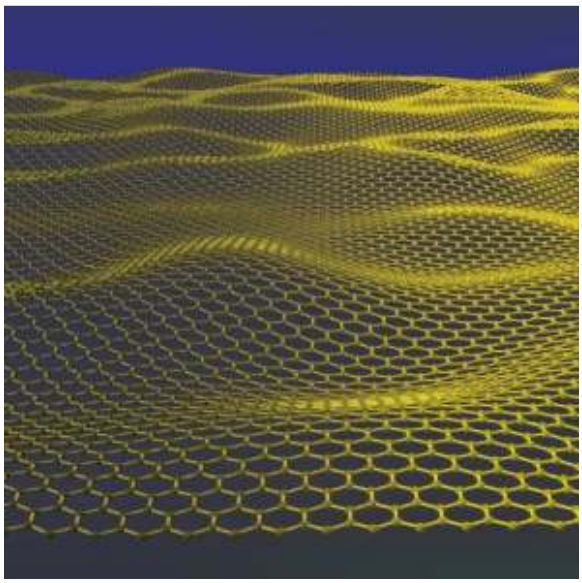

Figure 3.5 Graphene.

Graphene samples on 285 nm thick SiO2 layer and 2um thick Si is used. These samples are commercially availabe products in the market [213]. They are produced by coating graphene with CVD method on SiO2 layer which is created on thick Si substrate. Hall measurement to obtain the

mobility of graphene and carrier concentration is performed by utilizing Van der Pauw devices as shown in Figure 3.6. Average of several Hall measurements at room temperature from different regions of a 1cm x 1cm chip with different Van der Pauw devices resulted that the graphene samples have a mobility of 2286 $\frac{cm^2}{Vs}$, and $6.57x10^{12}cm^{-2}$ carrier concentration (p-doped - the majority carriers are holes). Refractive index of graphene is calculated according to Eqn.9 for different Fermi energies (hence different gate voltages).

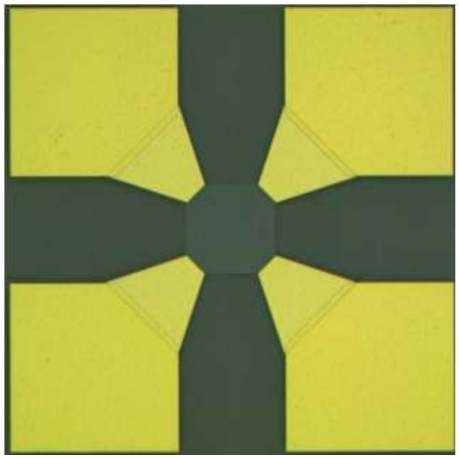

Figure 3.6 Van der Pauw device for Hall measurements.

We fabricated SRR arrays on a substrate of graphene+SiO2+Si. Fabrication is done by several different process steps. Firstly, ohmic contacts for the drain and the source with alignment marks are deposited on our graphene-SiO2-Si substrate (Figure 3.7). 20 nm titanium and 80 nm gold were deposited as ohmic metallization.

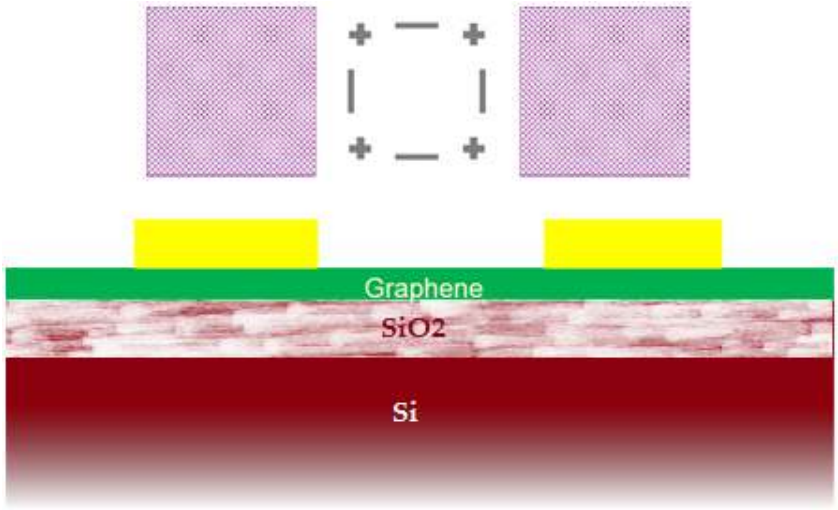

Figure 3.7: Ohmic contacts and alignment marks.

After that, the graphene layer which is not in the active region is cut out by mesa etching. By mesa etching the active area that connects source and drain is obtained, and the unwanted graphene on the chip is removed. Etching process is accomplished with ICP-RIE by exposing samples to O2 plasma for 20 seconds.

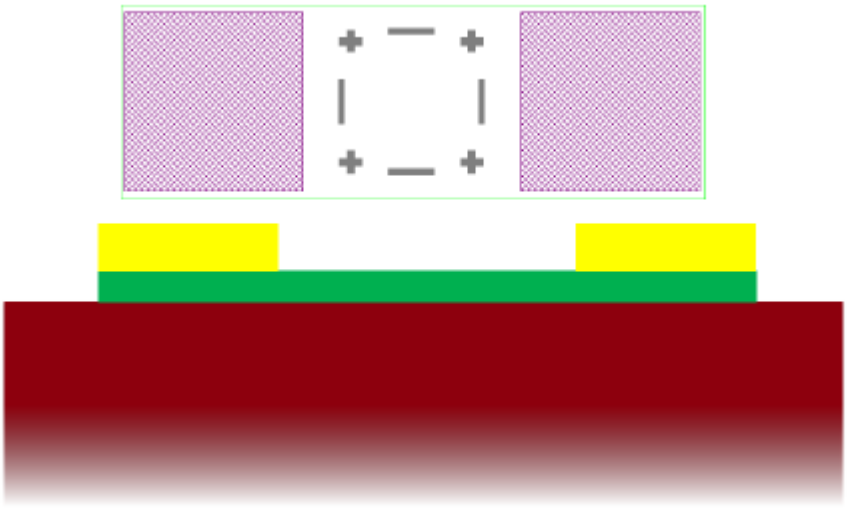

Figure 3.8: Mesa etching of active region.

SRR fabrication is done by electron beam lithography (Figure 3.9):

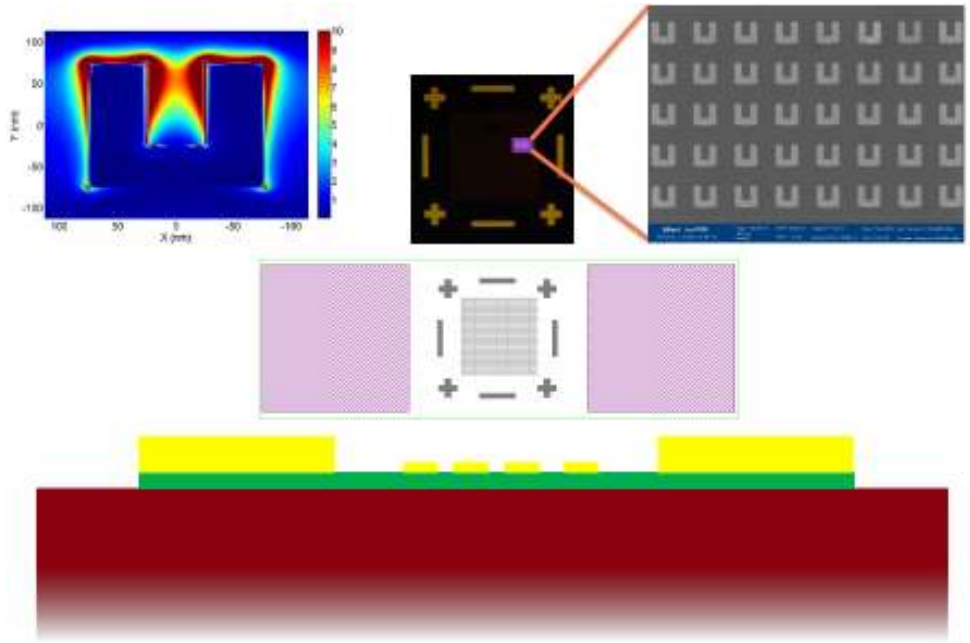

Figure 3.9: SRR fabrication.

After that interconnect metallization is done to establish connection interface for large electrical probes. 20 nm titanium and 200 nm gold were deposited as interconnect metals.

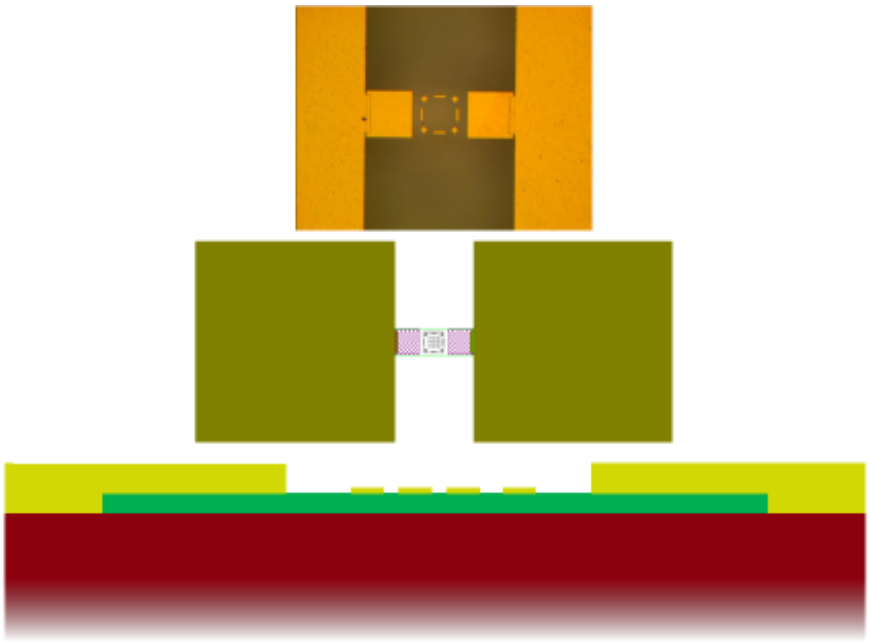

Figure 3.10: Interconnect metallization.

50 nm of SiO2 is coated on the active region in order to create a gating dielectric and then ITO is deposited on the SiO2 layer for making a gate contact.

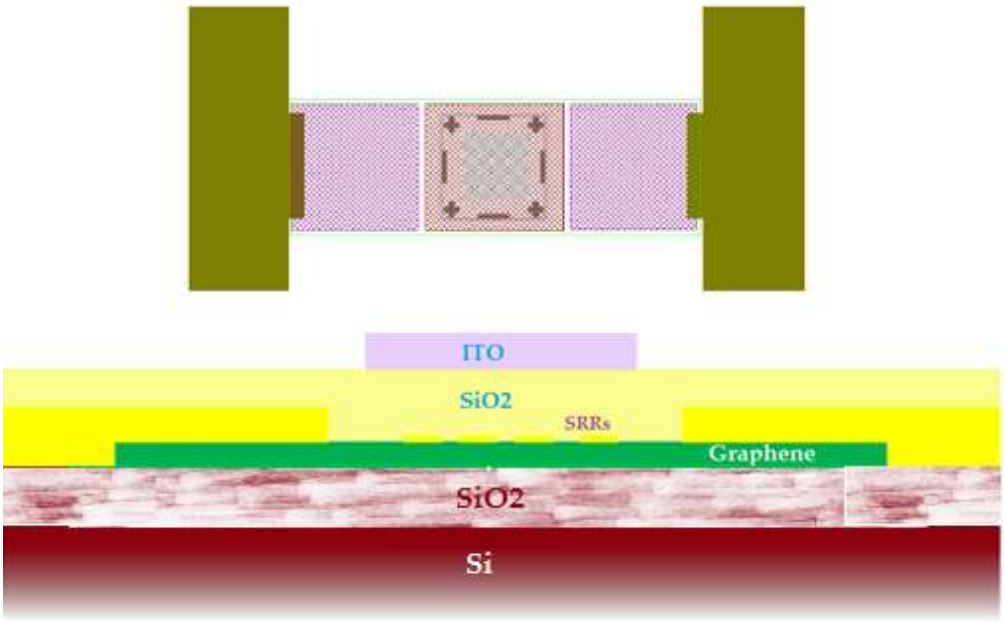

Figure 3.11: Gate Deposition.

Finally gate interconnect is deposited for gate probe and Some part of SiO2 is etched in order to reach the interconnects.

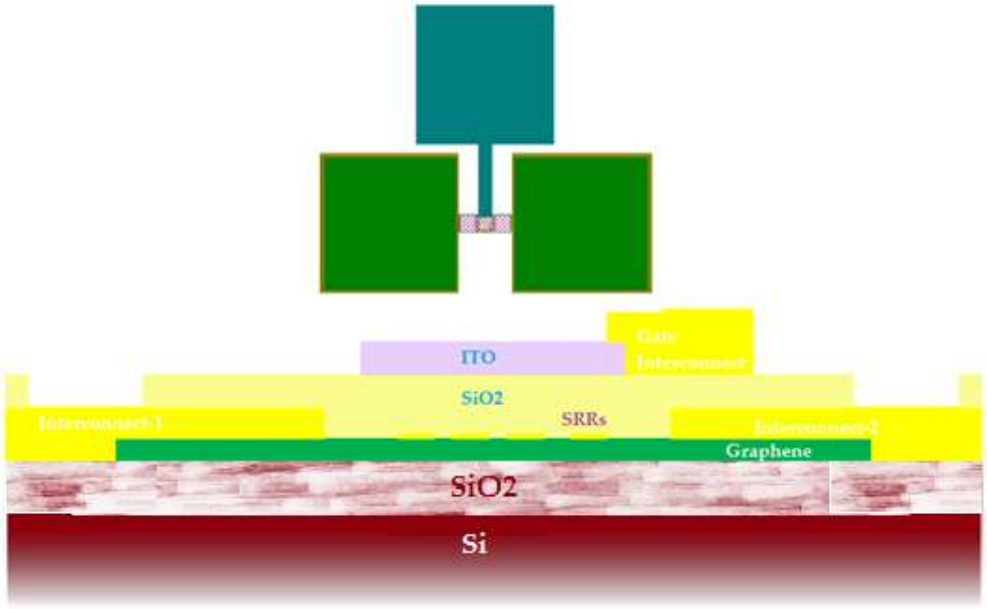

Figure 3.12: Gate interconnect deposition.

In experiments, the spectral response of structure before and after metamaterial deposition is measured by Horiba Photoluminescence System. SRR structures are fabricated by Electron Beam Lithography, metalization (2 nm Ti and 50nm Au) and subsequent lift-off processes. Scanning electron microscopy (SEM) image of af fabricated sample with plasmonic structures (SRR) on top of the graphene shees is shown in Figure 3.13.

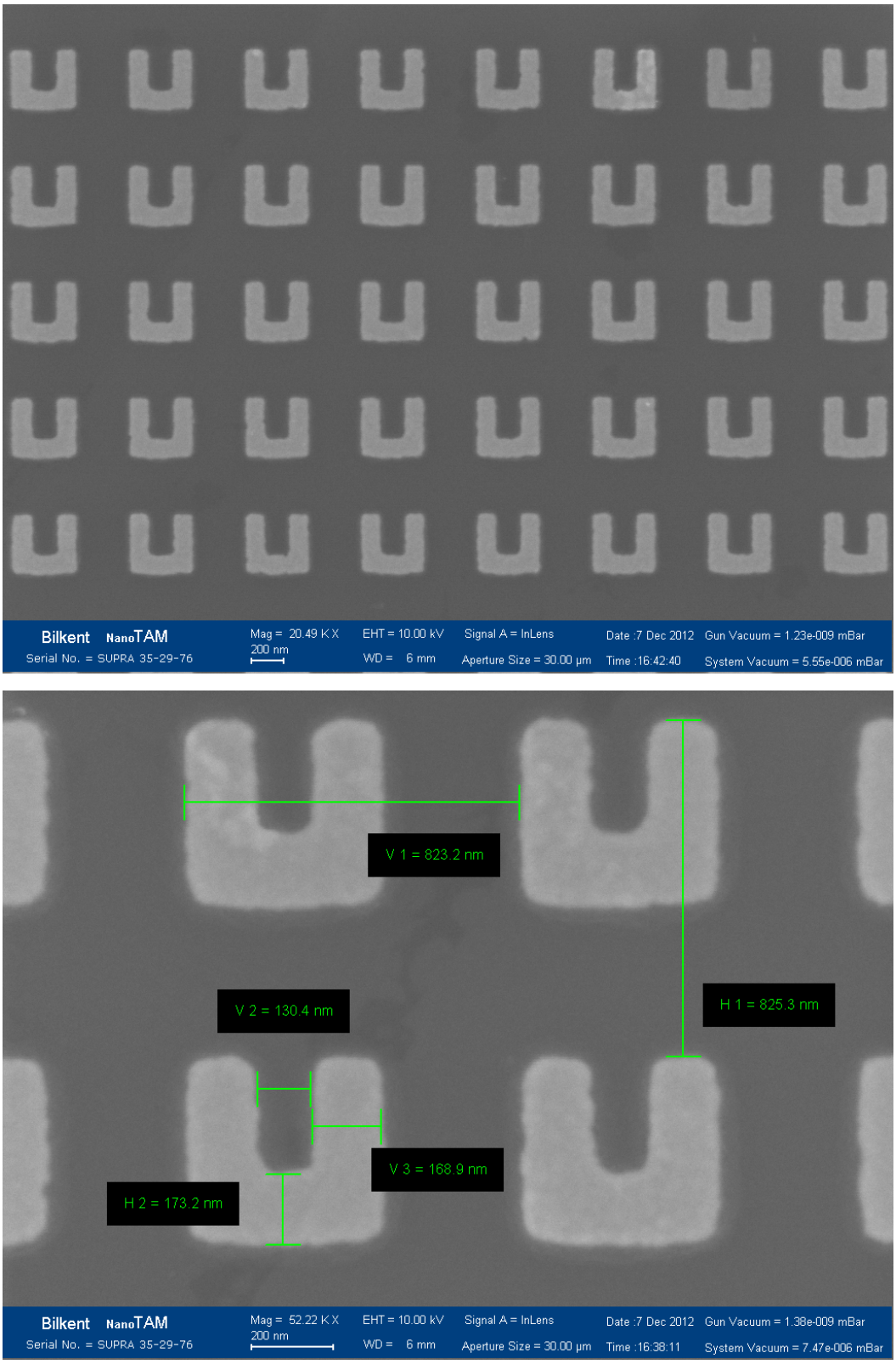

Figure 3.13: Fabricated SRR-graphene hybrid Structures.

In fabrication, we used the same graphene-SiO2-Si samples for both SRR on graphene and bare Si-SiO2 experiments. As can be seen in Figure 3.15, there are windows in first two columns, and everywhere else is covered with resist. Graphene is removed in the first two columns by O2 etch. First column is left empty for background measurements. The second column is SRR on Si-SiO2. Third and fourth columns are SRR on graphene-SiO2-Si.

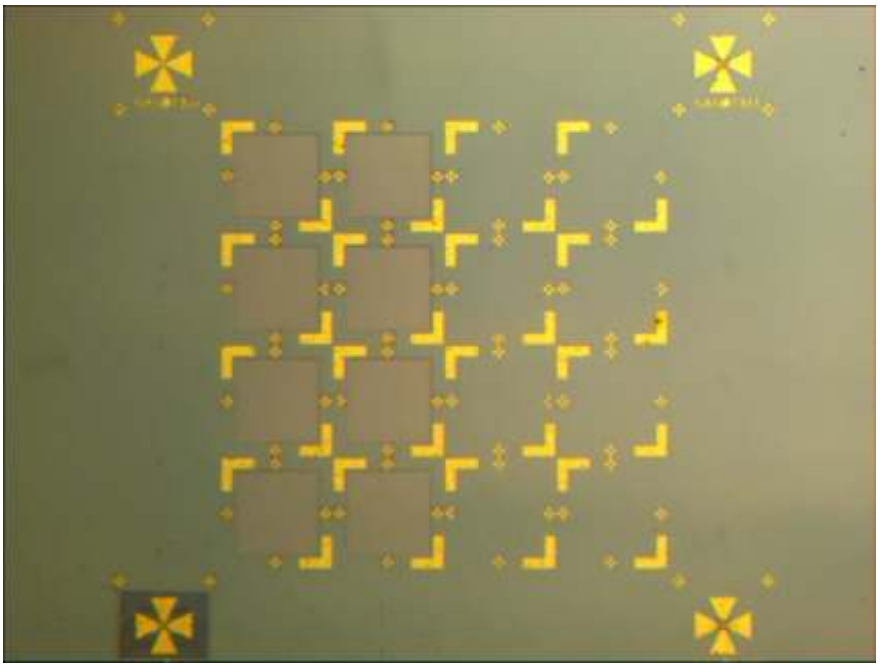

Figure 3.14: Fabricated SRR and SRR+graphene Structures.

3.4. Results

Transmission spectra of our structure are measured by Fourier transform infrared spectroscopy (FTIR) with capability of mid-infrared measurement. Aperture of 100umx100um is used for measurements. For reference, background measurements is done by removing graphene from the graphene-SiO2-Si substrate by O2 etch.

Before the optical measurements, dark current voltage measurements were performed. Charge neutrality point is observed to be at 80 V, as plotted in Fig.3.15.

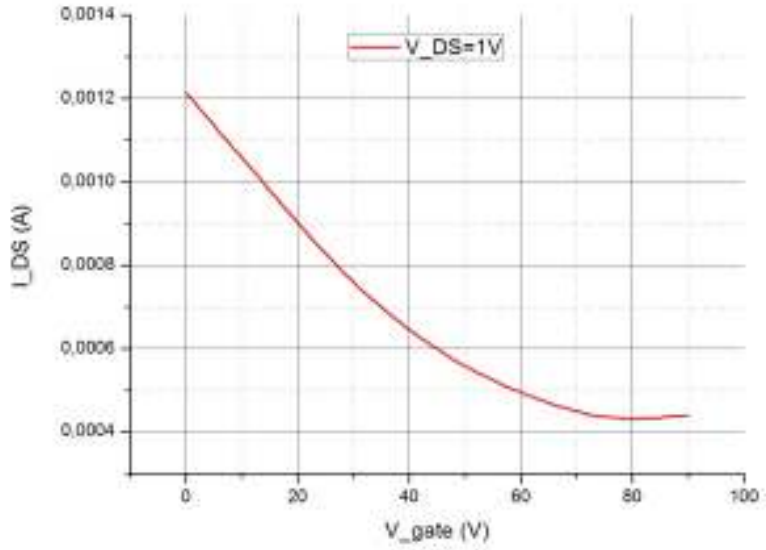

Figure 3.15: DC IV measurement.

The FTIR measurements of our sample for different gate voltages (hence Ef) are given in Figure 3.16. The transmission spectrum shows a strong resonance of SRR and also there is gate tuning as the gate voltage changes.

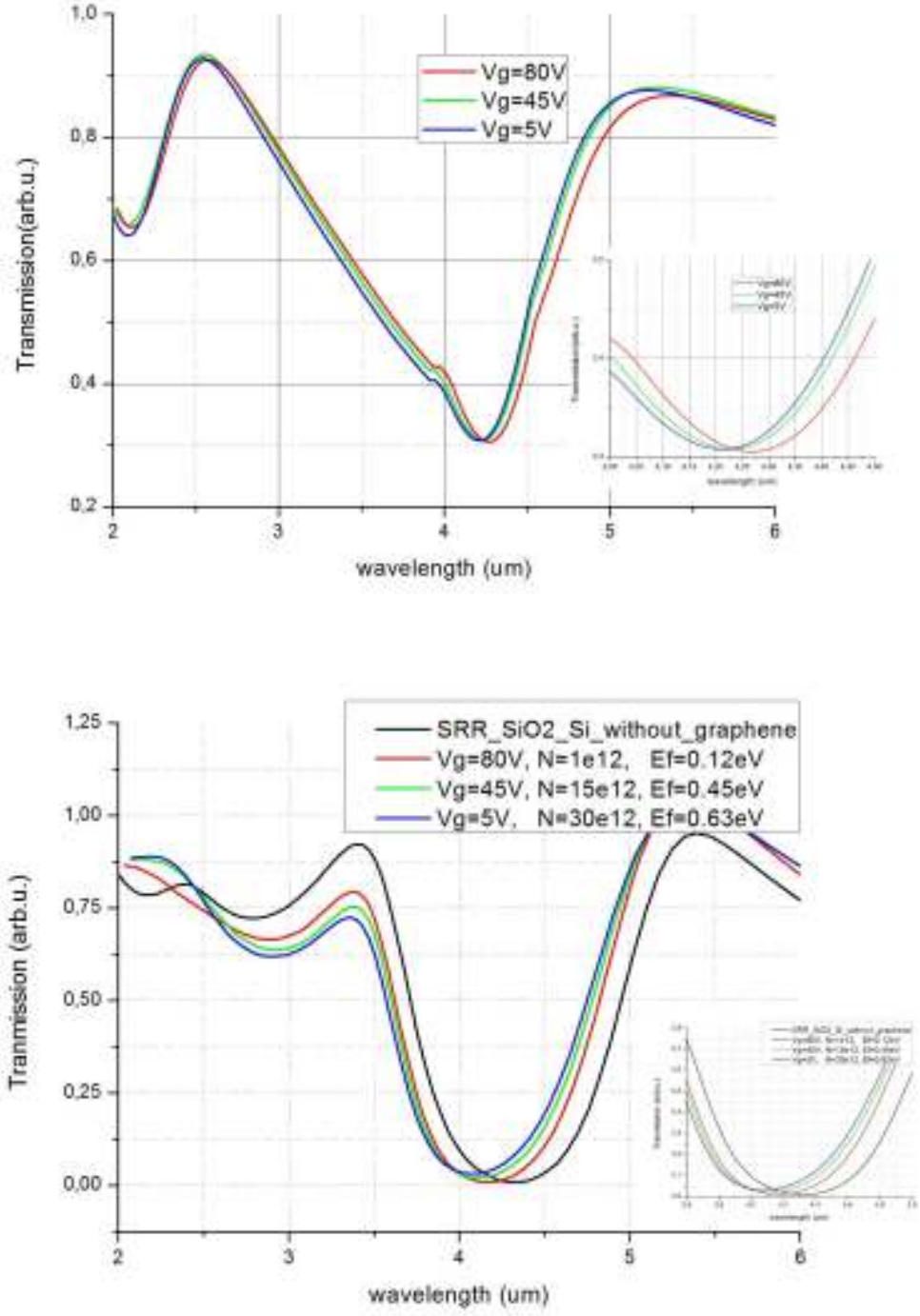

Figure 3.16: a) Measured optical transmission spectra of SRR strcutures for different gate voltages (Inset is zoomed graph). b) Simulated transmission spectra for different gate voltages and corresponding charge carrier concentrations.

Dynamical gate control of SRR resonance using graphene is demonstrated numerically (Figure 3.5) and experimentally (Figure 3.16). Table 3.2 summarizes the gate tuning results of simulations experimental measurements.

Sample	*Resonance (Sim.)*	*Resonance (Exp.)*
Vg=80V	4.18 um	4.27 um
Vg=45V	4.12 um	4.23 um
Vg=5V	4.07 um	4.20 um

Table 3.2: Resonances for different gate voltages (Sim. and Exp.).

In our simulations, we demonstrate electrical tuning of graphene-hybrid SRR over a broad wavelength range of 110 nm in the mid-infrared (4um) region (3% of the resonance frequency). Tranmission spectrum shows that resonance wavelength increases as the gate voltage increases; because gate voltage increase causes real part of permittivity to increase as a result of charge carrier concentration increase. Experimental results demonstrated a resonance shift of 70 nm shift. Electrically controllable plasmonic resonances of nano-rods on graphene have been shown before [159, 207] with very limited tuning ranges. However, we achieved electrical modulation of SRR resonance which is the first demonstration of electrical tuning of graphene based SRR in the contemporary literature according to our knowledge. There may be several reasons behind the lower tuning range of experimental results. Since the plasmonic (metallic) structures are in touch with graphene, they effect the graphene carrier concentration by additional electron doping. Therefore, we expect a deviation from the numerical results as a result of change in Fermi Level. One other reason is the fabrication errors that may cause deviation from

the numerical results. Surface roughness of the substrate and defects in graphene can cause a deviation from numerical results as a result of unexpected change in carrier concentration. Also, simulation parameters that we used to mimic the electrical response of graphene are not perfect. There are various approxmiation that we used in calculations which may be effective in our experimental results. Last but not the least counterproductive reason is the leakage from gate contact that we used in the experiments. Since we did not want to block the light transmitted light passing through plasmonic structures and graphene, we used a gate contact which does not covers the active graphene region. Therefore, leakage in gate contact might be major the source of less tuning compared to simulations. Achieving a greater degree of plasmonic resonance tuning, by understanding the interaction of graphene with metal structures, decreasing the gate leakage and making better electrical models for graphene, is an ongoing work.

3.5 Summary

In summary, we demonstrated that graphene can be used to electrically control the resonance of plasmonic structures like SRRs in the mid infrared spectrum. A novel approach of gate tuning of SRR resonance is demonstrated by utilizing promising properties of graphene for plasmonics. Also, electrical properties of graphene is investigated. Fabrication of electrically gated graphene based plasmonic structures are realized. We obtained a frequency shift by putting graphene layer between substrate and SRR layer. Moreover, we obtained a better resonance (steeper dip at resonance) which is a result of better confinement of resonance plasmons in monolayer graphene.

Electrical tuning of plasmonic resonance by using graphene with varying gate bias is achieved both experimentally (70nm) and numerically (110nm). This effect is studied with theoretical modeling and confirmed experimentally. Electrically controllable plasmonic resonances of nano-rods on graphene have been shown before with very limited tuning ranges[159,207]. But there is no demonstration of strong plasmonic resonance like SRRs before. Therefore, we achieved electrical modulation of SRR resonance which is the first demonstration of electrical tuning of graphene based SRR in the contemporary literature according to our knowledge.

As a future work, we will try to achieve a greater degree of plasmonic resonance tuning, by understanding the interaction of graphene with metal structures, decreasing the gate leakage and making better electrical models for graphene.

Graphene based nanophotonics is an intense research due to a wide range of applications of this phenomenon. As SRRs are already being realized at optical frequencies [82], it is possible to use these SRR-graphene-based structures for new optical applications such as novel photovoltaic, ultrafast miniature photodetectors and optical switches. Results of this chapter show that graphene is a good candidate to pave the way of tunable optical electrical filters, modulators, compact photonic devices. The research for novel applications of graphene on plasmonic devices will be a future work for us to conduct.

Chapter 4

Three Dimensional Nanostructures

4.1. Introduction

Photonic metamaterials are subjected to an intense research till they are introduced to represent a new world of novel optical devices. Mie resonances of the nanoscale building blocks are the main reason behind peculiar optical properties of photonic metamaterials. They are regarded as the best candidates for designing novel sensors, solar cells, nano-antennas etc [160,163,166,175,184,191].

Designing novel photonic devices needs novel fabrication techniques. Contemporary nanofabrication processes are mostly based on thin film technology which is 2D fabrication technique. However, 3D nanofabrication offers a number of advantages over those based on thin film technology like increasing the surface area of nanostructure to enhance sensitivity of sensors, improving efficiency of solar cells etc.

Obtaining a bulk 3D metamaterial is the ultimate goal of scientists. Also, definition of 3D metamaterial is controversial too. The number of layers

required reach the bulk 3D regime depends on the coupling between adjacent layers - interlayer spacing [26]. Some theoretical works suggests that at least four functional layer is required if the distance between adjacent layer is small [154]. Optical behavior converges after the number of adjacent layer increases more than four.

Direct Laser Writing is the 3D counterpart of 2D electron beam lithography. Femto-second laser pulses are focused into a small volume of photoresist. Two-photon absorption ensures only a nanoscale volume of photoresist is sufficiently focused by light. Computer aided scanning devices are utilized to manufacturing patterns in a photoresist by utilizing piezoelectric actuators with lateral resolution up to 100nm [192]. 100nm is very low feature size compared to contemporary electron beam lithography systems which have resolution down to 10nm. However, a novel femto-second laser system is utilized to access resolution much lower than 100 nm [208].

4.2 Femto-second Laser Writing

The field of photonics has increasing interest for last decades. There are variety of photonics devices designed by relying on the planar 2D lithography techniques. However, fabrication technology needs to develop towards 3D architectures. Patterning nanoscale metals in 3D is very difficult. However, femto-second laser direct writing or multiphoton absorption lithography has emerged that solves most of the problems of 3D nanoscale metallic writing [209].

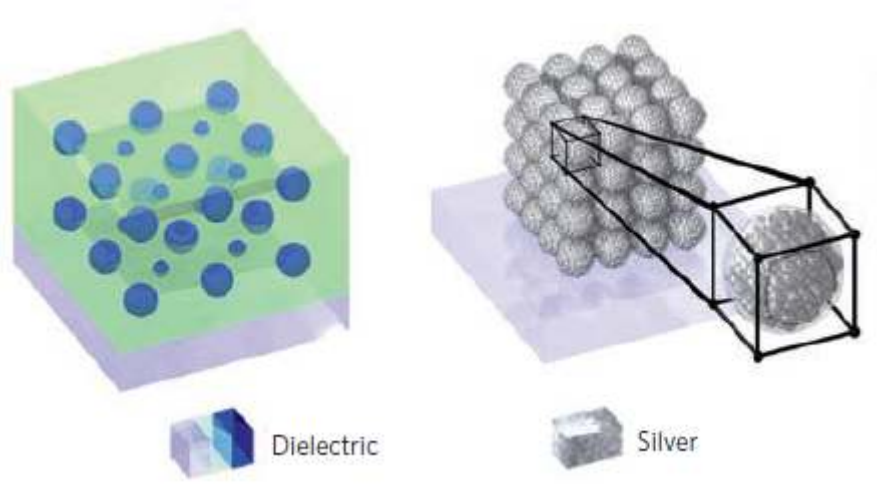

Figure 4.1: 3D patterns composed of (a) dielectric spheres and (b) metallic spheres [26].

Femtosecond-laser-direct-writing technique is used for creating three-dimensional (3D) patterns in polymers and glasses. Patterning in polymers and glasses is relatively easy compared to patterning metals in 3D. Patterning metals in 3D is a challenge. Standard 2D nanofabrication technique requires combination of several nanofabrication tools and several material processing steps. For instance, we need several sample exposure, sample development, metal deposition and metal liftoff procedures to complete ultraviolet lithography and photolithography. This steps are repeated multiple times to design a 3D structure. Complexity and difficulty of stacking and aligning multiple layers limits the practical implementation of novel 3D metamaterials. Here, a method to fabricate silver nanostructures embedded inside a polymer matrix using a femto-second laser centered is utilized. This novel method enables the fabrication of novel photonic devices which are not feasible using other techniques. Potential applications of 3D direct laser writing are negative index metamaterials, cloaking and perfect lenses at optical regime.

Non-linear photonic interaction between femtosecond laser pulses and polymer structure makes nanoscale fabrication possible. When the ultra-short laser pulses centered at 800 nm are focused into a small volume, they are absorbed by the polymer structure and multiple photons can converge in time and space to collectively bridge the target's energy gap and create an electronic transition [208]. Multiphoton absorption leads the material change and makes some region of the polymer structure metallic. A direct writing technique [210] for patterning a nanocomposite material with disconnected silver nanostructures in a polymer matrix is used for 3D writing. Nanoscale structures in the form of bulk material instead of 2D surface structures can be fabricated using this technique.

Femto-second laser writing was limited to the patterning of dielectric media. Recently advances have been made in direct writing of metals [53, 166]. One of the methods for creating 3D metal nanostructures is to utilize a metal deposition step for direct laser writing by coating 3D polymer structures [124,125] or by filling volumetric voids [128]. However, this approach does not let the creation of disconnected metallic structures. 3D metallic array composed of disconnected metallic structure is needed to obtain 3D photonics metamaterials [129,130]. Here we utilized a silver growth technique for femto-second laser direct writing of 3D nanostructures.

A chemical mixture of a 0.16M AgNO3 solution with polyvinylpyrrolidone (PVP) as support polymer and water (H20) as solvent is used. PVP is used as polymer because it helps to control nanoparticle synthesis [134,135]. Solution of AgNO3, PVP and H2O is

coated onto a substrate and baked to create a polymer matrix doped with silver ions [208].

A femto-second laser system is utilized to pattern silver nanodots in PVP-silver solvent (Figure 4.2). In this system, microscope objective with numerical aperture of 0.8 is used the focus the femtosecond laser pulses into PVP-silver solution. 11 MHz ultrafast Ti:sapphire laser system is used as a source and commercially available high precision and long travel 3-axis translation stage is used for scanning the sample in 3-directions. Also, an acoustic modulator shutters the laser pulses to control the exposure.

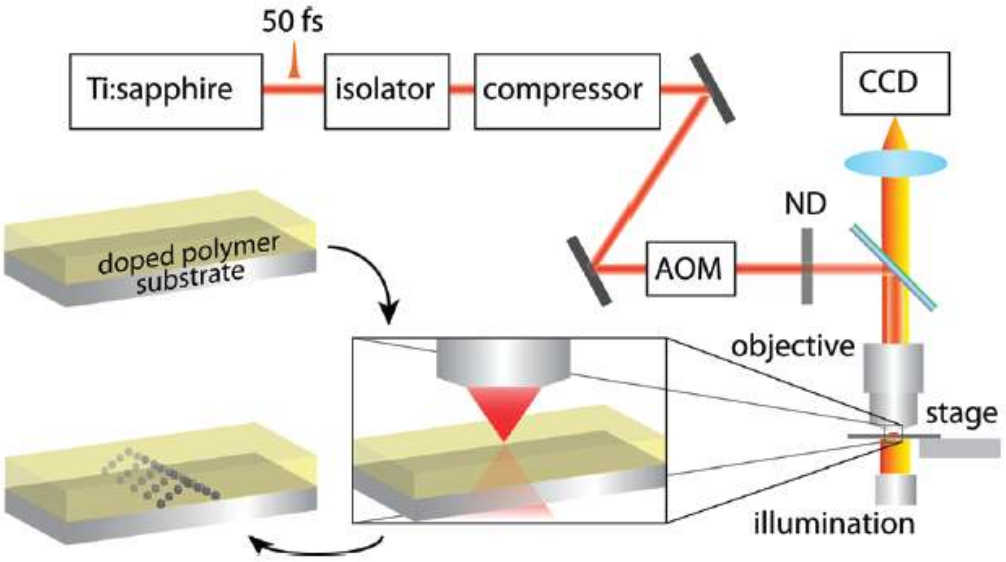

Figure 4.2: Schematic of the fabrication process [208].

When the laser is focused inside nanoscale volume, nonlinear light matter interactions occurs and metal-ion photoreduction process makes silver nanoparticle growth (Figure 4.3). Size of the silver nanodots can be varied by changing the exposure.

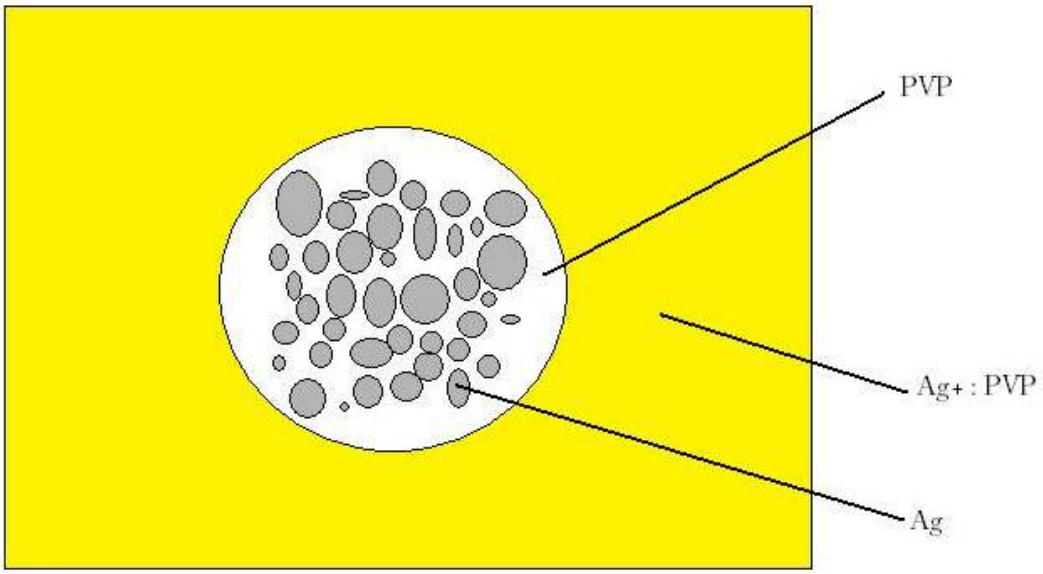

Figure 4.3: Material Schematic.

After the writing process, we utilized transmission electron microscopy (TEM) to determine the silver nanodots nucleation (Figure 4.4)

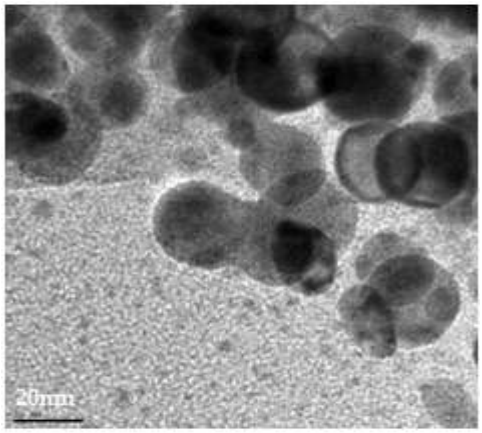

Figure 4.4: TEM image of fabricated silver nanodots.

Silver nanodots features of 10 nm diameter is obtained by direct laser writing. Diffraction experiment of fabricated nanodot array (Figure 4.5) confirms that silver nanodots are grown in areas irradiated by femto-second laser.

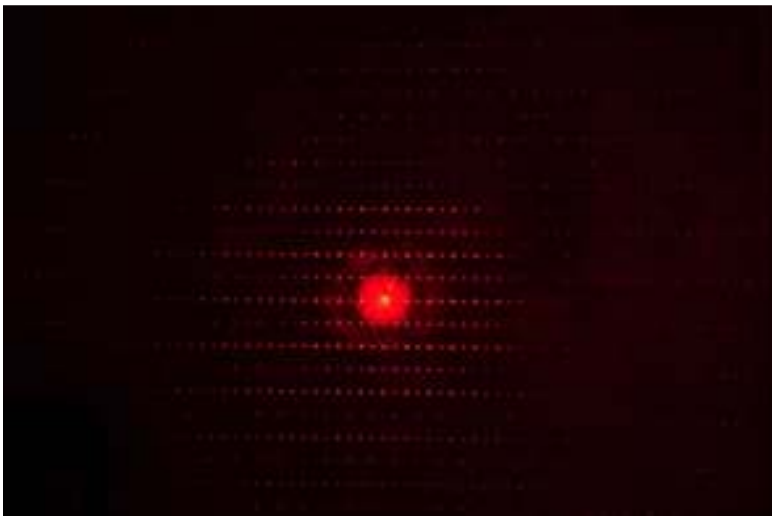

Figure 4.5: Diffraction experiment by shining a laser beam to the square lattice pattern.

Nanoscale fabrication of metals has many applications ranging from optical or biological sensors to solar cells. Therefore, metallic fabrication in nanoscale is very important. Since 3D metamaterials offer a new world of applications, 3D metallic nanoscale fabrication is very important too. Multiphoton absorption is utilized by femto-second laser writing into a dielectric PVP material. This technique is a good candidate to creation of 3D metamaterials which was used to be limited by current fabrication techniques. We will utilize this technique to further investigate 3D nanoscale structures that may be used as a base for optical 3D metamaterials.

4.3 Random Alignment, Random Radius Silver Nanodots

Characterizing silver nanodots is the first step towards designing 3D optical metamaterials; because basic building block of a femto-second 3D

direct laser system is a dot. Also, nanodots have peculiar properties which are under investigation.

Random arrays of silver nanodots are created and simulated for different filling factors. Also, each filling factor data is the average of 20 different simulations. A script is written to create silver nanodots at random positions for creating a specific filling factor which is defined as:

$$\text{Filling Factor (F)} = \frac{Total\_Volume\_of\_Silver\_Nanodots}{Total\_Volume(Silver\_Nanodots + PVP)}$$

Both the diameter of the spheres and alignment is changed for each simulation and same filling factor data are collected to get the average of these data. To design a lattice of silver nanodots, radius of all dots are chosen randomly ranging from 3 nm to 7 nm (1 nm variations) at each simulations. Radius of each dot is randomized too which makes our simulation completely random in sizes which mimics the real fabrication process.

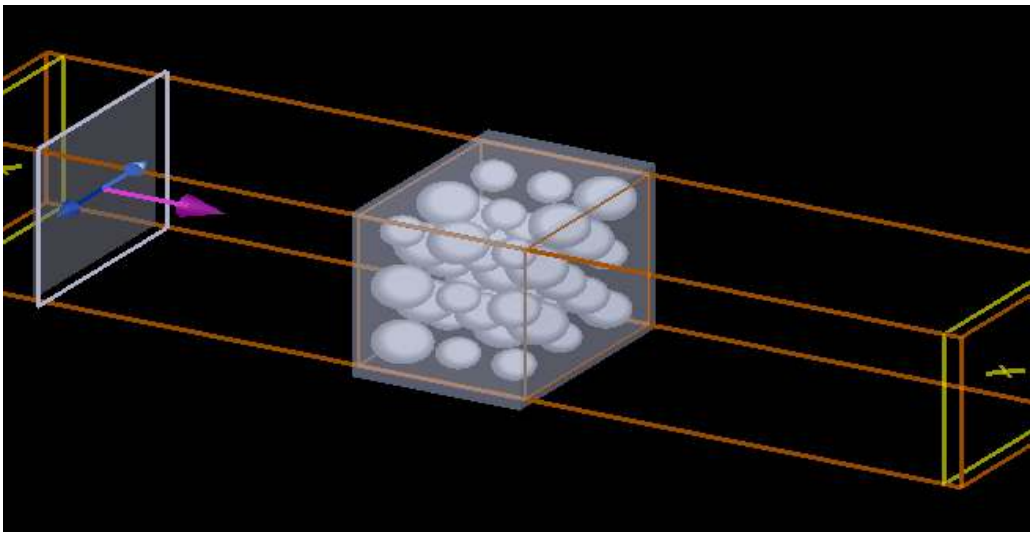

Figure 4.6: Random silver nanodots radius ranging from 3 nm to 10 nm.

One of the most common characterization tools for the metamaterial structures is the retrieval procedure [64,68-70,211]. We used Smith et al [152]' s retrieval analysis to obtain constitutive parameters. Each data is the average of ten different samples with same filling factor. The effective parameters (ε, μ) of the metamaterial are calculated by retrieval analysis. The amplitude and phase of the transmission and reflection data are used to retrieve the real and imaginary parts of the effective permittivity, permeability, and a refractive index. The retrieval approach outlined in Ref. [152] is used for the retrieval analysis in this work. The advantage of this procedure is the selection of the correct branch of the effective refractive index and effective impedance. The ambiguity in the determination of the correct branch was resolved by using an analytic continuation procedure [95].

The effective parameters of silver nanodot structure is retrieved by using the amplitudes and phases of transmission (S_{21}) and reflection (S_{11}) data. The S-parameters are related to refractive index and impedance by [69]:

$$S_{11} = \frac{\left(z - 1/z + 1\right)\left(1 - e^{-j2nk_0 d}\right)}{1 - \left(z - 1/z + 1\right)^2 e^{j2nk_0 d}} \tag{4.1}$$

$$S_{21} = \frac{\left(1 - \left(z - 1/z + 1\right)^2\right)e^{jnk_0 d}}{1 - \left(z - 1/z + 1\right)^2 e^{j2nk_0 d}} \tag{4.2}$$

where d is the thickness of homogenous slab of structure under test and k_0 is the free space propagation constant.

The refractive index (n) and impedance (z) are obtained by inverting the Eqs. (4.1) and (4.2) as [23];

$$z = \pm\sqrt{\frac{(1+S_{11})^2 - S_{21}^2}{(1-S_{11})^2 - S_{21}^2}} \tag{4.3}$$

$$e^{jnk_0 d} = X \pm j\sqrt{1-X^2} \tag{4.4}$$

where $X = \frac{1}{2S_{21}\left(1-S_{11}^2+S_{21}^2\right)}$.

The effective permittivity (ε_{eff}) and permeability (μ_{eff}) are obtained from the effective index and impedance by using the relations, $\varepsilon = \frac{n}{z}$ and $\mu = nz$.

In the retrieval procedure, a 3-by-3 silver nanodot array structure with random radius ranging from 3 nm to 7 nm is employed. The effective permittivity and permeability values were then retrieved from the transmission and reflection coefficients.

Real part of the refractive index shows us that as the filling factor increases, refractive index increases too. However, when the filling factor reaches 74% (each dot touches the neighbor dot) which is the highest atomic packing factor (APF) of Face-Centered-Cubic (Structure), silver nanodots' characteristics converges to bulk silver characteristics (Figure 4.7).

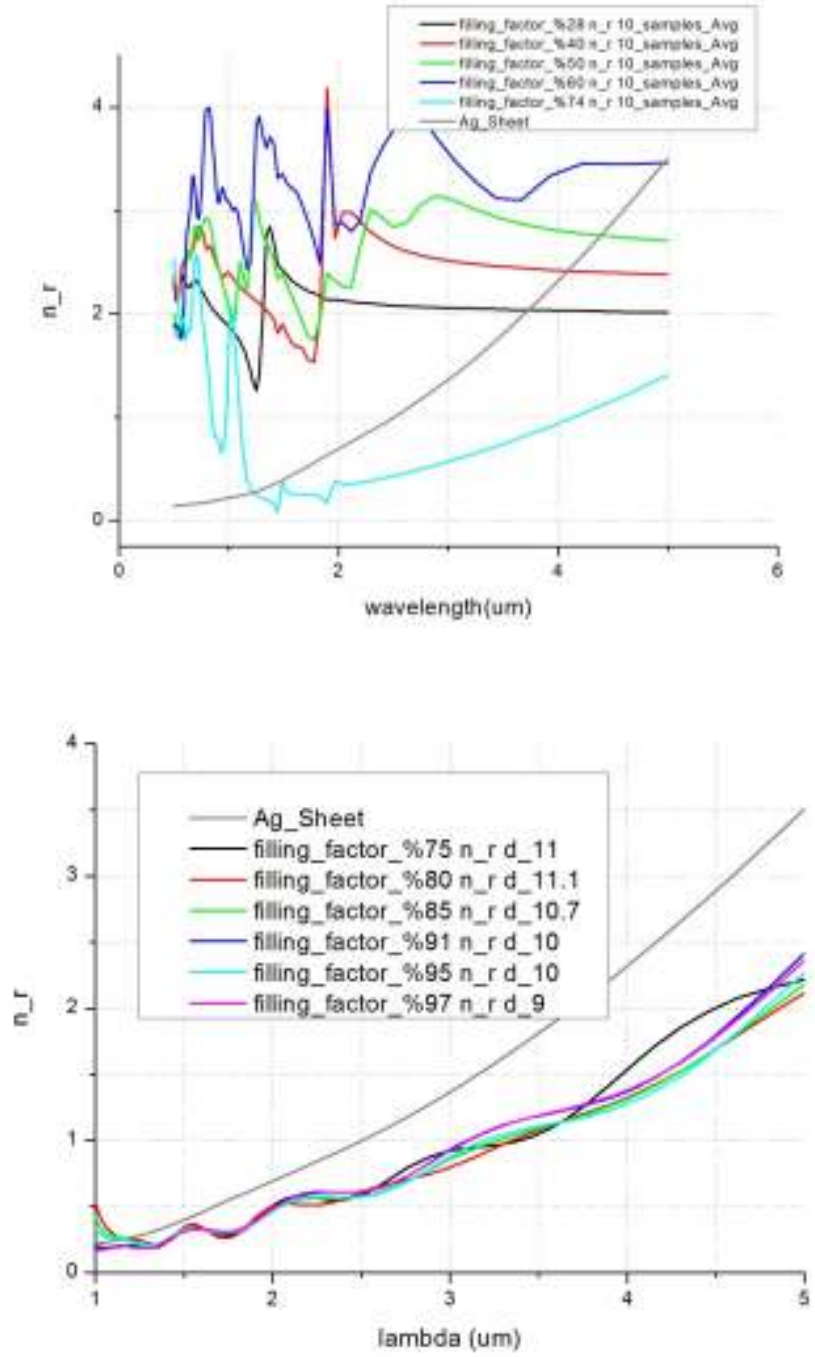

Figure 4.7: Real part of refractive index.

Touching silver nanodots make the cross-coupling relation more different then gapped samples. When the silver dots touches (for 74% case), the retrieved parameters become similar as Ag_sheet which is different for gapped samples (lower filling factor samples).

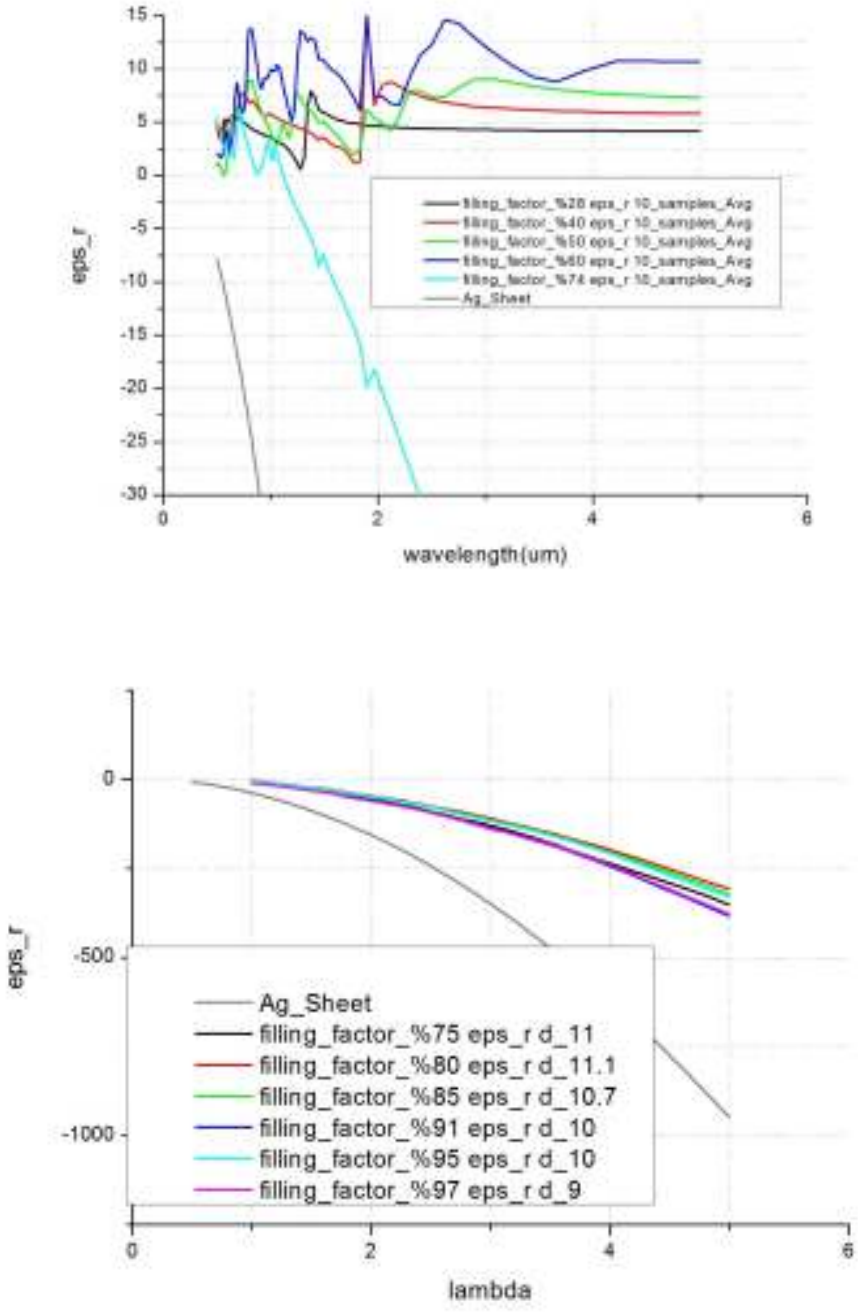

Figure 4.8: Real part of permittivity.

As the filling factor increases, the coupling between nanodots increases and therefore, deviates from smaller filling factor samples. Since there is no magnetic excitation, real part of permeability is converged to 1 for all the combinations. Epsilon deviation is the source of refractive index deviation. Therefore, coupling is electrical not magnetic.

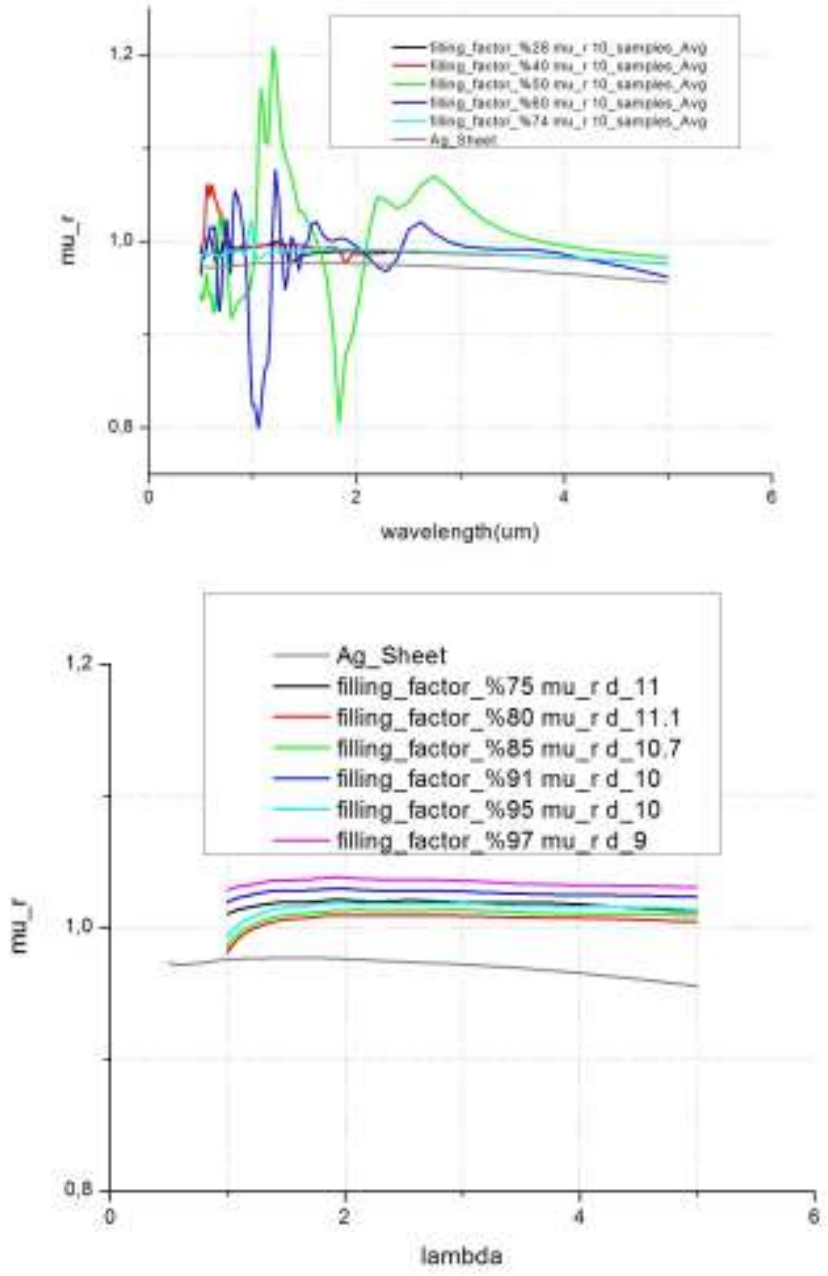

Figure 4.9: Real part of permeability.

Loss for Ag sheet is more effective. Therefore, imaginary part of Ag is very high compared to silver nano-dots which are coupled each other.

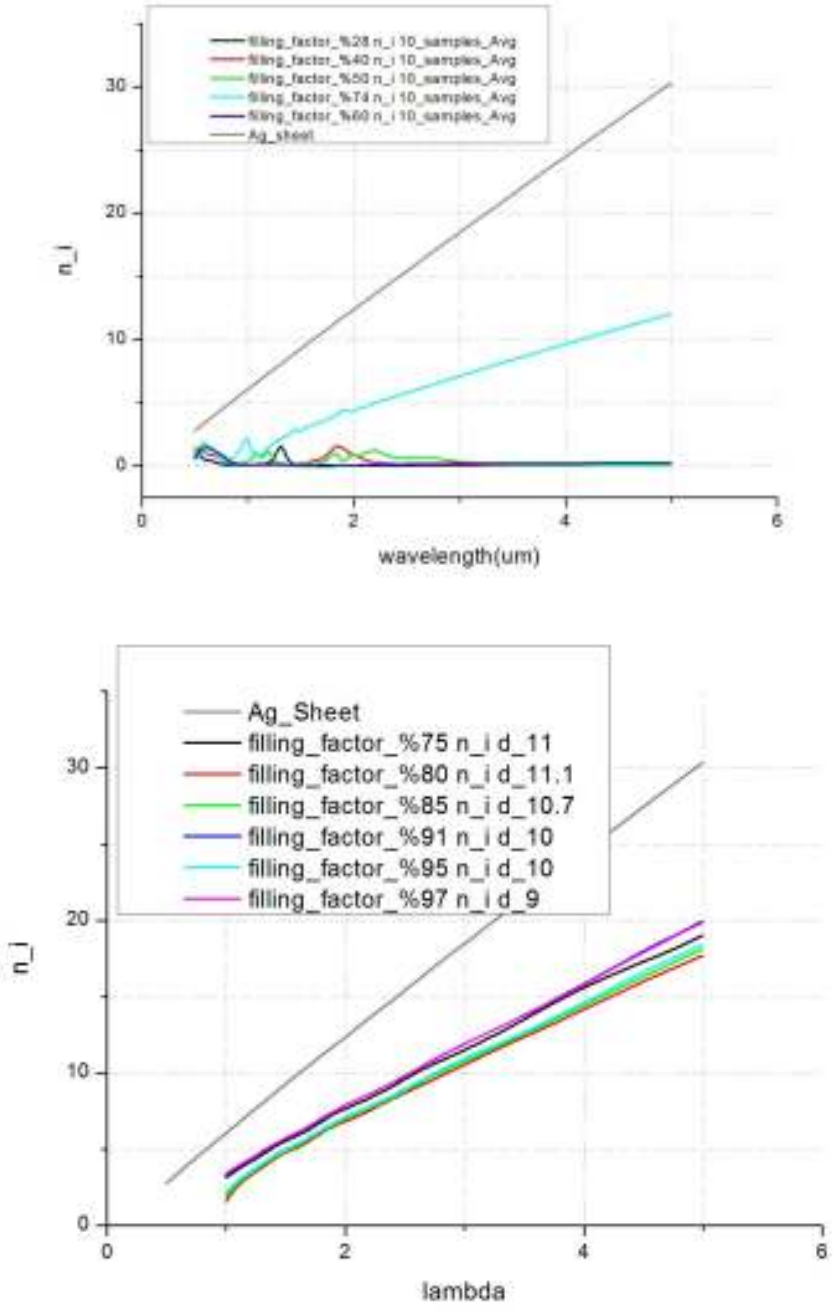

Figure 4.10: Imaginary part of refractive index.

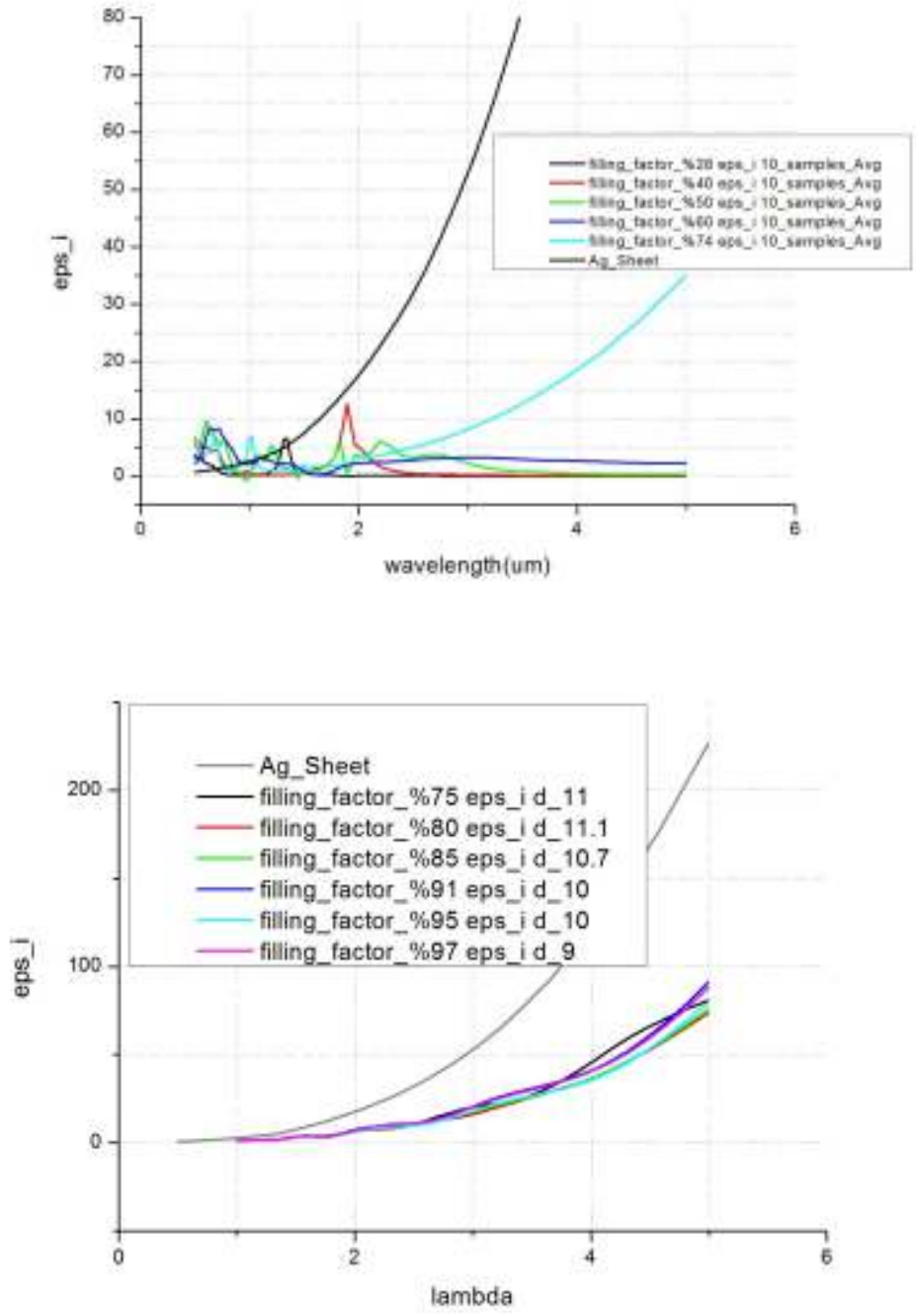

Figure 4.11: Imaginary part of permittivity.

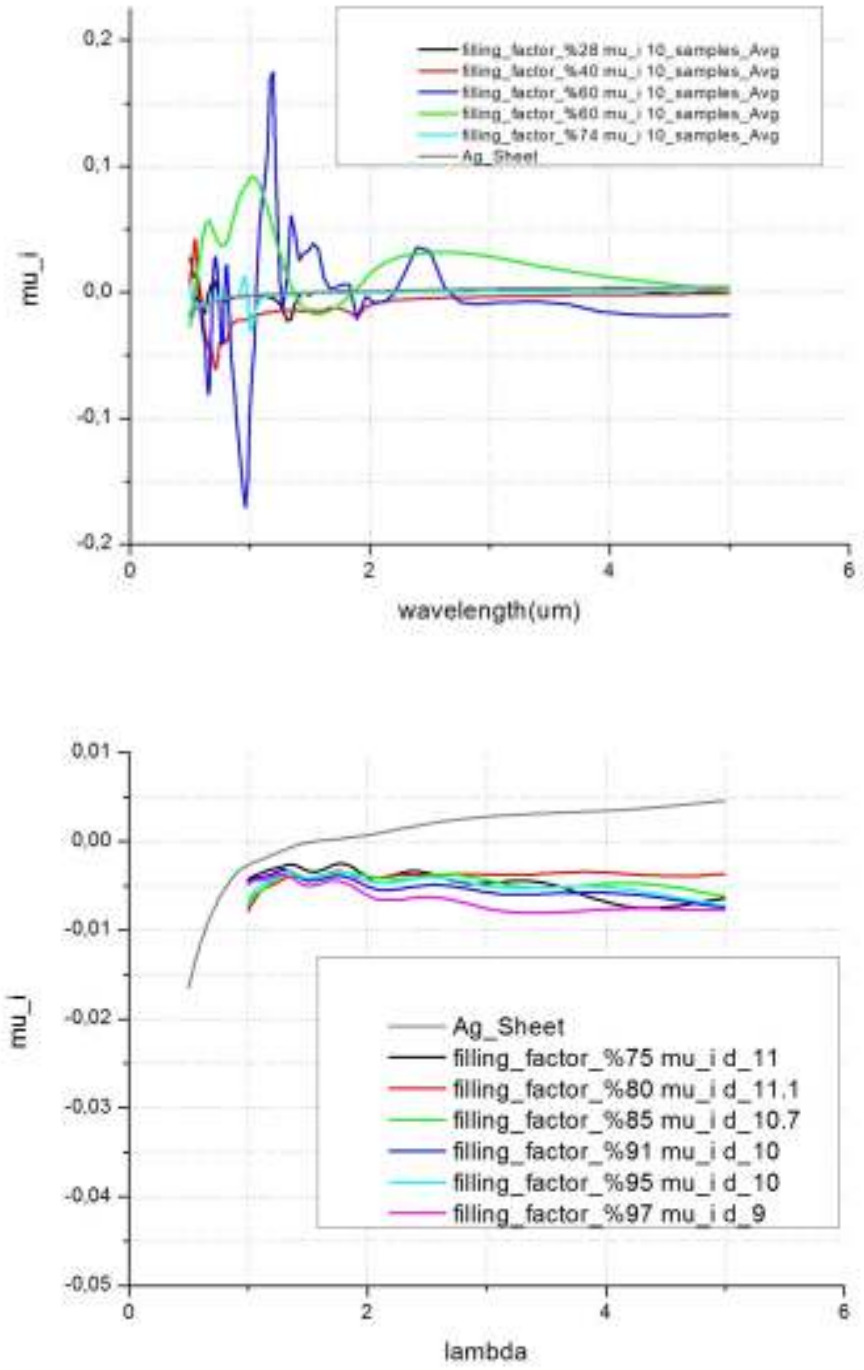

Figure 4.12: Imaginary part of permeability.

In the above simulations, 10 different random trials for same parameters gave very similar results. The suggested gapped structures show very

different characteristics then Ag plate because of inter coupling between the gapped dots. Also, the filling factor increase is correlated with the refractive index variation, yet permeability is 1 after 1um for all the combinations. As the filling factor increases, the coupling between nanodots increases and therefore, deviates from smaller filling factor samples. Also, there is a threshold limit of 74% in which the random allignment of spheres behaves almost likely a bulk Ag sheet.

4.4 Summary

In summary, simulation results indicate that gapped dots' intercoupling deviates their optical characteristics from bulk silver significantly. Also, as the filling factor of the FCC lattice increases, the refractive index increases as a result of increase in effective permittivity.

In this chapter, we investigated 3D fabricated nanodot array structure operating at optical frequencies. Simulations confirmed a deviation from bulk silver. In addition, increased index with increased filling factor till a certain threshold is verified by using the retrieval procedure. After the threshold random nano spheres behave like bulk Ag sheet. Since the simplest building block of a 3D manufacture optical metamaterial is a simple dot, we investigated the optical characteristics of nanodots here to write more complex plasmonic devices like SRRs in the future. Femto-second laser writing is a promising tool for designing optical novel devices faster and cheaper. The research for novel metamaterial designs by utilizing femto-second laser writing will be future work for us to conduct.

Chapter 5

Conclusions and Future Work

The work of this dissertation is motivated by the need for novel plasmonic devices for photonics. Since photonics is the flourishing technology ranging from communication to life sciences, more plasmonic devices that can enable new technological breakthroughs at photonics should be suggested. In this dissertation, the transmission and propagation characteristics of novel metamaterial-based plasmonic structures are investigated; and new approaches for the design of novel devices are proposed. This chapter includes a concise summary of the results that are achieved in this dissertation and possible future is mentioned.

In the second chapter, a detailed analysis on the theoretical background of metamaterial based plasmonics is provided. An analytical description of the constitutive parameters of metamaterials is given with theory. In

addition, we demonstrated several novel structures to increase the transmission through a sub-wavelength aperture. Enhanced transmission through a sub-wavelength aperture by placing a SRR structure in the near field of the aperture is achieved at both optical and microwave frequencies. 740-fold enhancement is obtained at microwave device and 200% enhancement is obtained at ~1.5um. Also, we manipulated the shape of sub-wavelength aperture. We utilized SRR-shaped apertures in order to increase the transmission though a sub-wavelength aperture and we obtained a 104-fold enhancement by utilizing SRR-shaped apertures at microwave and 275% enhancement at 1.5um.

Chapter 3 studied graphene based plasmonic structures. The electrical gate tuning characteristic of graphene-SRR hybrid structure is successfully demonstrated. We achieved electrical tuning of SRR resonance both numerically and experimentally which is the first demonstration of electrical tuning of graphene based SRR in the contemporary literature according to our knowledge. Graphene based nanophotonics is an intense research due to a wide range of applications of this phenomenon. The research for novel applications and increasing the tuning capability of graphene based plasmonic devices will be a future work for us to conduct.

In the fourth chapter, 3D fabricated nanodot array structure operating at optical frequencies is proposed and investigated. Transmission measurements and simulations confirmed a deviation from bulk silver. In addition, increased index with increased filling factor till a certain threshold is verified by using the retrieval procedure. Since the simplest building block of a 3D manufacture optical metamaterial is a simple dot,

we investigated the optical characteristics of nanodots here. The research for novel metamaterial designs by utilizing femto-second laser writing will be future work for us to conduct.

Research for improving novel applications suggested in this study will be future work for us to conduct. We will investigate the possibility of utilizing different sub-wavelength structures in order to manipulate optical characteristics of plasmonic devices. Also, we will further investigate the possibility of utilizing outstanding electrical and mechanical properties of graphene for designing plasmonic devices. Our proposed structures can be used in new research areas and applications ranging from electronics to life sciences.

The results show us that novel plasmonic devices will broaden the photonics applications. This dissertation presents a platform for understanding the characteristics of plasmonic devices and theoretical basics to develop practical applications. Since, plasmonics field is a flourishing research field, there is a great potential for further development on plasmonics devices for photonics. We presented several possible novel devices in this dissertation. Nowadays, there are plenty of plasmonic devices being designed by researchers. Although demonstrations of novel plasmonic devices in the laboratory level seems to minor steps, I believe the realization of phenomenal technological breakthroughs is about to happen.

Bibliography

[1] V.G. Veselago, "The electrodynamics of substances with simultaneously negative values of permittivity and permeability," *Sov. Phys. Uspekhi*, vol.10, p.509, 1968.

[2] J.B. Pendry, A.J. Holden, D.J. Robbins, W.J. Stewart, "Magnetism from Conductors and Enhanced Nonlinear Phenomena," *IEEE Trans. Microwave Theory Tech.*, vol.47, p.2075, 1999.

[3] D.R. Smith, W.J. Padilla, D.C. Vier, S.C. Nemat-Nasser, S. Schultz, "Composite medium with simultaneously negative permeability and permittivity," *Phys. Rev. Lett*, vol. 84, p.4184, 2000.

[4] B. Edwards, A. Andrea, E. Michael, M.S. Young, N. Engheta, "Experimental verification of epsilon-near-zero metamaterial coupling and energy squeezing using a microwave waveguide," *Phys. Rev. Lett.*, 100, 033903, 2008.

[5] W.J. Padilla, A.J. Taylor, C. Highstrete, M. Lee, R.D. Averitt "Dynamical electric and magnetic metamaterial response at terahertz frequencies," *Phys. Rev. Lett.*, 96, 107401, 2006.

[6] R. Liu, Q. Cheng, T. Hand, J.J. Mock, T.J. Cui, S.A. Cummer, D.R. Smith, "Experimental Demonstration of Electromagnetic Tunneling Through an Epsilon-Near-Zero Metamaterial at Microwave Frequencies," *Phys. Rev. Lett.*, 100, 023903, 2008.

[7] S. Feng, K. Halterman, "Parametrically Shielding Electromagnetic Fields by Nonlinear Metamaterials," *Phys. Rev. Lett.,* 100, 063901, 2008.

[8] Y. Cheng, J.Y. Xu, X.J. Liu, "One-dimensional structured ultrasonic metamaterials with simultaneously negative dynamic density and modulus," *Phys. Rev. B* 77, 045134, 2008.

[9] X.Q. Lin, T.J. Cui, J.Y Chin, X.M. Yang, Q. Cheng, R. Liu, "Controlling electromagnetic waves using tunable gradient dielectric metamaterial lens," *Applied Physics Letters*, 92, 131904, 2008.

[10] K.L. Tsakmakidis, A.D. Boardman, O. Hess, ″Trapped rainbow storage of light in metamaterials,″ *Nature,* 450, 397–401, 2007.

[11] J. Valentine, S. Zhang, T. Zentgraf, E. Ulin-Avila, D.A. Genov, G. Bartal, X. Zhang, "Three-dimensional optical metamaterial with a negative refractive index," *Nature,* vol. 455, 376-379, 2008.

[12] H.T. Chen, W.J. Padilla, J.M.O. Zide, A.C. Gossard, A. J. Taylor, R.D. Averitt, "Active terahertz metamaterial devices," *Nature,* 444, 597-600, 2006.

[13] N.C. Panoiu, R.M. Osgood, "Numerical investigations of negative refractive index metamaterials at infrared and optical frequencies," *Opt. Comm.,* 223, 331–337, 2003.

[14] C.M. Soukoulis, S. Linden, M. Wegener, "Negative refractive index at optical frequencies," *Science* 315, 47-49, 2007.

[15] T. Li, H. Liu, F.M. Wang, Z.G. Dong, S.N. Zhu, X. Zhang, "Coupling effect of magnetic polariton in perforated metal/dielectric layered metamaterials and its influence on negative refraction transmission," *Opt. Express* 14, 11155–11163, 2006.

[16] A. Alu, N. Engheta, "Three-dimensional nanotransmission lines at optical frequencies: A recipe for broad band negative-refraction optical metamaterials," *Phys. Rev. B*, 75, 024304, 2007.

[17] I.I. Smolyaninov, Y.J. Hung, C.C. Davis, "Magnifying superlens in the visible frequency range," *Science*, 315, 1699-1701, 2007.

[18] X. Zhang, Z. Liu, "Superlenses to overcome the diffraction limit," *Nature Mater.*, 7, 435-441, 2008.

[19] M. C. K. Wiltshire, J.B. Pendry, I.R. Young, D.J. Larkman, D.J. Gilderdale, J.V. Hajnal, "Microstructured Magnetic Materials for RF Flux Guides in Magnetic Resonance Imaging," *Science*, vol. 291, 2001.

[20] Z.W. Liu, H. Lee, Y. Xiong, C. Sun, X. Zhang, "Far field optical hyperlens magnifying sub-diffraction-limited objects," *Science*, 315, 1686, 2007.

[21] Z. Jacob, L.V. Alekseyev, E. Narimanov, "Optical hyperlens: Far-field imaging beyond the diffraction limit," *Opt. Exp.*, 14, 8247-8256, 2006.

[22] J.B. Pendry, D. Schurig, D.R. Smith, "Controlling electromagnetic fields," *Science* 312, 1780-1782, 2006.

[23] A.J. Hoffman, L. Alekseyev, S.S. Howard, K.J. Franz, D. Wasserman, V.A. Podolskiy, E.E. Narimanov, D.L. Sivco, C Gmachl, "Negative refraction in semiconductor metamaterials," *Nature Mater* 6, 946-950, 2007.

[24] T.W. Ebbesen, H.J. Lezec, H.F. Ghaemi, T. Thio, P.A. Wolff, "Extraordinary optical transmission through sub-wavelength hole arrays," *Nature* 391, 667–669, 1998.

[25] H.A. Bethe, "Theory of diffraction by small holes," *Phys. Rev.* 66, 163-182, 1994.

[26] C. M. Soukoulis and M. Wegener, "Past achievements and future challenges in the development of three-dimensional photonic metamaterials," *Nat. Photonics*, vol. 5, no. 9, pp. 523-530, Sep. 2011.

[27] V. J. Logeeswaran, Stameroff, A. N.; Islam, M. S.; Wu, W.; Bratkovsky, A. M.; Kuekes, P. J.; Wang, S. Y.; Williams, R. S., "Switching between positive and negative permeability by photoconductive coupling for modulation of electromagnetic radiation," *Appl. Phys. A: Mater. Sci. Process.*, 87, 209-216, 2007.

[28] A. Bostwick, F. Speck, T. Seyller, K. Horn, M. Polini, R. Asgari, A. H. MacDonald, E. Rotenberg, "Observation of plasmarons in quasi-freestanding doped graphene," *Science* 328, 999–1002, 2010.

[29] A. Grbic and G. Eleftheriades, "Overcoming the diffraction limit with a planar left-handed transmission-line lens," *Phys. Rev. Lett.,* vol. 92, no. 11, Mar. 2004.

[30] J. Krenn, Perspective on plasmonics, "Interview", *Nature Photonics*, vol 6, November 2012.

[31] Wu, W.; Yu, Z. N.; Wang, S. Y.; Williams, R. S.; Liu, Y. M.; Sun, C.; Zhang, X.; Kim, E.; Shen, Y. R.; Fang, N. X., "Midinfrared metamaterials fabricated by nanoimprint lithography," *Appl. Phys. Lett.*, 90, 063107, 2007.

[32] Jon A. Schuller, Edward S. Barnard, Wenshan Cai, Young Chul Jun, Justin S. White and Mark l. Brongersma, "Plasmonics for extreme light concentration and manipulation," *Nature Materials* Vol 9, 193-205, March 2010.

[33] L. Sahin, K. Aydin, G. Turhan-Sayan, E. Ozbay, "Enhanced transmission of electromagnetic waves through split-ring resonator-shaped apertures," *Journal of Nanophotonics*, vol. 5, 051812, 2011.

[34] W. L. Barnes, W. A. Murray, J. Dintinger, E. Deveaux, and T. W. Ebbesen, "Surface Plasmon Polaritons and their role in the enhanced transmission of light through periodic arrays of subwalength holes in a metal film," *Phys. Rev. Lett.* 92, 107401 2004.

[35] H. J. Lezec and T. Thio, "Diffracted Evanescent Wave Model for Enhanced and Supressed Optical Transmission through Subwavelength Hole Arrays," *Optics Express* **12**(16), 3629 (2004).

[36] P. Chaturvedi, K. Hsu, S. Zhang, and N. Fang, "New Frontiers of Metamaterials: Design and Fabrication," *MRS Bulletin*, volume 33, October 2008.

[37] S. Durant, Z. Liu, J. M. Steele, and X. Zhang, "Theory of the transmission properties of an optical far-field superlens for imaging beyond the diffraction limit," *J. Opt. Soc. Am. B* Vol. 23, No. 11, November 2006.

[38] L. Sahin, "Transmission and Propagation Properties Of Novel Metamaterials," *Master of Science Thesis*, Middle East Tech. Univ., 2009.

[39] J.B. Pendry, A.J. Holden, W.J. Stewart, I. Youngs, "Extremely Low Frequency Plasmons in Metallic Mesostructures," *Phys. Rev. Lett*, vol.76, Number 25 1996.

[40] J.B. Pendry, A.J. Holden, D.J. Robbins, W.J. Stewart, "Low frequency Plasmons in thin-wire structures," *J.Phys.: Condens. Matter*, vol.10, 4785-4809, 1998.

[41] D.R. Smith, D.C. Vier, W.J. Padilla, S. C. Nemat-Nasser, S.Schultz, "Loop-wire medium for investigating plasmons at microwave frequencies," *Appl. Phys. Lett.*, vol. 75, p1425, 1999.

[42] Y. Liu, R.F. Willis, K.V. Emtsev, T. Seyller, "Plasmon dispersion and damping in electrically isolated two-dimensional charge sheets," *Phys. Rev. B* 78, 201403, 2008.

[43] C. Tegenkamp, H. Pfnur, T. Langer, J. Baringhaus, H. Schumacher, "Plasmon electron-hole resonance in epitaxial graphene," *J. Phys. Condens. Matter* 23, 012001, 2011.

[44] V.W. Brar, S. Wickenburg, M. Panlasigui, C.H. Park, T.O. Wehling, Y. Zhang, R. Decker, Ç. Girit, A. V. Balatsky, S. G. Louie, A. Zettl, M.F. Crommie, "Observation of carrier-density-dependent many-body effects in graphene via tunneling spectroscopy," *Phys. Rev. Lett*. 104, 036805, 2010.

[45] R.A. Shelby, D.R. Smith, S.C. Nemat-Nasser, S. Schultz, "Microwave transmission through a two-dimensional, isotropic, left-handed metamaterial," *Appl. Phys. Lett.*, vol. 78, p489, 2001.

[46] D.R. Smith, N. Kroll, "Negative Refractive Index in Left-Handed Materials," *Phys. Rev. Lett.*, vol.85, Number 14, 2000.

[47] R.A. Shelby, D.R. Smith, S. Schultz, "Experimental verification of a negative index of refraction," *Science*, vol.292, p.77, 2001.

[48] C.G. Parazolli, R.B. Greegor, K. Li, B.E.C. Koltenbah, M. Tanielian, "Experimental verification and simulation of negative index of refraction using Snell's Law," *Phys. Rev. Lett.*, vol.90. Number 10, 2003.

[49] A.A. Houck, J.B. Brock, I.L. Chuang, "Experimental observations of a left-handed material that obeys Snell's Law," *Phys. Rev. Lett.*, Vol.90, Number 10, 2003.

[50] K. Aydin, K. Guven, C. M. Soukoulis, E. Ozbay, "Observation of negative refraction and negative phase velocity in left-handed metamaterials," *Appl. Phys. Lett.* 86, 124102, 2005.

[51] N. Seddon, T. Bearpark, "Observation of the inverse Doppler effect," *Science*, Vol.302, 1537-1540, 2003.

[52] J. Lu, T. Grzegorczyk, Y. Zhang, J. Pacheco Jr., B. Wu, J. Kong, M. Chen , "Čerenkov radiation in materials with negative permittivity and permeability," *Optics Express*, 2003.

[53] D.R. Smith, J.B. Pendry, M.C.K. Wiltshire, "Metamaterials and negative refractive index," *Science*, 305, 788, 2004.

[54] S.I. Maslowski, S.A. Tretyakov, P.A. Belov, "Wire media with negative effective permittivity: a quasi-static model," *Microwave Opt. Technol. Lett.*, 35:47, 2002.

[55] IEEE, *Research on the macro effect of the thin wire array in metamaterial by equivalent circuit method*, IEEE AP-S International Symposium and USNC/URSI National Radio Science Meeting, Washington D.C., USA, 2005.

[56] M. Bayindir, K. Aydin, E. Ozbay, P. Marko, C.M. Soukoulis, "Transmission properties of composite metamaterials in free space," *Appl. Phys. Lett.*, 81:120, 2002.

[57] R. Marques, J. Martel, F. Mesa, F. Medina, "Left-handed-media simulation and transmission of electromagnetic waves in subwavelength split-ring resonator-loaded metallic waveguides," *Phys. Rev. Lett.*, 89:183901, 2002.

[58] P. Markos, C.M. Soukoulis, "Transmission studies of left-handed materials," *Phys. Rev. B.*, 65:033401, 2001.

[59] K. Aydin, K. Guven, M. Kafesaki, L. Zhang, C.M. Soukoulis, E. Ozbay, "Experimental observation of true left-handed transmission peak in metamaterials," *Opt. Lett.,* 29, 2623, 2004.

[60] P. Gay-Balmaz, O.J.F. Martin, "Electromagnetic Resonances in individual and coupled split-ring resonators," *J. Appl. Phys*., 92:2929, 2002.

[61] C.R. Simovski, B. Sauviac, "Role of wave interaction of wires and split-ring resonators for the loss in a left handed composite," *Phys. Rev. E,* 70:046607, 2004.

[62] M. Shamonin, E. Shamonina, V. Kalinin, L. Solymar, "Properties of a metamaterial element: Analytical solutions and numerical simulations for a singly split double ring," *J. Appl. Phys.,* 95:3778, 2004.

[63] J. Zhou, T. Koschny, M. Kafesaki, E.N. Economou, J.B. Pendry, C.M. Soukoulis, "Saturation of magnetic response of split-ring resonators at optical frequencies," *Phys. Rev. Lett.,* 95, 223902, 2005.

[64] N. Katsarakis, M. Kafesaki, I. Tsiapa, E.N. Economou, C.M. Soukoulis, "High transmittance left-handed materials involving symmetric split-ring resonators," *Photon. Nanostruct: Fundam. Appl.* 5, 149, 2007.

[65] M. Born, E. Wolf, "Principles of Optics: Electromagnetic Theory of Propagation, Interference and Diffraction of Light," *Cambridge University Press*, The Edinburgh Building, Cambridge CB2 2RU, UK, 7. Edition, 1999.

[66] D.R. Smith, D. Schurig, J.B. Pendry, "Negative Refraction of modulated electromagnetic waves," *Appl. Phys. Lett.,* vol.81, p.2713, 2002.

[67] J.B. Pendry, "Negative Refraction makes a perfect lens," *Phys. Rev. Lett.*, vol.85, p.3966, 2000.

[68] D.R. Smith, S. Schultz, P. Markos, C.M. Soukoulis, "Determination of effective permittivity and permeability of metamaterials from reflection and transmission coefficients," *Phys. Rev. B.* 65, 195104, 2002.

[69] X. Chen, T.M. Grzegorczyk, B.I. Wu, J. Pacheco Jr., J.A. Kong, "Robust method to retrieve the constitutive effective parameters of metamaterials," *Phys. Rev. E* 70, 016608, 2004.

[70] T. Koschny, P. Markoš, E.N. Economou, D.R. Smith, D.C. Vier, C.M. Soukoulis, "Impact of the inherent periodic structure on the effective medium description of left-handed and related meta-materials," *Phys. Rev. B* 71, 245105, 2005.

[71] Zhou, J.; Koschny, T.; Kafesaki, M.; Economou, E. N.; Pendry, J. B.; Soukoulis, C. M., "Saturation of the magnetic response of split-ring resonators at optical frequencies," *Phys. Rev. Lett.*, 95, 223902, 2005.

[72] K. Aydin, Z. Li, L. Sahin, E. Ozbay, "Negative phase advance in polarization independent, multi-layer negative-index metamaterials," *Optics Express,* Vol.16, No.12, 8835, 2008.

[73] K. Aydin, E.Ozbay, "Experimental and numerical analyses of the resonances of split-ring resonators," *Phys. Stat. Sol.* 244, No.4, 1197-1201, 2007.

[74] K. Li, S.J. McLean, R.B. Greegor, C.G. Parazolli, M.H Tanielian, "Free-space focused-beam characterization of left-handed materials," *Appl. Phys. Lett*, 82, 2535, 2003.

[75] F. Martin, F. Falcone, J. Bonache, R. Marques, M. Sorolla, "Miniaturized Coplanar Waveguide Stop Band Filters Based on Multiple Tuned Split Ring Resonators," *IEEE Microwave Wireless Comp.*, 13, 511, 2003.

[76] J. Martel, R. Marques, F. Falcone, J.D. Baena, F. Medina, F. Martin, M. Sorolla, "A New LC Series Element for Compact Bandpass Filter Design," *IEEE Microwave Wireless Comp.*, 14, No.5, 2004.

[77] K. Aydin, E.Ozbay, "Identifying the magnetic response of split-ring resonators at microwave frequencies," *Opto-Electron Rev* 14, 193-199, 2006.

[78] B. Sauviac, C.R Simovski, S.A. Tretyakov, "Double split-ring resonators: Analytical modeling and numerical simulations," *Electromagnetics* 24, 317-338, 2004.

[79] E. Ozbay, K. Aydin, K. Guven, "Metamaterials with negative permeability and negative refractive index: experiments and simulations," *J. Opt. A: Pure and Appl. Opt.* 9, 301, 2007.

[80] J. Gomez Rivas, C. Schotsch, P. Haring Bolivar, H. Kurz "Enhanced transmission of THz radiation through subwavelength holes," *Physical Review B* 68, 201306, 2003.

[81] K. Aydin, I. Bulu, K. Guven, M. Kafesaki, C.M. Soukoulis, E. Ozbay, "Investigation of magnetic resonances for different split-ring resonator parameters and designs," *New Journal of Physics* 7, 168, 2005.

[82] F. Neubrech, A. Pucci, T.W. Cornelius, S. Karim, A. Garcia-Etxarri, J Aizpurua, "Giant infrared signals from molecular vibrations by the action of a tailored nanoantenna," *J. Phys. Rev. Lett.*, 101, 157403 , 2008.

[83] C.M. Soukoulis, M. Kafesaki, E.N. Economou, "Negative index materials: New frontiers in optics," *Adv. Mater.* 18, 1941, 2006.

[84] E. Ozbay, I. Bulu, H. Caglayan, "Transmission, refraction, and focusing properties of labyrinth based left-handed metamaterials," *Phys. Stat. Sol.* 244, No. 4, 1202–1210, 2007.

[85] P. Markos, C.M. Soukoulis, "Numerical studies of left-handed materials and arrays of split ring resonators," *Physical Review E,* Vol.65, 036622, 2002.

[86] T. Weiland, R. Schuhmann, R.B. Greegor, C.G. Parazzoli, A.M. Vetter, D.R. Smith, D.C. Vier, S. Schultz, "Ab initio numerical simulation of left-handed metamaterials: Comparison of calculations and experiments," *J. Appl. Phys.* 90 No.10, 2001.

[87] P. Markos, C.M. Soukoulis, "Transmission properties and effective electromagnetic parameters of double negative metamaterials," *Opt. Exp.* 11 649, 2003.

[88] N. Katsarakis, T. Koschny, M. Kafesaki E.N. Economou C.M. Soukoulis, "Electric coupling to the magnetic resonance of split ring resonators," *Applied Physics Letters,* vol.84, No.15, 2004.

[89] P. Mühlschlegel, H.J Eisler, O.J.F. Martin, B. Hecht, D.W. Pohl, "Resonant Optical Antennas," *Science*, 308, 1607−1609, 2005.

[90] J.D. Baena, R. Marques, F. Medina, J. Martel, "Artificial magnetic metamaterial design by using spiral resonators," *Phys. Rev. B* 69 014402, 2004.

[91] A.B. Movchan, S. Guenneau, "Split-ring resonators and localized modes," Phys. Rev. B 70 125116, 2004.

[92] S. Linden, C. Enkrich, M. Wegener, J. Zhou, T. Koschny, C.M. Soukoulis, "Magnetic Response of Metamaterials at 100 Terahertz," *Science*, 306, 1351, 2004.

[93] T. J. Yen, W. J. Padilla, N. Fang, D. C. Vier, D. R. Smith, J. B. Pendry, D. N. Basov, and X. Zhang, "Terahertz magnetic response from artificial materials," *Science* 303,1494, 2004.

[94] F.M. Grimaldi, "Physico-mathesis de Lumine, Coloribus, et Iride, Aliisque Sequenti Pagina Indicatis" *9* , Bologna, 1665.

[95] C. Genet, T.W. Ebbesen, "Light in tiny holes," *Nature*, Vol. 445, 39-46, January 2007.

[96] A. Alu, N. Engheta, "Wireless at the Nanoscale: Optical Interconnects using Matched Nanoantennas," *Phys. Rev. Lett*., 104, 213902, 2010.

[97] H. Çağlayan, "Enhanced Confined Microwave Transmission by Single Subwavelength Apertures," Page 29, M.Sc. Thesis, Bilkent Univ., August 2005.

[98] X. Shi, L. Hesselink, R. Thornton, "Ultrahigh light transmission through a C-shaped nanoaperture," *Optics Letters*, Vol. 28, No. 15, August 2003.

[99] X. Shi, L. Hesselink, "Design of a C aperture to achieve $\lambda/10$ resolution and resonant transmission," *Optical Society of America*, Vol. 21, No. 7, July 2004.

[100] L. Tang, D.A.B. Miller, A.K. Okyay, J.A. Matteo, Y. Yuen, K.C. Saraswat, L. Hesselink, "C-shaped nanoaperture-enhanced germanium photodetector," *Optics Letters*, vol. 31, No. 10, May 2006.

[101] P. Hansen, L. Hesselink, B. Leen, "Design of a subwavelength bent C-aperture waveguide," *Optics Letters*, vol.32, No.12, June 2007.

[102] R. Gordon, A. Brolo, "Increased cut-off wavelength for a sub-wavelength hole in a real metal," *Optics Express,* 13, 1933-1938, 2005.

[103] A. Roberts, "Electromagnetic theory of diffraction by a circular aperture in a thick, perfectly conducting screen," *J. Opt. Soc. Am*., A 4, 1970-1983, 1987.

[104] F.J. Garcia-Vidal, E. Moreno, J.A. Porto, L. Martin-Moreno, "Transmission of Light through a single rectangular hole," *Phys. Rev. Lett.* 95, 103901, 2005.

[105] W.A. Challener, C.B. Peng, A.V. Itagi, D. Karns, W. Peng, Y.Y. Peng, X.M. Yang, X.B. Zhu, N.J. Gokemeijer, Y.T. Hsia, G. Ju, R.E. Rottmayer, M.A. Seigler, E.C. Gage, "Heat-assisted magnetic recording by a near-field transducer with efficient optical energy transfer," *Nat Photonics*, 3, 220−224, 2009.

[106] T.D. Visser, "Plasmonics: Surface Plasmons at work?", *Nature Physics*, Vol2, August 2006.

[107] P. Lalanne, J.P Hugonin, "Interaction between optical nano-objects at metallo-dielectric interfaces," *Nature Physics*, Vol.2, 551-556, 2006.

[108] H.F. Schouten, N. Kuzmin, G. Dubois, T.D. Visser, G. Gbur, P.F.A. Alkemade, H. Blok, G.W. Hooft, D. Lenstra, E.R. Eliel, "Plasmon-assisted Two-Slit Transmission: Young's Experiment Revisited," *Phys. Rev. Lett.* 94, 053901, 2005.

[109] K.L. Klein Koerkamp, S. Enoch, F.B. Segerink, N.F. van Hulst, L. Kuipers, "Strong Influence of Hole Shape on Extraordinary Transmission through Periodic Arrays of Subwavelength Holes," *Phys. Rev. Lett.* 92, 183901, 2004.

[110] M.J. Levene, J. Korlach, S.W. Turner, M. Foquet, H.G. Craighead, W.W. Webb, "Zero-mode waveguides for single molecule analysis at high concentrations," *Science* 299, 682–686, 2003.

[111] E. Betzig, J.K. Trautman, "Near-field optics: microscopy, spectroscopy, and surface modification beyond the diffraction limit," *Science* 257, 189–194 1992.

[112] G. Gbur, H.F. Schouten, T.D. Visser, "Achieving super resolution in near-field optical data readout systems using surface plasmons," *Appl. Phys. Lett.* 87, 191109, 2005.

[113] J. Fujikata, T. Ishi, H. Yokota, K. Kato, M. Yanagisawa, M. Nakada, K. Ishihara, K. Ohashi, T. Thio, "Surface plasmon enhancement effect and its application to nearfield optical recording," *Trans. Magn. Soc. Jpn* 4, 255–259, 2004.

[114] W. Srituravanich, N. Fang, C. Sun, Q. Luo, X. Zhang, "Plasmonic nanolithography," *Nano Lett.* 4, 1085–1088, 2004.

[115] X. Luo, T. Ishihara, "Sub-100nm photolithography based on plasmon resonance," *Jpn J. Appl. Phys.* 43, 4017–4021, 2004.

[116] D.B. Shao, S.C. Che, "Surface-plasmon-assisted nanoscale photolithography by polarized light," *Appl. Phys. Lett.* 86, 253107, 2005.

[117] H. Rigneault, J. Capoulade, J. Dintinger, J. Wenger, N. Bonod, E. Popov, T.W. Ebbesen, P. Lenne, "Enhancement of single-molecule fluorescence detection in subwavelength apertures," *Phys. Rev. Lett.* 95, 117401, 2005.

[118] T. Ishi, J. Fujikata, K. Makita, T. Baba, K. Ohashi, "Si nano-photodiode with a surface plasmon antenna," *Jpn J. Appl. Phys*. 44, L364–L366, 2005.

[119] J.B. Pendry, L. Martin-Moreno, F.J. Garcia-Vidal, "Mimicking surface Plasmons with structured surfaces", *Science* 305, 847–848, 2004.

[120] F.J. Garcia-Vidal, L. Martin-Moreno, J.B. Pendry, "Surfaces with holes in them: new plasmonic metamaterials," *J. Opt. Pure Appl.* Opt. 7, S97–S101, 2005.

[121] A. Degiron, H.J. Lezec, N. Yamamoto, T.W. Ebbesen, "Optical transmission properties of a single subwavelength aperture in a real metal," *Opt Comm*. 239, 61-66, 2004.

[122] F.J. Garcia de Abajo, "Colloquium: Light scattering by particle and hole arrays," *Reviews of Modern Physics*, volume 79, 1267-1290, 2007.

[123] K.R. Catchpole, A. Polman, "Plasmonic solar cells," *Opt Express*, 16, 21793–21800, 2008.

[124] M. S. Rill, C. Plet, M. Thiel, I. Staude, G. von Freymann, S. Linden, and M. Wegener, "Photonic metamaterials by direct laser writing and silver chemical vapor deposition," *Nature Mater.* 7, 543, 2008.

[125] N. Takeyasu, T. Tanaka, and S. Kawata, "Fabrication of 3D metal/polymer microstructures by site-selective metal coating," *Appl. Phys. A: Mater. Sci. Process.* 90, 205, 2007.

[126] H.T. Chen, H. Lu, A. K. Azad, R. D. Averitt, A.C. Gossard, S. A. Trugman, J.F. O'Hara, A.J. Taylor, "Electronic control of extraordinary terahertz transmission through subwavelength metal hole arrays," *Opt. Express*, 16, 7641–7648, 2008.

[127] H.T. Chen, W.J. Padilla, M.J. Cich, A.K. Azad, R.D. Averitt, A.J. Taylor, "A metamaterial solid-state terahertz phase modulator," Nat. Photon., 3, 148–151, 2009.

[128] J. K. Gansel, M. Thiel, M. S. Rill, M. Decker, K. Bade, V. Saile, G. von Freymann, S. Linden, and M. Wegener, "Gold helix photonic metamaterial as broadband circular polarizer," *Science* 325(5947), 1513, 2009.

[129] A. N. Grigorenko, "Negative refractive index in artificial metamaterials," *Opt. Lett.* 31(16), 2483, 2006.

[130] A. Ishikawa, T. Tanaka, and S. Kawata, "Magnetic Excitation of Magnetic Resonance in Metamaterials at Far-Infrared Frequencies," *Appl. Phys. Lett.* 91, 113118, 2007.

[131] Z. Fei, A.S. Rodin, G.O. Andreev, W. Bao, A.S. McLeod, M. Wagner, L.M. Zhang, Z. Zhao, M. Thiemens, G. Dominguez, M.M. Fogler, A.H.C. Neto, C.N. Lau, F. Keilmann, D.N. Basov, "Gate-tuning of graphene plasmons revealed by infrared nano-imaging ," Nature, 487, 82–85, 2012.

[132] J.N. Chen, M. Badioli, P. Alonso-Gonzalez, S. Thongrattanasiri, F. Huth, J. Osmond, M. Spasenovic, A. Centeno, A. Pesquera, P. Godignon, A.Z. Elorza, N. Camara, F.J.G. de Abajo, R. Hillenbrand, F.H.L. Koppens, "Optical nano-imaging of gate-tunable graphene plasmons," Nature, 487, 77–81, 2012.

[133] H.G. Yan, X. S. Li, B. Chandra, G. Tulevski, Y.Q. Wu, M. Freitag, W.J. Zhu, P. Avouris, F.N. Xia, "Mid-infrared plasmons in scaled graphene nanostructures," *Nat. Nanotechnol.*, 7, 330–334, 2012.

[134] Y. Sun and Y. Xia, "Shape-Controlled Synthesis of Gold and Silver Nanoparticles," *Science* 298(5601), 2176, 2002.

[135] B. Wiley, Y. G. Sun, B. Mayers, and Y. N. Xia, "Shape-Controlled Synthesis of Metal Nanostructures: The Case of Silver," *Chem.-Eur. J.* 11(2), 454, 2005.

[136] O. Glushko, R. Brunner, R. Meisels, S. Kalchmair and G. Strasser, "Extraordinary transmission in metal hole arrayphotonic crystal hybrid structures," *Optics Express* , Vol. 20, No. 15, 17175, 2012.

[137] G. Li, F. Xiao, K. Li, K. Alameh and A. Xu, "Theory, Figures of Merit, and Design Recipe of the Plasmonic Structure Composed of a Nano-Slit Aperture Surrounded by Surface Corrugations," *Journal Of Lightwave Technology*, Vol. 30, No. 15, 2012.

[138] Y. Yao, M.A. Kats, G. Patrice, Y. Nanfang, Y. Song, J. Kong, F. Capasso,"Broad Electrical Tuning of Graphene-Loaded Plasmonic Antennas," *Nano Letters*, 2013.

[139] L.A. Falkovsky, A.A. Varlamov, "Space-time dispersion of graphene conductivity," *Eur. Phys. J. B* 56, 281–284, 2007.

[140] L.A. Falkovsky, "Optical properties of graphene," *International Conference on Theoretical Physics*, Dubna-Nan, Book of abstracts, p.28, 2008.

[141] Y. Lee, K. Hoshino, A. Alu and X. Zhang, "Efficient directional beaming from small apertures using surface-plasmon diffraction gratings," *Applied Physics Letters*, 101, 041102, 2012.

[142] G. D. Mahan, "Many-Particle Physics," 2nd ed. *Plenum Press*, New York, 1990.

[143] H. Ehrenreich and M. H. Cohen, "Self-Consistent Field Approach to the Many-Electron Problem," *Phys. Rev.* 115, 786-70, 1959.

[144] S. Adam, E. H. Hwang, V. M. Galitski, S. Das Sarma, "A self-consistent theory for graphene transport," 18392–18397, *PNAS*, vol. 104, no. 47, 2007.

[145] K. Nomura, A.H. MacDonald, "Quantum transport of massless Dirac fermions," *Phys. Rev. Lett.* 98, 076602, 2007.

[146] S. S. Akarca-Biyikli, I. Bulu and E. Ozbay, "Enhanced transmission of microwave radiation in one-dimensional metallic gratings with sub-wavelength aperture," *Applied Physics Letters*, 85 ,1098, 2004.

[147] H. Caglayan, I. Bulu and E. Ozbay, "Extraordinary grating-coupled microwave transmission through a subwavelength annular aperture," *Optics Express*, 13, 1666, 2005.

[148] T. Ando, "Screening effect and impurity scattering in monolayer graphene," *J. Phys. Soc. Jpn* 75, 074716, 2006.

[149] E. H. Hwang, S. Adam, S. Das Sarma, "Carrier transport in two-dimensional graphene layers," *Phys. Rev. Lett*. 98, 186806, 2007.

[150] J.C. Charlier, P.C. Eklund, J. Zhu, A.C. Ferrari, "Electron and Phonon Properties of Graphene: Their Relationship with Carbon Nanotubes," *Carbon Nanotubes Topics in Applied Physics* volume 111, pp 673-709, 2008.

[151] J.H. Chen, C. Jang, S. Adam, M. S. Fuhrer, E. D. Wıllıams, M. Ishigami, "Charged-impurity scattering in graphene," *Nature Physics* Vol 4, 2008.

[152] D.R. Smith, D.C. Vier, T. Koschny, C.M. Soukoulis "Electromagnetic parameter retrieval from inhomogeneous metamaterials", *Phys Rev E* 71, 036617, 2005.

[153] M. Liu, X. Yin, E. Ulin-Avila, B. Geng, T. Zentgraf, L. Ju, F. Wang, X. Zhang, "A graphene-based broadband optical modulator," Nature, 64 Vol.474, 2011.

[154] J.F. Zhou, T. Koschny, M. Kafesaki, C.M. Soukoulis, "Negative refractive index response of weakly and strongly coupled optical metamaterials," *Phys. Rev. B* 80, 035109, 2009.

[155] M. Jablan, H. Buljan, M. Soljačić, "Plasmonics in graphene at infrared frequencies," *Physical Review B* 80, 245435 2009.

[156] P. Avouris, Z. Chen, V. Perebeinos "Carbon-based electronics," *Nature Nanotechnology* 2 : 605–15, 2007.

[157] J. Zhou, T. Koschny, M. Kafesaki E. N. Economou, J. B. Pendry, C. M. Soukoulis, "Saturation of the magnetic response of spli-ring resonators at optical frequencies" Phys. Rev. Lett., 95, 223902, 2005.

[158] W. Strupinski, K. Grodecki, A. Wysmolek,R. Stepniewski, T. Szkopek, P. E. Gaskell, A. Grüneis, D. Haberer, R. Bozek, J. Krupka, J. M. Baranowski, "Graphene Epitaxy by Chemical Vapor Deposition on SiC,"*Nano Lett.*, 11 (4), pp 1786–1791, 2011.

[159] N.K. Emani, T.F. Chung, X. Ni, A.V. Kildishev, Y.P. Chen, A. Boltasseva, 'Electrically Tunable Damping of Plasmonic Resonances with Graphene' *Nano Letters*, vol 12, no. 10, pp. 5202–5206, 2012.

[160] E. Ozbay, "Plasmonics: Merging Photonics and Electronics at Nanoscale Dimensions," *Science*, 13, Vol. 311 no. 5758 pp. 189-193, 2006.

[161] R. Marqués, F. Mesa, J. Martel and F. Medina, "Comparative Analysis of Edge- and Broadside-Coupled Split Ring Resonators for Metamaterial Design-Theory and Experiments," *IEEE Trans. on Antennas and Propagation*, 51, No. 10, 2003.

[162] K. Aydin, A. O. Cakmak, L. Sahin, Z. Li, F. Bilotti, L. Vegni and E. Ozbay, "Split-ring-resonator-coupled enhanced transmission through a single subwavelength aperture," *Phys. Rev. Lett.*, 102, 013904, 2009.

[163] C. M. Soukoulis, S. Linden, M. Wegener, "Negative refractive index at optical wavelengths," *Science*, 315, 47–49, 2007.

[164] E. Ozbay, K. Aydin, E. Cubukcu and M. Bayindir, "Transmission and Reflection Properties of Composite Double Negative Metamaterials in Free Space," *IEEE Trans. on Antennas and Propagation*, 51, 2592, 2003.

[165] K. Aydin, K. Guven, N. Katsarakis, C. M. Soukoulis and E. Ozbay, "Effect of disorder on magnetic resonance band gap of split-ring resonator structures," *Optics Express*, 12, 5896, 2004.

[166] V. M. Shalaev, "Optical negative-index metamaterials," *Nature Photon.* 1, 41–48, 2007.

[167] R. F. Harrington, "Time-Harmonic Electromagnetic Fields," *IEEE Press Wiley Interscience*, p365-p367, 2001.

[168] J. Dintiger, S. Klein and T. W. Ebbessen, "Molecule-surface plasmon interactions in hole arrays: enhanced absorption, refractive index changes, and all optical switching," *Adv. Mater (Wienheim, Ger.)*, 18, 1267-1270, 2006.

[169] I. I. Smolyaninov, A. V. Zayats, A. Stanishevsky and C. C. Davis, "Optical control of photon tunneling through an array of nanometer-scale cylindrical channels," *Phys. Rev. B*, 66, 205414, 2002.

[170] C. Janke, J. Gómez Rivas, P. Haring Bolivar and H. Kurz, "All-optical switching of the transmission of electromagnetic radiation through subwavelength apertures," *Opt. Lett.*, 30, 2357–2359, 2005.

[171] J. Dintinger, I. Robel, P. V. Kamat, C. Genet and T. W. Ebbesen, "Terahertz all-optical molecule-plasmon modulation," *Adv. Mater. (Weinheim, Ger.)*, 18, 1645–1648, 2006.

[172] E. Altewischer, M. P. van Exter and J. P. Woerdman, "Plasmon-assisted transmission of entangled photons," *Nature London*, 418, 304-306, 2002.

[173] I. Bulu, H. Caglayan and E. Ozbay, "Beaming of Light and Enhanced Transmission via Surface Modes of Photonic Crystals," *Optics Letters*, 30, 3078, 2005.

[174] I. Bulu, H. Caglayan and E. Ozbay, "Highly directive radiation from sources embedded inside photonic crystals," *Applied Physics Letters*, 83, 3263, 2003.

[175] N. I. Zheludev, "The road ahead for metamaterials," *Science* 328, 582–583, 2010.

[176] C. Enkrich, M. Wegener, S. Linden, S. Burger, L. Zschiedrich, F. Schmidt, J. F. Zhou, T. Koschny T and C. M. Soukoulis, "Magnetic Metamaterials at Telecommunication and Visible Frequencies," *Phys. Rev. Lett.*, 95, 203901, 2005.

[177] User Manual, Version 5.0, CST GmbH, Darmstadt, Germany, 2005, http://www.cst.de.

[178] User Manual, Release 6.5, Lumerical, http://docs.lumerical.com/en/fdtd/reference_guide.html

[179] A. K. Geim and K.S. Novoselov, "The rise of graphene," *Nature Materials* 6, 183-191, 2007.

[180] L. Ju, B. Geng, C. Girit, M. Martin, Z. Hao, H. A. Bechtel, X. Liang, A. Zettl, Y. R. Shen and F. Wang, "Graphene Plasmonics for tunable teraheartz metamaterials," *Nature Nanotechnology*, Advance Online Publication, DOI: 10.1038/NNANO.2011.146 2011.

[181] N. Papasimakis, Z. Luo, Z. X. Shen, F. De Angelis, E. Di Fabrizio, A. E. Nikolaenko and N. I. Zheludev, "Graphene in a photonic metamaterial," *Optics Express* 8, 8353-8359, 2010.

[182] F. Bonaccorso, Z. Sun, T. Hasan and A. C. Ferrari, "Graphene photonics and optoelectronics," *Nature Photonics* 4, 611-622, 2010.

[183] F. H. L. Koppens, D. E. Chang and F. J. Garcia de Abajo, "Graphene Plasmonics: A platform for strong light-matter interactions," *Nano Letters* 11, 3370-3377, 2011.

[184] C. M. Soukoulis, M. Wegener, "Optical metamaterials: More bulky and less lossy," *Science* 330, 1633–1634, 2010.

[184] A. H. Castro Neto, F. Guinea, and N. M. R. Peres, "Drawing conclusions from graphene," *Physics World* 19, 33-37, 2006.

[185] K. S. Novoselov, E. McCann, S. V. Morozov, V. I. Fal'ko, M. I. Katsnelson, U. Zeitler, D. Jiang, F. Schedin, and A. K. Geim, "Unconventional quantum Hall effect and Berry's phase of 2π in bilayer graphene," *Nat. Phys*. 2 (3),177–180, 2006.

[186] K. S. Novoselov, A. K. Geim, S. V. Morozov, D. Jiang, M. I. Katsnelson, I. V. Grigorieva, S. V. Dubonos, A. A. Firsov, "Two-dimensional gas of massless Dirac fermions in graphene," *Nature* 438, 197-200, 2005.

[187] K. I. Bolotin, K. J. Sikes, Z. Jiang, M. Klima, G. Fudenberg, J. Hone, P. Kim and H.L. Stormer, "Ultrahigh electron mobility in suspended graphene," *Solid State Commun*. 146, 351-355, 2008.

[188] K. S. Novoselov, A. K. Geim, S. V. Morozov, D. Jiang, Y. Zhang, S. V. Dubonos, I. V. Grigorieva, and A. A. Firsov, "Electric field effect in atomically thin carbon films," *Science* 306 (5696), 666-669, 2004.

[189] Y. Zhang, Y. W. Tan, H. L. Stormer, and P. Kim, "Experimental observation of the quantum Hall effect and Berry's phase in graphene," *Nature* 438 (7065), 201–204, 2005.

[190] X. Du, I. Skachko, A. Barker, and E. Y. Andrei, "Approaching ballistic transport in suspended graphene," *Nat. Nanotechnol*. 3 (8), 491-495, 2008.

[191] S. Zhang, W. Fan, B. K. Minhas, A. Frauenglass, K. J. Malloy, S. R. J. Brueck. "Mid-infrared resonant magnetic nanostructures exhibiting a negative permeability," *Phys. Rev. Lett.* 94, 037402 2005.

[192] J. Fischer, G. von Freymann, M. Wegener, "The materials challenge in diffraction-unlimited direct-laser-writing optical lithography," *Adv. Mater.* 22, 3578–3582 2010.

[193] Z. Q. Li, E. A. Henriksen, Z. Jiang, Z. Hao, M. C. Martin, P. Kim, H. L. Stormer, D. N. Basov, "Dirac charge dynamics in graphene by infrared spectroscopy," *Nature Phys*. 4, 532-535, 2008.

[194] F. Wang, Y. Zhang, C. Tian, C. Girit, A. Zettl, M. Crommie, Y. Ron Shen, "Gate-variable optical transitions in graphene," *Science* 320, 206-209, 2008.

[195] T. Hasan, Z. Sun, F. Wang, F. Bonaccorso, P. H. Tan, A. G. Rozhin, A. C. Ferrari, "Nanotube–polymer composites for ultrafast photonics," *Adv. Mater.* 21, 3874-3899, 2009.

[196] Z. Sun, T. Hasan, F. Torrisi, D. Popa, G. Privitera, F. Wang, F. Bonaccorso, D. M. Basko, A. C. Ferrari, "Graphene mode-locked ultrafast laser," *ACS Nano* 4, 803-810, 2010.

[197] R. J. Stoehr, R. Kolesov, J. Pflaum, J. Wrachtrup, "Fluorescence of lasercreated electron–hole plasma in graphene," *Physical Review B*, volume 82, 2010.

[198] T. Gokus, R. R. Nair, A. Bonetti, M. Böhmler, A. Lombardo, K. S. Novoselov, A. K. Geim, A. C. Ferrari, A. A. Green, M. C. Hersam, A. Hartschuh, "Excited state energies and decay dynamics in carbon nanotubes and graphene," *E-MRS Spring Meeting*, 2010.

[199] T. Kampfrath, L. Perfetti, F. Schapper, C. Frischkorn, M. Wolf, "Strongly coupled optical phonons in the ultrafast dynamics of the electronic energy and current relaxation in graphite," *Phys. Rev. Lett.* 95, 187403, 2005.

[200] K.M. Mak, J. Shan, T.F. Heinz, "Electronic structure of few-layer graphene: experimental demonstration of strong dependence on stacking sequence," *Phys. Rev. Lett.* 104, 176404, 2009.

[201] M. Breusing, C. Ropers, T. Elsaesser, "Ultrafast carrier dynamics in graphite," *Phys. Rev. Lett.* 102, 086809, 2009.

[202] X. S. Li, W. W. Cai, J. H. An, S. Kim, J. Nah, D. X. Yang, R. D. Piner, A. Velamakanni, I. Jung, E. Tutuc, S. K. Banerjee, L. Colombo, and R. S. Ruoff, "Large-area synthesis of high-quality and uniform graphene films on copper foils," *Science* 324(5932), 1312–1314, 2009.

[203] V. V. Khardikov, E. O. Iarko, and S. L. Prosvirnin, "Trapping of light by metal arrays," *J. Opt.* 12 (2010) 045102, 2010.

[204] R. R. Nair, P. Blake, A.N. Grigorenko, K. S. Novoselov, T.J. Booth, T. Stauber, N.M.R. Peres, A.K. Geim, "Fine Structure Constant Defines Visual Transparency Of Graphene," *Science*, 320, 1308, 2008.

[205] K.F. Mak, Y.M. Sfeir, Y. Wu, C.H. Lui, J. A. Misewich, T.F. Heinz, "Measurement of the Optical Conductivity of Graphene," *Phys. Rev. Lett*. 101, 196405, 2008.

[206] P. Y. Yu, M. Cardona, "Fundamentals of Semiconductors," *Springer*: New York, 2004.

[207] J. Kim, H. Son, D. J. Cho, B. Geng, W. Regan, S. Shi, K. Kim, A. Zettl, Y. Shen, F. Wang, "Electrical Control of Optical Plasmon Resonance with Graphene," *Nano Lett*., 12, 5598−5602, 2012.

[208] K. Vora, S. Kang, S. Shukla, E. Mazur, "Fabrication of disconnected three dimensional silver nanostructures in a polymer matrix," *Applied Physics Letters*, 100, 063120, 2012.

[209] C. N. LaFratta, J. T. Fourkas, T. Baldacchini, and R. A. Farrer, Angew. Chem., "Multiphoton Fabrication," Int. Ed. 46(33), 6238, 2007.

[210] R. R. Gattass, E. Mazur, "Femtosecond laser micromachining in transparent materials," *Nature Photonics* 2, 219 - 225, 2008.

[211] R.S. Penciu, M. Kafesaki, T.F. Gundogdu, E.N. Economou, C.M. Soukoulis, "Theoretical study of left-handed behavior of composite metamaterials," *Photon. Nanostruct: Fund. Appl*. 4, 12, 2006.

[212] A. Bostwick, T. Ohta, T. Seyller, K. Horn, E. Rotenberg, "Quasiparticle dynamics in graphene," *Nature Phys*. 3, 36–40 2007.

[213] Graphene Market, https://graphene-supermarket.com/CVD-Graphene-on-SiO2-Si/